ISTANBUL TECHNICAL UNIVERSITY ★ GRADUATE SCHOOL OF SCIENCE ENGINEERING AND TECHNOLOGY

NONLINEAR DYNAMIC BEHAVIOUR OF TAPERED SANDWICH PLATES WITH MULTI-LAYERED FACES SUBJECTED TO AIR BLAST LOADING

Ph.D. THESIS

Sedat SÜSLER

Department of Aeronautics and Astronautics Engineering

Aeronautics and Astronautics Engineering Programme

DECEMBER 2015

ISTANBUL TECHNICAL UNIVERSITY ★ GRADUATE SCHOOL OF SCIENCE ENGINEERING AND TECHNOLOGY

NONLINEAR DYNAMIC BEHAVIOUR OF TAPERED SANDWICH PLATES WITH MULTI-LAYERED FACES SUBJECTED TO AIR BLAST LOADING

Ph.D. THESIS

Sedat SÜSLER
(511082103)

Department of Aeronautics and Astronautics Engineering

Aeronautics and Astronautics Engineering Programme

Thesis Advisor: Prof. Dr. Halit Süleyman TÜRKMEN

DECEMBER 2015

İSTANBUL TEKNİK ÜNİVERSİTESİ ★ FEN BİLİMLERİ ENSTİTÜSÜ

ÇOK KATMANLI YÜZEYLERE SAHİP KALINLIKÇA SİVRİLEN SANDVİÇ PLAKLARIN ANLIK BASINÇ YÜKLEMESİ ALTINDAKİ LİNEER OLMAYAN DİNAMİK DAVRANIŞI

DOKTORA TEZİ

Sedat SÜSLER
(511082103)

Uçak ve Uzay Mühendisliği Anabilim Dalı

Uçak ve Uzay Mühendisliği Programı

Tez Danışmanı: Prof. Dr. Halit Süleyman TÜRKMEN

ARALIK 2015

Sedat SÜSLER, a Ph.D. student of ITU Graduate School of Science Engineering and Technology student ID 511082103, successfully defended the thesis entitled "NONLINEAR DYNAMIC BEHAVIOUR OF TAPERED SANDWICH PLATES WITH MULTI-LAYERED FACES SUBJECTED TO AIR BLAST LOADING", which he prepared after fulfilling the requirements specified in the associated legislations, before the jury whose signatures are below.

Thesis Advisor : **Prof. Dr. Halit Süleyman TÜRKMEN** ....
İstanbul Technical University

Jury Members : **Prof. Dr. Vedat Ziya DOĞAN** ....
Istanbul Technical University

Prof. Dr. Mehmet Alaittin ARPACI ....
Istanbul Technical University

Assoc. Prof. Dr. Hasan KURTARAN ....
Gebze Technical University

Assoc. Prof. Dr. Zafer KAZANCI ....
Turkish Air Force Academy

Date of Submission : 02 November 2015
Date of Defense : 15 December 2015

To my family,

FOREWORD

Foremost, I would like to express my gratitude to my advisor Prof. Dr. Halit S. Türkmen for his support, providing guidance and sharing his profound knowledge. I would like to thank Assoc. Prof. Dr. Zafer Kazancı for his support and help to configure the basic of this study. I would also like to thank Prof. Dr. Vedat Z. Doğan, Prof. Dr. M. Alaittin Arpacı and Assoc. Prof. Dr. Hasan Kurtaran for their constructive comments and suggestions. I would like to specially thank my dear wife Belkıs for her love and patience at all times. I am very grateful to my mother Seniha Süsler, my sister Seda Güler and her family, my nephew Eren and my brother in law Murat, for their endless support and encouragement. I would like to appreciate my wife's parents Ayhan & Keriman Erzincanlı, her brother Burak, my aunt Sebahat Dikbay and my older aunt Nazike Özgirgin for their lovely support. In addition, I would also like to appreciate Tech. Müslüm Çakır and my colleague Erdem Akay for their help with experimental studies and having good time at laboratory. Finally, I would like to thank all my good friends, especially Fırat Korkmaz, Serhan Özen, Fulya Şahiner, Çağrı Yalçın, Erdem Sönmez, Serhat Yılmaz and Alkım Deniz Şenalp for my beautiful memories. I also acknowledge Istanbul Technical University research fund for supporting my Ph.D. study.

December 2015 Sedat SÜSLER

TABLE OF CONTENTS

Page

ABBREVIATIONS

Ref.	: Reference
FEM	: Finite Element Method
Eq.	: Equation
t_sand	: Tapered Sandwich Plate
App	: Appendix
3D	: Three Dimensional
CNC	: Computer Numerical Control
CAD	: Computer Aided Design
ASTM	: American Society for Testing and Materials
sp gr	: Specific Gravity
DAQ	: Data Acquisition
ICP	: Integrated Circuit Piezoelectric
AAF	: Anti-Aliasing Filter

LIST OF TABLES

Page

LIST OF FIGURES

Page

NONLINEAR DYNAMIC BEHAVIOUR OF TAPERED SANDWICH PLATES WITH MULTI-LAYERED FACES SUBJECTED TO AIR BLAST LOADING

SUMMARY

A sandwich structure is a class of composite material which is manufactured by attaching two thin laminated stiff faces to a core which is lighter and less stiff. Sandwich structures have a wide application area in aerospace, defence and marine industry. Sandwich and laminated composite components such as panels can have variable thickness in some cases while the others have constant thickness according to design, geometric necessities and minimum weight requirements. A tapered effect in thickness can be sometimes sufficient to obtain the variable thickness. The crucial point to design more durable sandwich structures is predicting dynamic responses of them when they are subjected to various types of transient dynamics loadings. This study focuses on the sandwich structure as a plate and the transient dynamic load as explosive air blast waves.

Air blast loads occur on supersonic and hypersonic flights due to turbulences, sonic boom and shock waves. Sonic boom is a phenomenon and aerospace structures are subjected to sonic booms that cause shock waves while aircrafts, rockets and missiles reach and pass the speed of sound on flights. On the other hand, an explosion is another phenomenon which is the result of a rapid release of energy because of an explosive event. Chemical explosions like bombs, nuclear explosions, fuel explosions, etc. can be a blast source which causes overpressure.

In this study, nonlinear dynamic behaviour of composite sandwich plates with variable thickness subjected to time dependent pressure pulse has been investigated by an analytical model, experimental model and finite element method (FEM). Tapered plate subjected to air blast loading is considered as a design model for the variable thickness and pressure pulse. The tapered sandwich plate has a honeycomb core and laminated composite face sheets. In the first part of study, the tapering thickness is varying for both sandwich core and face sheets together in case of simply supported boundary conditions for all edges. Moreover, a tapered sandwich plate which has a thickness varying for only sandwich core, is analysed for clamped boundary conditions for all edges to include the experimental model into the second part of study. Clamped sandwich plate with both tapered sandwich core and tapered face sheets is also considered.

The theoretical method is based on a sandwich plate theory including the large deformation effects, such as geometric nonlinearities, in-plane stiffness and inertias, and shear deformation. The geometric nonlinearity effects are taken into account by using the von Kármán large deflection theory of thin plates. The classical sandwich plate theory for plates with constant thickness which have one-layered face sheets found in the literature is developed to analyse the tapered sandwich plates with multi-

layered face sheets. The equations of motion for the plate are derived by the use of the virtual work principle. Approximate solution functions are assumed for the space domain and substituted into the equations of motion. The Galerkin method is used to obtain the nonlinear differential equations in the time domain. The finite difference method is applied to solve the system of coupled nonlinear equations. Finally, the equations of motion are reduced into a form that can be easily solved by one of the methods for solution of linear equation systems such as LU decomposition. The displacement-time and strain-time histories are obtained on certain points through the tapered direction. Then, the results obtained by using the present method are compared with the ones obtained by using a commercial finite element package ANSYS and the experimental method. The effects of taper ratio, the stacking sequence and the fiber orientation angle on the dynamic responses of the tapered sandwich plates are also investigated for the simply supported boundary condition.

The simply supported and clamped tapered plates are discretized using 28x28 eight nodded layered shell elements (Shell281) which have the geometric nonlinearity capability for the FEM. Shell 281 has six degrees of freedom which are at each node. Three degrees of freedom is in translation while three is in rotation. These types of shell elements are not only typically described as geometrically planar elements, but also they are spatially 3D elements. Shell elements are very used to model thin and thick shell and plate structures which are subjected to bending. The total number of elements, 784 is satisfactory and is chosen as based on the mesh sensitivity analysis. The individual laminas (laminated faces and core) are assumed to be perfectly bonded in the finite element model. Finite element analysis is examined for only tapered sandwich plate that has both a tapering core and tapered faces because of the restrictions of defining the tapering function in FEM.

The experimental studies contain manufacturing a tapered sandwich plate, determining mechanical properties of the constituents and finally simulating an environment of the blast effect with a two stage procedure. At first, blast load tests for transient pressure measurement on a plexiglass model plate are done. Then, air blast load tests on the real tapered sandwich clamped plate are carried out for measuring strain and acceleration at certain points. Acceleration data work useful on obtaining displacement-time histories experimentally. The experimental model presented here can reduce the period of time and can be defined as low cost in comparison with conventional tests by using the mentioned two stage procedure. Polyester film membranes for bursting which are used in this study are also very practical and cheap for the blast testing.

There is a good correlation between not only the results of theory and FEM for simply supported tapered sandwich plate but also the results of the experimental model and theory with FEM for the clamped tapered plate. The closed form solution presented here costs much lower computer time compared to the FEM. The experimental studies are a troublesome process anyway which have a long period of time. However, the testing process is strongly needful for the validation of the theory. The code is once validated with the test, then the theory can be carried out the desired design of plates. Because, it is very easy to change design parameters for the theory. The method present here can be used in preliminary design of sandwich and laminated plates with variable thickness. The method is very capable of predicting the nonlinear dynamic response of the tapered sandwich plate with multi-layered faces. The thickness variation is taken as a linear function of coordinate axis in this study. However, the thickness variation could be taken as the second or third degree functions of coordinate axis. The blast pressure is uniformly distributed on the tapered plate. Tapered sandwich plates could be more functional under the effect of non-uniform pressure distribution. The thicker part of the tapered plate could be subjected to higher pressure load while the thinner part is subjected to lower pressure load.

ÇOK KATMANLI YÜZEYLERE SAHİP KALINLIKÇA SİVRİLEN SANDVİÇ PLAKLARIN ANLIK BASINÇ YÜKLEMESİ ALTINDAKİ LİNEER OLMAYAN DİNAMİK DAVRANIŞI

ÖZET

Sandviç yapılar, katmanlı iki ince yüzey arasına hafif ve daha kalın bir çekirdek malzemenin tutturulmasıyla üretilen bir kompozit malzeme türüdür. Çekirdek malzemenin dayanımı yüzeylerin malzeme özelliğine göre çok daha düşüktür. Oluşturulan yeni malzeme türü çok sağlam ve eğilmeye karşı çok dirençli olur. Sandviç yapılar, havacılık-uzay, savunma ve denizcilik endüstrisinde çok geniş bir uygulama alanına sahiptir. Tasarım süreci, geometrik gereklilikler ve ağırlığın optimize edilmesi gibi nedenlerle sandviç veya katmanlı kompozit komponentlerin bazı durumlarda değişken kalınlığa, bazen de sabit kalınlığa sahip olması gerekebilir. Değişen kalınlık etkisinin lineer olarak sivrilme şeklinde verilmesi yaygın bir uygulama olarak komponentler için yeterli olabilir. Daha dayanıklı sandviç yapılar tasarlamanın kritik noktalarından biri, bu yapılar çeşitli tipteki anlık dinamik yüklemelere maruzken verdikleri dinamik cevapları doğru tahmin etmektir.

Patlama ile oluşan anlık basınca sahip hava yükleri, süpersonik ve hipersonik uçuşlarda gerçekleşen türbülans, sonik patlama ve şok dalgaları nedeniyle oluşur. Hava-uzay yapıları, şok dalgaları yaratan sonik patlama hadisesine uçakların, uzaya çıkan araçların, roketlerin ve füzelerin atmosferde uçuş sırasında ses hızına ulaşıp geçmesi neticesinde maruz kalır. Bununla birlikte, bir infilak neticesinde açığa çıkan ani enerji yayılımı patlamaya neden olur. Bomba gibi kimyasal patlayıcılar, nükleer kaza ve bombalar, yakıt patlamaları gibi etkiler, anlık basınç ile oluşan ve aşırı basınca neden olan patlamalara örnektir.

Bu çalışmada, zamana bağlı basınç darbesi yüklerine maruz, kalınlığı değişen kompozit sandviç plakların lineer olmayan dinamik davranışı analitik ve deneysel model ile sonlu elemanlar metodu kullanılarak incelenmiştir. Kalınlığı değişen plak, kalınlıkça lineer olarak sivrilmiş şekilde tanımlanmış ve bu plak tasarımı, basıncın dinamik etkisi olarak patlama ile oluşan anlık basınç yüklemesine maruz bırakılmıştır. Sivrilen sandviç plak, bal peteği yapısına sahip çekirdeğe ve katmanlı kompozit sandviç yüzeylere sahiptir. Çalışmanın ilk kısmında, kalınlıkça sivrilmenin bal peteği yapısı ve katmanlı hibrid kompozit yüzeylerin ikisinde de birlikte olduğu dört kenarı da basit mesnetli bir sandviç plak tasarımına ait sonuçlar elde edilmiştir. İkinci kısımda, deneysel çalışmalar ile elde edilen sonuçları da kapsayacak şekilde, kalınlıkça sivrilmenin sadece bal peteği yapısında olduğu ve sabit kalınlığa sahip katmanlı kompozit yüzeyler içeren dört kenarı da ankastre olan imal edilmiş bir sandviç plağa ait sonuçlar karşılaştırılmıştır. Üretilen sandviç plak için kalınlıkça sivrilmenin bal peteği yapısı yanında, sanki katmanlı kompozit yüzeylerde de olduğu kabulü yapılarak, bu tip bütünüyle sivrilen sandviç plaklar için de ankastre sınır koşulları için sonuçlar elde edilmiştir.

Kullanılan teorik yöntem, büyük yer değiştirme etkilerini hesaba katacak şekilde geometrik açıdan lineer olmama etkilerini, düzlem içi katılık ve ataletleri ile kayma deformasyonu içeren bir sandviç plak teorisine dayanır. Geometrik olarak lineer olmama etkileri, plaklar için kullanılan von Kármán büyük yer değiştirme teorisi kullanılarak yönteme dahil edilmiştir. Literatürde bulunan, bir katmanlı yüzeylere sahip sabit kalınlıkta bir sandviç plağa uygulanabilen sandviç plak teorisi geliştirilerek kalınlıkça sivrilen ve çok katmanlı yüzeylere sahip sandviç plakların analizinde kullanılabilecek bir teori haline getirilmiştir. Plak için gerekli hareket denklemleri virtüel iş prensibi kullanılarak türetilmiştir. Uzay bölgesi için yaklaşık çözüm fonksiyonları kabul edilmiş ve hareket denklemleri içine eklenmiştir. Bunun için yaklaşık çözüm tekniği olan Galerkin metodu kullanılmıştır. Daha sonra, zaman bölgesinde lineer olmayan diferansiyel denklemleri elde edilmiştir. Lineer olmayan bağlaşık denklem sisteminin çözümü için sonlu farklar yöntemine başvurulmuştur. Bu işlemler sonunda hareket denklemleri, lineer denklem sistemlerinin çözümü için kullanılan yöntemlerden biri olan LU ayrıştırma ile kolaylıkla çözülebilen lineer bir forma dönüştürülmüş olur. Daha sonra plak üzerinde belirlenmiş noktalardaki yer değiştirme-zaman ve birim uzama-zaman grafikleri basit mesnetli ve ankastre sınır koşulları için elde edilmiştir. Elde edilen bu sonuçlar, sonlu elemanlar yöntemini kullanan ticari bir program olan ANSYS ile ve deneysel yöntemle elde edilen sonuçlarla karşılaştırılmıştır. Basit mesnetli sınır koşullarına sahip sivrilen plağın dinamik davranışına, farklı sivrilme açılarının ve katman diziliminde fiber yönelim açılarının etkisi de ayrıca araştırılmıştır.

Sonlu elemanlar çözümü için dört kenarı basit mesnetli ve ankastre olarak ayrı ayrı tanımlı iki sivrilen plak, 28x28 sekiz düğüm noktalı katmanlı kabuk elemanlara bölünmüştür. Shell281 olarak tanımlanan bu eleman, geometrik yönden lineer olmama kapasitesine sahiptir ve her düğüm noktasında altı serbestlik derecesi mevcuttur. Üç serbestlik derecesi yer değiştirme, üç serbestlik derecesi de dönme için kullanılır. Shell 281 kabuk elemanları, genel anlamda sadece düzlemsel elemanlar olarak tanımlanmaz, aynı zamanda bu elemanlar uzaysal olarak üç boyutlu elemanlardır. Kabuk sonlu elemanlar, eğilmeyle sonuçlanmış bir yüklemeye maruz ince ve kalın kabuk ile plak yapıların sonlu elemanlar modellenmesinde yaygın olarak kullanılırlar. Bu çalışmada, plak sonlu elemanlar modellenmesinde kullanılan 784 eleman sayısı tatmin edici bir miktardır ve ağ oluşturma için yapılan hassasiyet analizi sonucunda elde edilmiştir. Sandviç yapının her bir yüzeyinin katmanları ve çekirdek yapı, ayrı ayrı birer tabaka olarak tanımlanmış ve birbirine mükemmel şekilde yapıştırılmış olarak kabul edilmiştir. Sonlu elemanlar analizi sadece, tamamı sivrilen sandviç plak olarak tanımlanan, çekirdeğin ve sandviç yüzeylerin kalınlıklarının birlikte lineer değiştiği basit mesnetli ve ankastre plaklar için yapılmıştır. Bunun nedeni, kabuk elemanlarla yapılan sonlu elemanlar modellemesinde programın, tanımlanmış ve daha sonra plağa atanmış sivrilme fonksiyonunu, tüm katmanlar için aynı anda sadece tek bir fonksiyon şeklinde tanımlayabilme imkanı vermesidir.

Deneysel çalışmaların içeriği, kalınlıkça sivrilen bir sandviç plak üretimini, üretilen sandviç plağın bileşenlerinin malzeme özelliklerinin belirlenmesini ve nihayetinde anlık basınç oluşturabilen iki aşamalı bir patlama testi ortamının yaratılmasını kapsar. Katmanlı karbon-epoksi sandviç yüzeylerin malzeme özelliklerinin belirlenmesi için kuponlar üzerinde yoğunluk, çekme ve kayma testleri yapılmıştır. Çekirdek kısmın malzeme özelliklerinin bir kısmı literatürden alınarak, diğer kısmı da çeşitli hesaplamalar yapılarak elde edilmiştir. Patlama testinin birinci aşamasında, gerçek sivrilen sandviç plak yerine pleksiglas bir model plak patlama sonucu oluşan anlık basınca maruz bırakılarak, sandviç plak ile aynı yüzeysel boyutlara sahip bir alandaki basınç dağılımı belirlenen noktalarda basınç sensörleri ile yapılan ölçümler sonucu elde edilir. Basınç ölçümleri bittikten sonra model plak sökülür ve üzerinde çeşitli noktalara birim uzama ölçer ve ivme ölçer yapıştırılmış üretilen sandviç plak sisteme monte edilir ve patlama testleri birçok kez tekrarlanarak gerçekleştirilir. Basınç, birim uzama ve ivme verileri, veri toplama cihazları yardımıyla bilgisayar hafızasına kaydedilir. Elde edilen ivme dataları, deneysel olarak elde edilmiş yer değiştirme-zaman grafiklerine dönüştürülür. Bu çalışmada kullanılan iki aşamalı deneysel modelin, benzer deney metotlarına göre deney zamanını ve maliyetini azaltıcı etkisi olabilir. Öncelikle, plak ile membran arasındaki uzaklık, membran sayısına bağlı olan patlama basıncı ve plak boyutları değişmiyorsa, model plak ile basınç ölçümü yapmak yeterlidir. İkinci aşama patlama testi, sadece birim uzama ve ivme ölçümü özelinde, farklı katman dizilimlerine, fiber açılarına yada değişik malzeme özelliklerine sahip birçok kompozit plağa hızlıca seri bir şekilde yapılabilir. Kullanılan basınç sensörleri, delik açma yoluyla montajlanan, maliyeti düşük ve patlama etkisi ile zarar görmesi çok düşük ihtimal olan sensörlerdendir. Bu çalışmada kullanılan, patlama etkisi yaratmak için yüksek basınç bölgesi oluşturan poliyester film membranlar, kullanımı çok pratik, test için hazırlama evresi çok kısa ve çok ucuz olduklarından, deney yöntemine kattıkları süre ve maliyet avantajı yadsınamaz bir gerçektir.

Sadece basit mesnetli sivrilen sandviç plak için teorik ve sonlu elemanlar yöntemi sonuçları arasında değil, ayrıca ankastre sivrilen sandviç plak için deneysel, teorik ve sonlu elemanlar yöntemi sonuçları arasında da iyi bir uyum olduğu gözlenmiştir. Kullanılan kapalı çözüm yöntemi, ANSYS çözüm süresi ile karşılaştırıldığında, çok daha az çözüm zamanı harcamıştır. Ayrıca, sadece çekirdek katmanının sivrildiği kalınlıkça sivrilen plak tipi, teorik yöntem ile çözülebilirken, ANSYS kabuk elemanlarla sonlu elemanlar modellenmesi dahi yapılamamaktadır. Bu tip plağın üç boyutlu model üzerinden sonlu elemanlarla modellenmesi, sadece çözüm zamanını çok daha arttırmakla kalmaz, aynı zamanda modelleme süresini de birkaç kat arttırır. Problemin deneysel çalışmalarıysa, uzun zaman gerektiren zahmetli bir işlem gibi gözükse de, teorik ve sonlu elemanlar yöntemlerinin doğrulanması adına fazlasıyla gerekli görülmüştür. Bununla birlikte, teorik sonuçlar ilk aşamada testle doğrulandıktan sonra, arzu edilen diğer plaklar üzerinde hızlıca çözümler elde edilebilir. Çünkü, teorik kapalı çözüm, bir plağın tasarım parametrelerinin hızlıca değiştirilebileceği şekilde nümerik parametrik bir FORTRAN bilgisayar programı şeklinde kodlanmıştır. Kullanılan teorik yönteme dayalı program, bu çalışmanın başlangıcı sayılabilecek geçmiş kalınlıkça sivrilen katmanlı kompozit plak çalışmalarını da dahil ederek, kalınlıkça lineer sivrilen sandviç ve katmanlı kompozit plakların ön tasarım evresinde kullanılabilir. Yöntemin, çok katmanlı kompozit yüzeylere sahip kalınlıkça sivrilen sandviç plakların lineer olmayan dinamik davranışının tahmin edilmesindeki kabiliyeti yüksektir. Bu çalışmada, kalınlık değişimi koordinat ekseninin lineer bir fonksiyonu olarak tanımlansa da, kalınlık değişimi farklılaştırılarak ikinci yada üçüncü dereceden fonksiyonlar olarak da tanımlanabilirdi. Oluşturulan parametrik programa bu fonksiyonların da dahil edilmesi kalınlığı değişen kompozit plakların hızlı ön tasarım seçeneklerini genişletecektir. Deneysel olarak elde edilen basınç dağılımı sonuçlarını da hesaba katarak, patlama sonucu sivrilen plak üzerinde basıncın üniform dağılım gösterdiği kabul edilmiştir. Kalınlıkça sivrilen sandviç plaklar, üniform olmayan basınç dağılımı etkisi altında daha fonksiyonel olabilir. Plağın daha kalın bölümünün daha yüksek basınç değerlerine maruz kalırken, daha ince bölümünün daha düşük basınç değerlerine maruz kaldığı bir basınç dağılımının etkisi altındaki bir plak davranışı incelenebilir.

1. INTRODUCTION

1.1 General

A sandwich structure is a class of composite material which is manufactured by attaching two thin laminated stiff faces to a core which is lighter and less stiff. They have the capability of specific bending stiffness, so they are called bending dominant structures in industry [1]. Sandwich structures have a wide application area in aerospace, defence and marine industry. Sandwich and laminated composite components such as panels can have variable thickness in some cases while the others have constant thickness according to design, geometric necessities and minimum weight requirements. As an example for an application area, sandwich structures with variable thickness are used for wing skin panels by taking the airfoil shapes because of aerodynamic concerns and structural efficiency. Thus, the thickness varies along the chord line from the leading edge to the trailing edge [1,2]. Helicopter rotor blades are most applicable.

A tapered effect in thickness can be sometimes sufficient to obtain the variable thickness. For example, tapered sandwich panels with two faces with constant thickness and a tapered core are used for most of the flight control surfaces and wing trailing edges of aircrafts. An illustrated figure shows lightweight and strong sandwich panels that can have either constant thickness for aircraft floor panels, bulkheads and wing skin panels or tapered core honeycomb for control surfaces and wing trailing edges in Figure 1.1 [3]. As a further example, a tapered sandwich core region between face sheets is found on V-22 Osprey fuselage not only for geometric requirements but also to improve the load transfer in Figure 1.2. There are tapered sandwich panels attached to frame and spars on Boeing’s Model 360 helicopter fuselage [4].

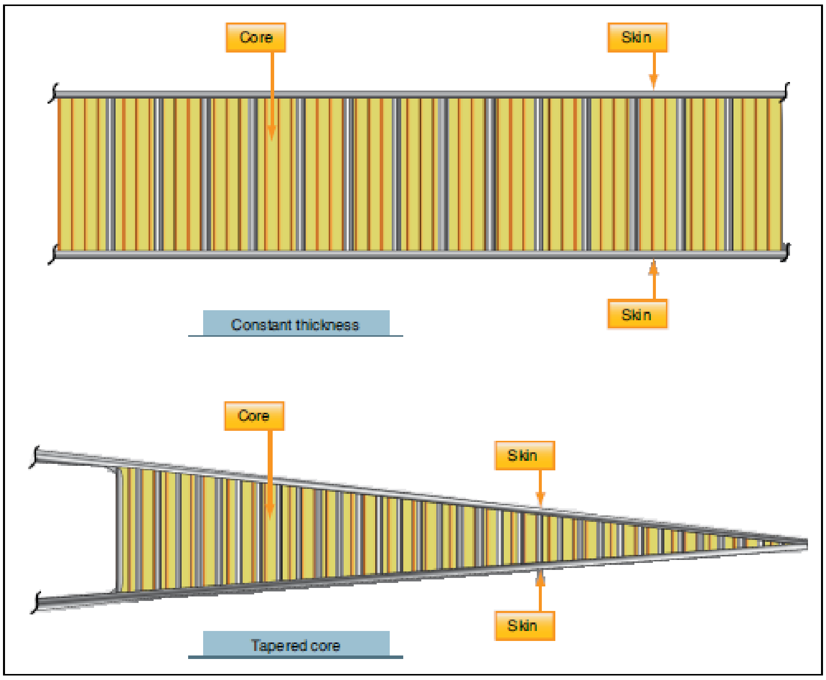

Figure 1.1 : Honeycomb panels with constant and tapered thickness [3].

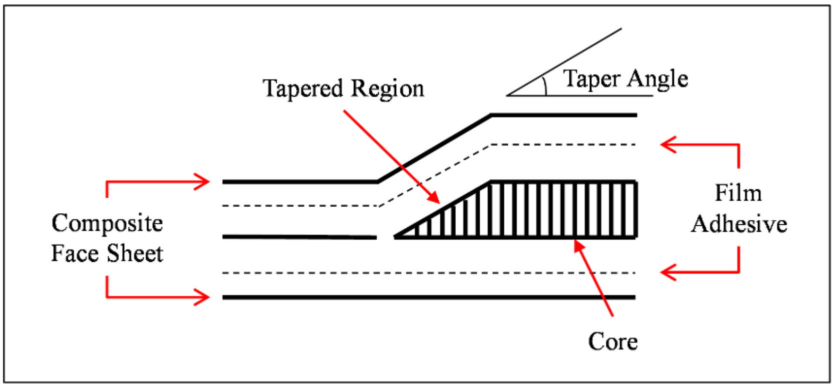

Figure 1.2 : Tapered sandwich region of V-22 Osprey fuselage [4].

The crucial point to design more durable sandwich structures is predicting dynamic responses of them when they are subjected to various types of transient dynamics loadings. This study focuses on the sandwich structure as a plate and the transient dynamic load as explosive air blast waves.

The plates are described as structural elements which have small thickness compared to other dimensions of the plane. They become resistant to transverse loads by leading to shear forces, bending and twisting moments. The advantage is that a plate is much stiffer than a beam because of their two dimensional load carrying mechanism. They are lighter structures and are used in all fields of engineering. Besides, the lighter the plate is, the more economic it is.

Laminated and sandwich composite plates can be faced with air blast loads on supersonic and hypersonic flights and under the effects of all kinds of explosions in the atmosphere and the underwater. The effects of explosions on plates must be evaluated without detrimental particle impact. Because, the impact is another research area on plates and cannot be confused with the blast waves that are based on overpressure.

Air blast loads occur on supersonic and hypersonic flights due to turbulences, sonic boom and shock waves. Sonic boom is a phenomenon and aerospace structures are subjected to sonic booms that cause shock waves while aircrafts, rockets and missiles reach and pass the speed of sound on flights. On the other hand, an explosion is another phenomenon which is the result of a rapid release of energy because of an explosive event. Chemical explosions like bombs, nuclear explosions, fuel explosions, etc. can be a blast source which causes overpressure. Figure 1.3 shows the most typical blast wave curve as a pressure-time history. As seen in the figure, there is an arrival time because of the distance from the centre of explosion. Then, there is a suddenly jump to a peak pressure called overpressure. An immediate decay starts and continues with a positive and negative phase durations which can be described as a quasi-exponential signification.

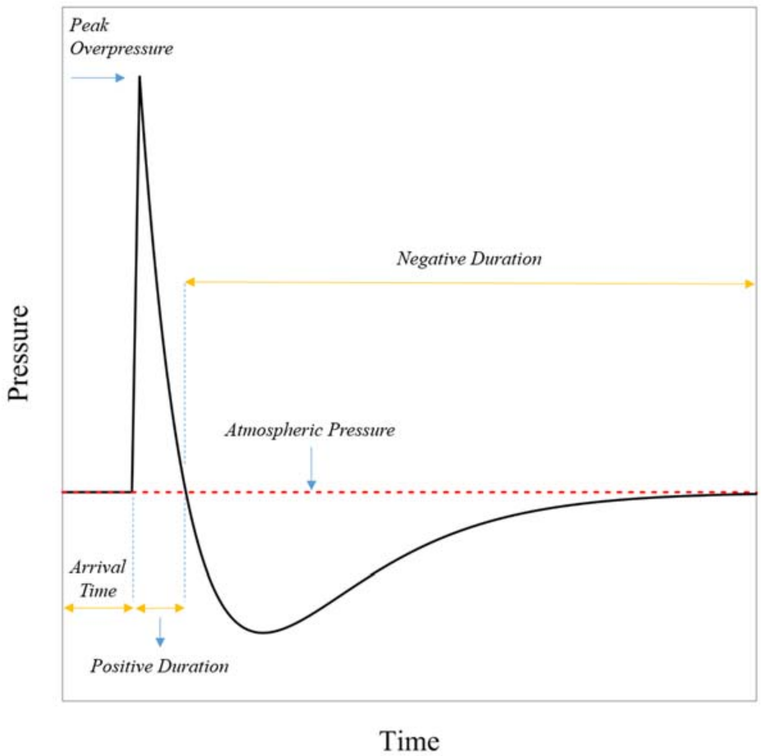

Figure 1.3 : Typical pressure-time history of a blast wave.

Distance from the blast source is an important factor that effects the peak pressure of the blast load. Table 1.1 lists the relation between distance and peak overpressure in the air at 15 °C and standard atmosphere pressure by comparing two different explosive power.

Table 1.1 : Distance from the blast source versus peak overpressure [5].

Chemical Explosion (1 Kg TNT)			Nuclear Explosion (1 Kt TNT)		
Distance (m)	Peak Pressure (bar)	Arrival Time (ms)	Distance (m)	Peak Pressure (bar)	Arrival Time (s)
0.1	332.95	0.007	10	3242.4	0.2
0.5	39.52	0.142	20	425.56	1.3
1	9.96	0.506	75	10.94	30.4
2	2.05	1.897	150	2.24	133
3	0.81	3.94	250	0.82	336
4	0.44	6.34	350	0.44	575
5	0.29	8.92	450	0.29	833
10	0.1	22.7	850	0.1	1940

1.2 Literature Review

Many studies have been done on both linear and nonlinear analysis of isotropic and laminated composite plates with constant thickness subjected to time dependent loads such as air blast. The nonlinear damped vibration of a simply supported laminated composite plate on the effect of blast load was studied theoretically by Kazancı and Mecitoğlu [6]. In another study, in-plane stiffness and inertias are considered in the theoretical solution of laminated composite plate under the blast load [7]. Moreover, Upadhyay et al. [8] studied non-linear dynamic response of laminated composite plates subjected to different pulse loadings and compared their work with Ref. [7] by using third order shear deformation plate theory. Türkmen and Mecitoğlu [9] investigated the nonlinear structural response of laminated composites subjected to blast loading experimentally. In another study, Louca and Pan [10] analysed the response of stiffened and unstiffened plates subjected to blast loading by using a single energy based formulation. Theoretical and experimental results are compared for geometrically nonlinear vibrations of rectangular plates with different boundary conditions by Amabili [11,12]. Chen et al. [13] developed a semi-analytical finite strip method for the nonlinear transient response to dynamic loading of simply supported laminated rectangular plates. Şenyer and Kazancı [14] numerically analysed nonlinear response of a simply supported laminated hybrid composite plate subjected to several blast loads that are sonic boom pulses, gust and nuclear explosions. Baştürk et al. [15] focused on deflections of simply supported laminated basalt composite plates forced by several time dependent external pulses by using an analytical model also consisting of a parametric study. Baştürk et al. [16] also studied nonlinear damped vibrations of a simply supported hybrid laminated epoxy composite plate including basalt, kevlar and e-glass laminates subjected to air blast load.

Dynamic responses of sandwich panels have been also investigated by several authors. Kazancı [17] studied dynamic response of orthotropic sandwich composite plates induced by time dependent pressure pulses theoretically. Hause and Librescu [18] investigated the dynamic response of anisotropic sandwich panels subjected to external blast pulses. Linear and non-linear dynamic response of sandwich flat panels subjected to blast load was studied by Librescu et al. [19]. Yang et al. [20] performed finite element solutions on the dynamic response of circular sandwich panel constructions under global and local blast loading and compared different sandwich set-ups with the aid of commercial package ABAQUS. Nayak et al. [21,22] analysed the transient response of orthotropic composite sandwich plates by using new finite element formulations based on a refined higher order plate theory. Balkan and Mecitoğlu [23] carried out theoretical and experimental studies for the nonlinear dynamic behaviour of viscoelastic sandwich composite plates with constant thickness under non-uniform blast load.

The plates which have constant thickness are considered only in the studies above. The effect of variable thickness, generally tapering thickness, is also important in a design process. Researches on structures with variable thickness have been generally limited to static, free vibration or stress and damage analysis theoretically, numerically and experimentally. He et al. [24] reviewed many studies until the year 2000 about tapered laminated composite structures in the scope of interlaminar stress analysis and delamination analysis. Barton [25] researched about fundamental frequency of an isotropic plate with a linear thickness. Nallim and Grossi [26] investigated natural frequencies of tapered orthotropic rectangular plates with a central free hole. In the other two studies, free vibration analysis of isotropic tapered plate without [27] and with [28] nonlinearity effects were computed using differential quadrature method. Civalek [29] focused on natural frequencies of orthotropic rectangular plates with linearly varying thickness by using discrete singular convolution method. Nguyen et al. [30] analysed honeycomb sandwich panels with locally stepped facings in static bending problems. Vel et al. [31] developed a tapered sandwich theory that predicts the stresses and deflection of tapered sections and tested on bending of sandwich panels with laminated anisotropic facings. Rabinovitch and Frostig [32] studied about the bending behaviour of a unidirectional sandwich panel with curved faces and a flexible core with variable thickness. There had been also methodological studies about static analysis of sandwich plates with variable thickness by small deflection theory [33,34]. On the other hand, Ganesan and Liu [35] studied on predictions about failure and post buckling nonlinear response of tapered composite plates under the effect of uniaxial compression by developing a nonlinear finite element formulation on the first order shear deformation theory. Rasul and Ganesan [36] then extended the previous study to buckling of tapered curved composite plates by using a similar finite element method. Mustapha and Ye [37] investigated the characteristics of guided waves for damage inspection in tapered sandwich plates with a high density foam core.

Dynamic responses of composite plates with variable thickness subjected to time dependent loads are very limited. In a study, response of composite beams with tapering and parabolic thickness subjected to a point harmonic excitation was studied by using a finite element model [38]. Susler et al. [39,40] conducted two studies on nonlinear dynamic behaviour of laminated composite plates with tapering and parabolic thickness subjected to air blast load as a time dependent transient load.

1.3 Purpose of Thesis

In this study, nonlinear dynamic behaviour of composite sandwich plates with variable thickness subjected to time dependent pressure pulse has been investigated by an analytical model, experimental model and FEM (finite element method). Tapered plate subjected to air blast loading is considered as a design model for the variable thickness and pressure pulse. The tapered sandwich plate has a honeycomb core and laminated composite face sheets. In the first part of study, the tapering thickness is varying for both sandwich core and face sheets together in case of simply supported boundary conditions for all edges. Moreover, a tapered sandwich plate which has a thickness varying for only sandwich core, is analysed for clamped boundary conditions for all edges to include the experimental model into study. Clamped sandwich plate with both tapered sandwich core and tapered face sheets is also considered.

The theoretical method is based on a sandwich plate theory including the large deformation effects, such as geometric nonlinearities, in-plane stiffness and inertias, and shear deformation. The geometric nonlinearity effects are taken into account by using the von Kármán large deflection theory of thin plates. The classical sandwich plate theory for plates with constant thickness which have one-layered face sheets found in the literature is developed to analyse the tapered sandwich plates with multi-layered face sheets. The equations of motion for the plate are derived by the use of the virtual work principle. Approximate solution functions are assumed for the space domain and substituted into the equations of motion. The Galerkin method is used to obtain the nonlinear differential equations in the time domain. The finite difference method is applied to solve the system of coupled nonlinear equations. Finally, the equations of motion are reduced into a form that can be easily solved by one of the methods for solution of linear equation systems such as LU decomposition. The displacement-time and strain-time histories are obtained on certain points through the tapered direction. Then, the results obtained by using the present method are compared with the ones obtained by using a commercial finite element package ANSYS and the experimental model. The effects of taper ratio, the stacking sequence and the fiber orientation angle on the dynamic responses of the tapered sandwich plates are also investigated for the simply supported boundary condition.

The experimental studies of whole thesis contain manufacturing a tapered sandwich plate, determining mechanical properties of the constituents and finally simulating an environment of the blast effect by setting up a shock tube testing mechanism.

1.4 Organization of Thesis

The main body of this thesis is divided into 6 parts. Following this introductory part which has a general overview and literature review, is Chapter 2. This chapter focuses on the detailed explanation of the theoretical model. Chapter 3 describes the FEM and solution obtained by ANSYS. Experimental studies about the tapered sandwich plate are described in Chapter 4. Chapter 5 covers the results and comparison of theoretical results with other models. Chapter 6 expresses the conclusions and suggests several ideas for related future studies.

As distinguished from the text, References and Appendices are listed after Chapter 6, respectively. Table of Contents, Abbreviations, List of Tables, List of Figures, English Summary and Turkish Summary are written before Chapter 1, respectively.

2. THEORETICAL MODEL

2.1 Equations of Motion

The tapered rectangular sandwich plate with the length a, the width b, and the blast load are depicted in Figure 2.1. The thickness denoted by $h(x)$ is varying for both core (c) and laminated top (f_T) and bottom (f_B) face sheets in Eq. (2.1). If the thickness of the sandwich varies for only core, Eq. (2.2) is obtained. The taper ratio is defined by β and the Cartesian axes are used in the derivation of the formulation.

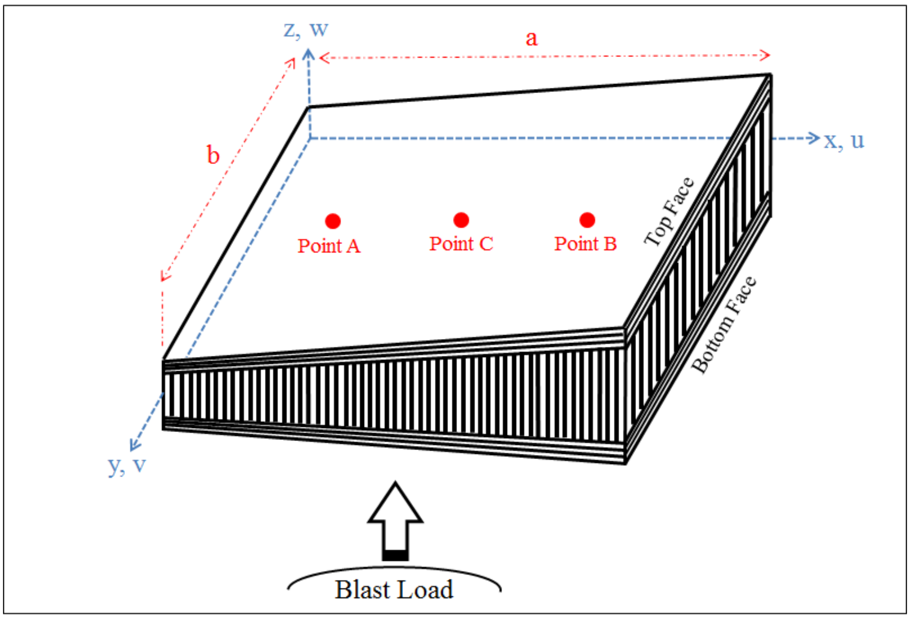

Figure 2.1 : The schematic view of the tapered sandwich composite plate.

$$h(x) = \left((h_c)_0 + \left(h_{f_T}\right)_0 + \left(h_{f_B}\right)_0 \right)\left(1 + \beta \frac{x}{a}\right) \tag{2.1}$$

$$h(x) = (h_c)_0 \left(1 + \beta \frac{x}{a}\right) + h_{f_T}(x) + h_{f_B}(x) \quad ; \quad h_{f_i}(x) = h_{f_i} \tag{2.2}$$

Some assumptions are used while theorizing the problem. Linear elastic material behaviour is considered only. The each face of the sandwich plates are defined as specially orthotropic laminates. The layers and the core are all perfectly bonded and delamination is not allowed. The shear stresses are not changed through the thickness of the core. Out-of-plane transverse normal strain is omitted [41]. Lastly, it is a common way in literature for sandwich constructions to define the lateral displacement by dividing it into contributions of bending and shear:

$$w = w_b + w_s \tag{2.3}$$

According to Weierstrass approximation theorem, polynomial functions can define uniformly any continuous function on a closed interval in mathematical analysis because of their easy computing property. This theorem is effective for defining the displacement field of a plate through the thickness. If displacement functions (u, v, w) are expanded in a series, the simplified functions for displacements in the x, y and z directions are then obtained by using first few terms in Eq. (2.4) [17]. u^0, v^0, w^0 are displacement components of the reference surface in the x, y and z directions, respectively. ψ_x and ψ_y are cross sectional rotations for xz and yz planes due to bending.

$$u = u^0 - z\psi_x = u^0 - z\frac{\partial w}{\partial x} \;;\; v = v^0 - z\psi_y = v^0 - z\frac{\partial w}{\partial y} \;;\; w = w^0 \tag{2.4}$$

Cross sectional rotations are written as Eq. (2.5) because of the partial deflection described in Eq. (2.3).

$$\psi_x = -\frac{\partial w_b}{\partial x} \;;\; \psi_y = -\frac{\partial w_b}{\partial y} \tag{2.5}$$

And if the partial differentials of total lateral displacement are used:

$$\frac{\partial w_s}{\partial x} = \frac{\partial w}{\partial x} + \psi_x \;;\; \frac{\partial w_s}{\partial y} = \frac{\partial w}{\partial y} + \psi_y \tag{2.6}$$

The strain-displacement relations for the von Kármán large deflection plate theory is then modified by using above equations in Eq. (2.7) [41]. The strains with the notation $(\,)^0$ denote the membrane strains. κ_x, κ_y and κ_{xy} are the curvatures.

$$\varepsilon_x = \varepsilon_x^0 + z\kappa_x = \frac{\partial u^0}{\partial x} + \frac{1}{2}\left(\frac{\partial w^0}{\partial x}\right)^2 - z\frac{\partial^2 w_b^0}{\partial x^2}$$

$$\varepsilon_y = \varepsilon_y^0 + z\kappa_y = \frac{\partial v^0}{\partial y} + \frac{1}{2}\left(\frac{\partial w^0}{\partial y}\right)^2 - z\frac{\partial^2 w_b^0}{\partial y^2}$$

$$\varepsilon_z = 0 \tag{2.7}$$

$$\gamma_{xy} = \gamma_{xy}^0 + z\kappa_{xy} = \frac{\partial u^0}{\partial y} + \frac{\partial v^0}{\partial x} + \frac{\partial w^0}{\partial x}\frac{\partial w^0}{\partial y} - 2z\frac{\partial^2 w_b^0}{\partial x \partial y}$$

$$\gamma_{xz} = \frac{\partial w_s^0}{\partial x} \ ; = \gamma_{yz} = \frac{\partial w_s^0}{\partial y}$$

The constitutive equations of stress-strain relations for the k^{th} layer of a laminated plate are expressed in Eq. (2.8) with the reduced stiffness matrix of the k^{th} layer.

$$\begin{Bmatrix} \sigma_x \\ \sigma_y \\ \tau_{xy} \end{Bmatrix}^k = \begin{bmatrix} \overline{Q}_{11} & \overline{Q}_{12} & 0 \\ \overline{Q}_{12} & \overline{Q}_{22} & 0 \\ 0 & 0 & \overline{Q}_{66} \end{bmatrix}^k \begin{Bmatrix} \varepsilon_x \\ \varepsilon_y \\ \gamma_{xy} \end{Bmatrix}^k$$

$$\begin{Bmatrix} \tau_{yz} \\ \tau_{xz} \end{Bmatrix}^k = \begin{bmatrix} \overline{Q}_{44} & 0 \\ 0 & \overline{Q}_{55} \end{bmatrix}^k \begin{Bmatrix} \gamma_{yz} \\ \gamma_{xz} \end{Bmatrix}^k \tag{2.8}$$

σ_x, σ_y, τ_{xy}, τ_{yz}, τ_{xz} are stress components. $[Q_{ij}]^k$ in the principal material axes and $[T]^k$ as a transformation matrix are used to obtain the reduced stiffness matrix in the global plate axes:

$$\left[\overline{Q}\right]^k = \left[T^{-1}\right]^k [Q]^k [T]^k \tag{2.9}$$

where:

$$[T]^k = \begin{bmatrix} \cos^2\theta & \sin^2\theta & 2\cos\theta\sin\theta \\ \sin^2\theta & \cos^2\theta & -2\cos\theta\sin\theta \\ -\cos\theta\sin\theta & \cos\theta\sin\theta & \cos^2\theta - \sin^2\theta \end{bmatrix} \tag{2.10}$$

θ is the fiber direction of each layer according to the global plate axis. As a result, the components of the reduced stiffness matrix are obtained as:

$$\begin{aligned}
\bar{Q}_{11} &= Q_{11}\cos^4\theta + Q_{22}\sin^4\theta + \left(2Q_{12} + 4Q_{66}\right)\sin^2\theta\cos^2\theta \\
\bar{Q}_{12} &= \left(Q_{11} + Q_{22} - 4Q_{66}\right)\sin^2\theta\cos^2\theta + Q_{12}\left(\sin^4\theta + \cos^4\theta\right) \\
\bar{Q}_{22} &= Q_{11}\sin^4\theta + Q_{22}\cos^4\theta + \left(2Q_{12} + 4Q_{66}\right)\sin^2\theta\cos^2\theta \\
\bar{Q}_{16} &= \left(Q_{11} - Q_{12} - 2Q_{66}\right)\sin\theta\cos^3\theta - \left(Q_{22} - Q_{12} - 2Q_{66}\right)\sin^3\theta\cos\theta \\
\bar{Q}_{26} &= \left(Q_{11} - Q_{12} - 2Q_{66}\right)\sin^3\theta\cos\theta - \left(Q_{22} - Q_{12} - 2Q_{66}\right)\sin\theta\cos^3\theta \\
\bar{Q}_{66} &= \left(Q_{11} + Q_{22} - 2Q_{12} - 2Q_{66}\right)\sin^2\theta\cos^2\theta + Q_{66}\left(\sin^4\theta + \cos^4\theta\right)
\end{aligned} \tag{2.11}$$

$\bar{Q}_{16}$ and $\bar{Q}_{26}$ in the equations above equal 0 because of considering only specially orthotropic laminates. Furthermore, sandwich core is considered as behaving isotropically. So, $\bar{Q}_{44} = Q_{44}$ and $\bar{Q}_{55} = Q_{55}$. The components of $[Q_{ij}]^k$ in Eq. (2.11) are shown as:

$$\begin{gathered}
Q_{11} = \frac{E_1}{1 - \nu_{12}\nu_{21}} \;;\; Q_{12} = Q_{21} = \frac{\nu_{12}E_2}{1 - \nu_{12}\nu_{21}} \;;\; Q_{22} = \frac{E_2}{1 - \nu_{12}\nu_{21}} \;;\; Q_{66} = G_{12} \\
Q_{44} = \left(G_{23}\right)_c \;;\; Q_{55} = \left(G_{13}\right)_c
\end{gathered} \tag{2.12}$$

E_1, E_2, G_{12}, ν_{12} and ν_{21} are material properties of the layers and G_{23} and G_{13} are shear modulus related to core.

The equations of equilibrium are described as Eq. (2.13). In these equations, N_x, N_y and N_{xy} are in-plane force components while M_x, M_y and M_{xy} are moment components. Q_y and Q_x are the shear forces and related to shear deflections with shear stiffness matrices (A_{ij} for i,j=4,5) and the shear correction factors (k_{44}, k_{55}). The coefficients in the matrices in Eq. (2.13) are A_{ij}, B_{ij} and D_{ij}. They are called extensional, coupling and bending stiffness matrices respectively.

$$
\begin{Bmatrix} N_x \\ N_y \\ N_{xy} \\ M_x \\ M_y \\ M_{xy} \end{Bmatrix} = \begin{bmatrix} A_{11} & A_{12} & 0 & B_{11} & B_{12} & 0 \\ A_{12} & A_{22} & 0 & B_{12} & B_{22} & 0 \\ 0 & 0 & A_{66} & 0 & 0 & B_{66} \\ B_{11} & B_{12} & 0 & D_{11} & D_{12} & 0 \\ B_{12} & B_{22} & 0 & D_{12} & D_{22} & 0 \\ 0 & 0 & B_{66} & 0 & 0 & D_{66} \end{bmatrix} \begin{Bmatrix} \varepsilon_x^0 \\ \varepsilon_y^0 \\ \varepsilon_{xy}^0 \\ \kappa_x \\ \kappa_y \\ \kappa_{xy} \end{Bmatrix} \tag{2.13}
$$

$$
\begin{Bmatrix} Q_y \\ Q_x \end{Bmatrix} = \begin{bmatrix} k_{44}A_{44} & 0 \\ 0 & k_{55}A_{55} \end{bmatrix} \begin{Bmatrix} \varepsilon_{yz} \\ \varepsilon_{xz} \end{Bmatrix}
$$

All of stiffness matrices are shown in Eq. (2.14) together for the faces and the core of a sandwich plate. As a result of equations of equilibrium, the transverse forces are carried only by the core while the face sheets carry bending moments.

$$
\begin{gathered}
A_{ij} = \sum_{k=1}^{n} \left(\bar{Q}_{ij}\right)_k \left(h_k - h_{k-1}\right) \;\; ; \; i,j = 1,2,6 \\
B_{ij} = 1/2 \sum_{k=1}^{n} \left(\bar{Q}_{ij}\right)_k \left(h_k^2 - h_{k-1}^2\right) \;\; ; \; i,j = 1,2,6 \\
D_{ij} = 1/3 \sum_{k=1}^{n} \left(\bar{Q}_{ij}\right)_k \left(h_k^3 - h_{k-1}^3\right) \;\; ; \; i,j = 1,2,6 \\
A_{ij}^c = \bar{Q}_{ij}^c h_c \;\; ; \; i,j = 4,5 \\
B_{ij}^c = 0
\end{gathered} \tag{2.14}
$$

Finally, the stiffness matrices for a tapered sandwich plate (*t_sand*) with symmetrical laminated face sheets can be arranged as Eq. (2.15), because the stiffness matrices above are given for a single skin plate. While the matrices are calculated, tapering thickness in Eq. (2.1) must be considered for a full tapered sandwich varying in the *x* direction and must be replaced in the equations below as the crux of this study.

Eq. (2.2) must be likewise used for a tapered sandwich plate that has a tapering core and non-tapered faces. So, Eq. (2.16) is obtained for the stiffness matrices of a tapered sandwich plate with symmetrical laminated face sheets. Besides the variable thickness effect, the neglected terms of $D_{ij}^{t\_sand}$ are also included in the stiffness matrices in Eq. (2.15) and Eq. (2.16) unlike the formulation of Riber [41].

$$A_{ij}^{t\_sand} = \left(A_{ij}^{f_{T1}} + A_{ij}^{f_{T2}} + \cdots + A_{ij}^{f_{Tn}} + A_{ij}^{f_{B1}} + A_{ij}^{f_{B2}} + \cdots + A_{ij}^{f_{Bn}} \right)_0 \left(1 + \beta \frac{x}{a} \right)$$

$$B_{ij}^{t\_sand} = 0$$

$$\begin{aligned}
D_{ij}^{t_sand} = & \left\{ \left(\frac{(h_c)_0 + \left(h_{f_{T1}}\right)_0}{2} \right)^2 + \frac{\left(h_{f_{T1}}\right)_0^2}{12} \right\} \left(1 + \beta \frac{x}{a} \right)^2 A_{ij}^{f_{T1}} \\
& + \left\{ \left(\frac{(h_c)_0 + \left(h_{f_{T2}}\right)_0}{2} + \left(h_{f_{T1}}\right)_0 \right)^2 + \frac{\left(h_{f_{T2}}\right)_0^2}{12} \right\} \left(1 + \beta \frac{x}{a} \right)^2 A_{ij}^{f_{T2}} + \cdots \\
& + \left\{ \left(\frac{(h_c)_0 + \left(h_{f_{Tn}}\right)_0}{2} + \left(h_{f_{T1}}\right)_0 + \cdots + \left(h_{f_{T(n-1)}}\right)_0 \right)^2 + \frac{\left(h_{f_{Tn}}\right)_0^2}{12} \right\} \left(1 + \beta \frac{x}{a} \right)^2 A_{ij}^{f_{Tn}} \\
& + \left\{ \left(\frac{(h_c)_0 + \left(h_{f_{B1}}\right)_0}{2} \right)^2 + \frac{\left(h_{f_{B1}}\right)_0^2}{12} \right\} \left(1 + \beta \frac{x}{a} \right)^2 A_{ij}^{f_{B1}} \\
& + \left\{ \left(\frac{(h_c)_0 + \left(h_{f_{B2}}\right)_0}{2} + \left(h_{f_{B1}}\right)_0 \right)^2 + \frac{\left(h_{f_{B2}}\right)_0^2}{12} \right\} \left(1 + \beta \frac{x}{a} \right)^2 A_{ij}^{f_{B2}} + \cdots \\
& + \left\{ \left(\frac{(h_c)_0 + \left(h_{f_{Bn}}\right)_0}{2} + \left(h_{f_{B1}}\right)_0 + \cdots + \left(h_{f_{\mathrm{B}(n-1)}}\right)_0 \right)^2 + \frac{\left(h_{f_{Bn}}\right)_0^2}{12} \right\} \left(1 + \beta \frac{x}{a} \right)^2 A_{ij}^{f_{Bn}}
\end{aligned} \tag{2.15}$$

$; \; where \;\; i, j = 1, 2, 6$

$$A_{ij}^{t\_sand} = \left(A_{ij}^{c} \right)_0 \left(1 + \beta \frac{x}{a} \right) \; ; \; where \;\; i, j = 4, 5$$

$$A_{ij}^{t\_sand} = A_{ij}^{f_{T1}} + A_{ij}^{f_{T2}} + \cdots + A_{ij}^{f_{Tn}} + A_{ij}^{f_{B1}} + A_{ij}^{f_{B2}} + \cdots + A_{ij}^{f_{Bn}}$$

$$B_{ij}^{t\_sand} = 0$$

$$\begin{aligned}
D_{ij}^{t_sand} = & \left\{ \left(\frac{(h_c)_0 \left(1+\beta \frac{x}{a}\right) + h_{f_{T1}}}{2} \right)^2 + \frac{h_{f_{T1}}{}^2}{12} \right\} A_{ij}^{f_{T1}} \\
& + \left\{ \left(\frac{(h_c)_0 \left(1+\beta \frac{x}{a}\right) + h_{f_{T2}}}{2} + h_{f_{T1}} \right)^2 + \frac{h_{f_{T2}}{}^2}{12} \right\} A_{ij}^{f_{T2}} + \cdots \\
& + \left\{ \left(\frac{(h_c)_0 \left(1+\beta \frac{x}{a}\right) + h_{f_{Tn}}}{2} + h_{f_{T1}} + \cdots + h_{f_{T(n-1)}} \right)^2 + \frac{h_{f_{Tn}}{}^2}{12} \right\} A_{ij}^{f_{Tn}} \\
& + \left\{ \left(\frac{(h_c)_0 \left(1+\beta \frac{x}{a}\right) + h_{f_{B1}}}{2} \right)^2 + \frac{h_{f_{B1}}{}^2}{12} \right\} A_{ij}^{f_{B1}} \\
& + \left\{ \left(\frac{(h_c)_0 \left(1+\beta \frac{x}{a}\right) + h_{f_{B2}}}{2} + h_{f_{B1}} \right)^2 + \frac{h_{f_{B2}}{}^2}{12} \right\} A_{ij}^{f_{B2}} + \cdots \\
& + \left\{ \left(\frac{(h_c)_0 \left(1+\beta \frac{x}{a}\right) + h_{f_{Bn}}}{2} + h_{f_{B1}} + \cdots + h_{f_{\mathrm{B}(n-1)}} \right)^2 + \frac{h_{f_{Bn}}{}^2}{12} \right\} A_{ij}^{f_{Bn}} \\
& ;\ where\ \ i,j = 1,2,6
\end{aligned} \tag{2.16}$$

$$A_{ij}^{t\_sand} = \left(A_{ij}^{c}\right)_0 \left(1+\beta \frac{x}{a}\right)\ ;\ where\ \ i,j = 4,5$$

Equations of motion are derived by using the principle of virtual work. The total virtual work of the internal and external forces acting on the system is zero for any virtual displacement, if a system is in equilibrium. The equation of virtual work in variational form for a laminated plate obtained by Kazancı [42] is developed to derive the equation of virtual work for a sandwich plate in Eq. (2.17). According to the virtual work principle in interval t_1 to t_2 in Eq. (2.17), by using stress-strain relations and constitutive equations and by taking into the assumption of no strain in the *z* direction, equation of virtual work in variational form for the sandwich plate is expressed as Eq. (2.18).

$$\begin{aligned}\delta U=&\int_{t_1}^{t_2} d_t\left(\iint_A\left(\sigma_x\delta\varepsilon_x+\sigma_y\delta\varepsilon_y+\tau_{xy}\delta\gamma_{xy}+\tau_{yz}\delta\gamma_{yz}+\tau_{xz}\delta\gamma_{xz}\right)d_A\right)\\&-\int_{t_1}^{t_2} d_t\left(\iint_A\bar{m}\left(\dot{u}\delta\dot{u}+\dot{v}\delta\dot{v}+\dot{w}\delta\dot{w}\right)d_A+\iint_A\left(q_x\delta u+q_y\delta v+q_z\delta w\right)d_A\right)=0\end{aligned}\tag{2.17}$$

$$\begin{aligned}\delta U=&\int_{t_1}^{t_2} d_t\left(\iint_A\left(N_x\delta\varepsilon_x^0+N_y\delta\varepsilon_y^0+N_{xy}\delta\varepsilon_{xy}^0\right)d_A\right)\\&+\int_{t_1}^{t_2} d_t\left(\iint_A\left(M_x\delta\kappa_x+M_y\delta\kappa_y+M_{xy}\delta\kappa_{xy}\right)d_A\right)\\&+\int_{t_1}^{t_2} d_t\left(\iint_A\left(Q_x\delta\varepsilon_{xz}+Q_y\delta\varepsilon_{yz}\right)d_A\right)\\&-\int_{t_1}^{t_2} d_t\left(\iint_A\bar{m}\left(\dot{u}\delta\dot{u}+\dot{v}\delta\dot{v}+\dot{w}\delta\dot{w}\right)d_A+\iint_A\left(q_x\delta u+q_y\delta v+q_z\delta w\right)d_A\right)=0\end{aligned}\tag{2.18}$$

$\bar{m}$ is the mass of unit area and q_x, q_y, q_z are the load vectors in the directions of coordinate axes in Eq. (2.17) and Eq. (2.18). Variational principles and integration by parts are applied to every integrated term above. The derivatives are removed for the variations δu, δv and δw. Equations of motion for a sandwich plate are derived in differential form as:

$$
\begin{aligned}
&-\frac{\partial N_x}{\partial x}-\frac{\partial N_{xy}}{\partial y}-q_x+\bar{m}\ddot{u}^0=0\\
&-\frac{\partial N_y}{\partial y}-\frac{\partial N_{xy}}{\partial x}-q_y+\bar{m}\ddot{v}^0=0\\
&\frac{\partial^2 M_x}{\partial x^2}-\frac{\partial^2 M_y}{\partial y^2}-2\frac{\partial^2 M_{xy}}{\partial x\partial y}-\frac{\partial}{\partial x}\left(N_x\left(\frac{\partial w_b}{\partial x}+\frac{\partial w_s}{\partial x}\right)\right)\\
&\quad-\frac{\partial}{\partial y}\left(N_y\left(\frac{\partial w_b}{\partial y}+\frac{\partial w_s}{\partial y}\right)\right)-\frac{\partial}{\partial x}\left(N_{xy}\left(\frac{\partial w_b}{\partial y}+\frac{\partial w_s}{\partial y}\right)\right)\\
&\quad-\frac{\partial}{\partial y}\left(N_{xy}\left(\frac{\partial w_b}{\partial x}+\frac{\partial w_s}{\partial x}\right)\right)-q_z++\bar{m}\ddot{w}_b{}^0=0\\
&\frac{\partial Q_x}{\partial x}-\frac{\partial Q_y}{\partial y}-\frac{\partial}{\partial x}\left(N_x\left(\frac{\partial w_b}{\partial x}+\frac{\partial w_s}{\partial x}\right)\right)-\frac{\partial}{\partial y}\left(N_y\left(\frac{\partial w_b}{\partial y}+\frac{\partial w_s}{\partial y}\right)\right)\\
&\quad-\frac{\partial}{\partial x}\left(N_{xy}\left(\frac{\partial w_b}{\partial y}+\frac{\partial w_s}{\partial y}\right)\right)-\frac{\partial}{\partial y}\left(N_{xy}\left(\frac{\partial w_b}{\partial x}+\frac{\partial w_s}{\partial x}\right)\right)-q_z++\bar{m}\ddot{w}_s{}^0=0
\end{aligned}
\tag{2.19}
$$

where $\ddot{u}^0$, $\ddot{v}^0$, $\ddot{w}_b^0$ and $\ddot{w}_s^0$ are the components of acceleration vector. Force components, moment components and shear forces in Eq. (2.19) are replaced by using Eq. (2.13). On the other hand, von Kármán strains in Eq. (2.13) are replaced with Eq. (2.7) and the stiffness matrices for a tapered sandwich plate in Eq. (2.13) are replaced with Eq. (2.15) or Eq. (2.16) depending on the type of tapered sandwich plate. In the end, nonlinear dynamic equations of a laminated sandwich plate in terms of mid-plane displacements will be obtained.

2.2 Boundary and Initial Conditions

Simply supported and clamped tapered plates for all edges are considered in this study. Boundary conditions of the simply supported plates for all edges can be given in the following form:

$$
\begin{gathered}
u^0(0,y,t)=u^0(a,y,t)=u^0(x,0,t)=u^0(x,b,t)=0\\
v^0(0,y,t)=v^0(a,y,t)=v^0(x,0,t)=v^0(x,b,t)=0\\
w^0(0,y,t)=w^0(a,y,t)=w^0(x,0,t)=w^0(x,b,t)=0\\
M_x=0 \text{ at } \mathrm{x}=0,\mathrm{a}\\
M_y=0 \text{ at } \mathrm{y}=0,\mathrm{b}
\end{gathered}
\tag{2.20}
$$

Clamped boundary conditions are shown for all edges of a plate as:

$$
\begin{gathered}
u^0(0,y,t)=u^0(a,y,t)=u^0(x,0,t)=u^0(x,b,t)=0 \\
v^0(0,y,t)=v^0(a,y,t)=v^0(x,0,t)=v^0(x,b,t)=0 \\
w^0(0,y,t)=w^0(a,y,t)=w^0(x,0,t)=w^0(x,b,t)=0 \\
\frac{\partial u^0}{\partial x}(0,y,t)=\frac{\partial u^0}{\partial x}(a,y,t)=\frac{\partial u^0}{\partial y}(x,0,t)=\frac{\partial u^0}{\partial y}(x,b,t)=0 \\
\frac{\partial v^0}{\partial x}(0,y,t)=\frac{\partial v^0}{\partial x}(a,y,t)=\frac{\partial v^0}{\partial y}(x,0,t)=\frac{\partial v^0}{\partial y}(x,b,t)=0 \\
\frac{\partial w^0}{\partial x}(0,y,t)=\frac{\partial w^0}{\partial x}(a,y,t)=\frac{\partial w^0}{\partial y}(x,0,t)=\frac{\partial w^0}{\partial y}(x,b,t)=0
\end{gathered}
\tag{2.21}
$$

The structure began to vibrate from the rest, so at the beginning, displacements and velocities are all become zero. Initial conditions for both types of boundary are stated in Eq. (2.22).

$$
\begin{gathered}
u^0\left(x,y,0\right)=0 \;\; ; \;\; v^0\left(x,y,0\right)=0 \;\; ; \;\; w^0\left(x,y,0\right)=0 \\
\dot{u}^0\left(x,y,0\right)=0 \;\; ; \;\; \dot{v}^0\left(x,y,0\right)=0 \;\; ; \;\; \dot{w}^0\left(x,y,0\right)=0
\end{gathered}
\tag{2.22}
$$

2.3 Solution Method

The equations of motion of the sandwich plate in terms of mid-plane displacements can be solved by a two-stage method by using Galerkin method for the space domain and finite difference method for the time domain, respectively. First, equations of motion are transformed into the new ones in time domain by choosing proper approximation functions for displacement field and applying Galerkin method.

Solution functions for simply supported tapered sandwich plate are chosen crucially by also considering the results of static large deformation analysis of tapered laminated plate by Susler et al. [39]. Only the first term of the series for in-plane displacements and first two terms for out-of-plane displacements for the simply supported plate are accounted. For tapered sandwich plate, the effect of Eq. (2.1) and Eq. (2.2) is also considered and out-of-plane displacements are divided into two parts. The solution functions for simply supported boundary conditions:

$$
\begin{aligned}
u^0 &= U(t)\, y^2 (y-b)^2 \sin\frac{2\pi x}{a} \\
v^0 &= V(t)\, x^2 (x-a)^2 \sin\frac{2\pi y}{b} \\
w^0 &= w_b^0 + w_s^0 \\
w_b^0 &= W_{1b}(t)\sin\frac{\pi x}{a}\sin\frac{\pi y}{b} + W_{2b}(t)\sin\frac{2\pi x}{a}\sin\frac{\pi y}{b} \\
w_s^0 &= W_{1s}(t)\sin\frac{\pi x}{a}\sin\frac{\pi y}{b} + W_{2s}(t)\sin\frac{2\pi x}{a}\sin\frac{\pi y}{b}
\end{aligned}
\tag{2.23}
$$

Solution functions for clamped tapered sandwich plates are derived by modifying solution functions of clamped laminated plates with constant thickness obtained by Kazancı [42]. Similarly, only the first term of the series for in-plane displacements and first two terms for out-of-plane displacements are accounted. After comparing some function candidates for w^0, more proper solution functions for a clamped tapered sandwich plate is:

$$
\begin{aligned}
u^0 &= U(t) x^2 (x-a)^2 (x-\frac{a}{2})\left(1-\cos\frac{2\pi y}{b}\right) \\
v^0 &= V(t) y^2 (y-b)^2 (y-\frac{b}{2})\left(1-\cos\frac{2\pi x}{a}\right) \\
w^0 &= w_b^0 + w_s^0 \\
w_b^0 &= W_{1b}(t)\left(1-\cos\frac{2\pi x}{a}\right)\left(1-\cos\frac{2\pi y}{b}\right) \\
&+ W_{2b}(t)\left(1-\cos\frac{2\pi x}{a}\right)\left(\sin\frac{2\pi x}{a}\right)\left(1-\cos\frac{2\pi y}{b}\right) \\
w_s^0 &= W_{1s}(t)\left(1-\cos\frac{2\pi x}{a}\right)\left(1-\cos\frac{2\pi y}{b}\right) \\
&+ W_{2s}(t)\left(1-\cos\frac{2\pi x}{a}\right)\left(\sin\frac{2\pi x}{a}\right)\left(1-\cos\frac{2\pi y}{b}\right)
\end{aligned}
\tag{2.24}
$$

U, V, W_{1b}, W_{2b}, W_{1s} and W_{2s} are time dependent parts of displacement components in approximate functions of tapered sandwich plate. As a result of first stage for solution, Eq. (2.25) shows time dependent coupled nonlinear equations of tapered simply supported and clamped sandwich plate with symmetrical face sheets. The coefficients – a_i, b_i, c_i, d_i, e_i and f_i – in Eq. (2.25) are given in the Appendices. App A involves the coefficients of solution for a simply supported tapered sandwich plate that has both tapered faces and tapered core.

$$
\begin{aligned}
& a_0\ddot{U}+a_1U+a_2V+a_3W_{1b}+a_4W_{2b}+a_5W_{1s}+a_6W_{2s}+a_7W_{1b}^2+a_8W_{2b}^2 \\
& \quad +a_9W_{1s}^2+a_{10}W_{2s}^2+a_{11}W_{1b}W_{2b}+a_{12}W_{1b}W_{1s}+a_{13}W_{1b}W_{2s}+a_{14}W_{2b}W_{1s} \\
& \quad +a_{15}W_{2b}W_{2s}+a_{16}W_{1s}W_{2s}+a_{17}=0 \\
& b_0\ddot{V}+b_1U+b_2V+b_3W_{1b}+b_4W_{2b}+b_5W_{1s}+b_6W_{2s}+b_7W_{1b}^2+b_8W_{2b}^2 \\
& \quad +b_9W_{1s}^2+b_{10}W_{2s}^2+b_{11}W_{1b}W_{2b}+b_{12}W_{1b}W_{1s}+b_{13}W_{1b}W_{2s}+b_{14}W_{2b}W_{1s} \\
& \quad +b_{15}W_{2b}W_{2s}+b_{16}W_{1s}W_{2s}+b_{17}=0 \\
& c_0\ddot{W}_{1b}+c_1U+c_2V+c_3W_{1b}+c_4W_{2b}+c_5W_{1s}+c_6W_{2s}+c_7UW_{1b}+c_8UW_{2b} \\
& \quad +c_9UW_{1s}+c_{10}UW_{2s}+c_{11}VW_{1b}+c_{12}VW_{2b}+c_{13}VW_{1s}+c_{14}VW_{2s}+c_{15}W_{1b}^3 \\
& \quad +c_{16}W_{2b}^3+c_{17}W_{1s}^3+c_{18}W_{2s}^3+c_{19}W_{1b}W_{2b}^2+c_{20}W_{1b}W_{1s}^2+c_{21}W_{1b}W_{2s}^2+c_{22}W_{2b}W_{1b}^2 \\
& \quad +c_{23}W_{2b}W_{1s}^2+c_{24}W_{2b}W_{2s}^2+c_{25}W_{1s}W_{1b}^2+c_{26}W_{1s}W_{2b}^2+c_{27}W_{1s}W_{2s}^2+c_{28}W_{2s}W_{1b}^2 \\
& \quad +c_{29}W_{2s}W_{2b}^2+c_{30}W_{2s}W_{1s}^2+c_{31}W_{1b}W_{2b}W_{1s}+c_{32}W_{1b}W_{2b}W_{2s}+c_{33}W_{1b}W_{1s}W_{2s} \\
& \quad +c_{34}W_{2b}W_{1s}W_{2s}+c_{35}=0 \\
& d_0\ddot{W}_{2b}+d_1U+d_2V+d_3W_{1b}+d_4W_{2b}+d_5W_{1s}+d_6W_{2s}+d_7UW_{1b}+d_8UW_{2b} \\
& \quad +d_9UW_{1s}+d_{10}UW_{2s}+d_{11}VW_{1b}+d_{12}VW_{2b}+d_{13}VW_{1s}+d_{14}VW_{2s}+d_{15}W_{1b}^3 \\
& \quad +d_{16}W_{2b}^3+d_{17}W_{1s}^3+d_{18}W_{2s}^3+d_{19}W_{1b}W_{2b}^2+d_{20}W_{1b}W_{1s}^2+d_{21}W_{1b}W_{2s}^2+d_{22}W_{2b}W_{1b}^2 \\
& \quad +d_{23}W_{2b}W_{1s}^2+d_{24}W_{2b}W_{2s}^2+d_{25}W_{1s}W_{1b}^2+d_{26}W_{1s}W_{2b}^2+d_{27}W_{1s}W_{2s}^2+d_{28}W_{2s}W_{1b}^2 \\
& \quad +d_{29}W_{2s}W_{2b}^2+d_{30}W_{2s}W_{1s}^2+d_{31}W_{1b}W_{2b}W_{1s}+d_{32}W_{1b}W_{2b}W_{2s}+d_{33}W_{1b}W_{1s}W_{2s} \\
& \quad +d_{34}W_{2b}W_{1s}W_{2s}+d_{35}=0 \\
& e_0\ddot{W}_{1s}+e_1U+e_2V+e_3W_{1b}+e_4W_{2b}+e_5W_{1s}+e_6W_{2s}+e_7UW_{1b}+e_8UW_{2b} \\
& \quad +e_9UW_{1s}+e_{10}UW_{2s}+e_{11}VW_{1b}+e_{12}VW_{2b}+e_{13}VW_{1s}+e_{14}VW_{2s}+e_{15}W_{1b}^3 \\
& \quad +e_{16}W_{2b}^3+e_{17}W_{1s}^3+e_{18}W_{2s}^3+e_{19}W_{1b}W_{2b}^2+e_{20}W_{1b}W_{1s}^2+e_{21}W_{1b}W_{2s}^2+e_{22}W_{2b}W_{1b}^2 \\
& \quad +e_{23}W_{2b}W_{1s}^2+e_{24}W_{2b}W_{2s}^2+e_{25}W_{1s}W_{1b}^2+e_{26}W_{1s}W_{2b}^2+e_{27}W_{1s}W_{2s}^2+e_{28}W_{2s}W_{1b}^2 \\
& \quad +e_{29}W_{2s}W_{2b}^2+e_{30}W_{2s}W_{1s}^2+e_{31}W_{1b}W_{2b}W_{1s}+e_{32}W_{1b}W_{2b}W_{2s}+e_{33}W_{1b}W_{1s}W_{2s} \\
& \quad +e_{34}W_{2b}W_{1s}W_{2s}+e_{35}=0 \\
& f_0\ddot{W}_{2s}+f_1U+f_2V+f_3W_{1b}+f_4W_{2b}+f_5W_{1s}+f_6W_{2s}+f_7UW_{1b}+f_8UW_{2b} \\
& \quad +f_9UW_{1s}+f_{10}UW_{2s}+f_{11}VW_{1b}+f_{12}VW_{2b}+f_{13}VW_{1s}+f_{14}VW_{2s}+f_{15}W_{1b}^3 \\
& \quad +f_{16}W_{2b}^3+f_{17}W_{1s}^3+f_{18}W_{2s}^3+f_{19}W_{1b}W_{2b}^2+f_{20}W_{1b}W_{1s}^2+f_{21}W_{1b}W_{2s}^2+f_{22}W_{2b}W_{1b}^2 \\
& \quad +f_{23}W_{2b}W_{1s}^2+f_{24}W_{2b}W_{2s}^2+f_{25}W_{1s}W_{1b}^2+f_{26}W_{1s}W_{2b}^2+f_{27}W_{1s}W_{2s}^2+f_{28}W_{2s}W_{1b}^2 \\
& \quad +f_{29}W_{2s}W_{2b}^2+f_{30}W_{2s}W_{1s}^2+f_{31}W_{1b}W_{2b}W_{1s}+f_{32}W_{1b}W_{2b}W_{2s}+f_{33}W_{1b}W_{1s}W_{2s} \\
& \quad +f_{34}W_{2b}W_{1s}W_{2s}+f_{35}=0
\end{aligned}
\tag{2.25}
$$

App B and App C shows the coefficients for two different clamped tapered sandwich plate configurations. App B is used for a full tapered sandwich plate similarly as the simply supported one while App C is used for a clamped tapered sandwich plate that has a tapering core and non-tapered faces. The initial conditions for all configurations are shown in Eq. (2.26).

$$\begin{aligned}
&U(0)=0,\, V(0)=0,\, W_{1b}(0)=0,\, W_{2b}(0)=0,\, W_{1s}(0)=0,\, W_{2s}(0)=0 \\
&\dot{U}(0)=0,\, \dot{V}(0)=0,\, \dot{W}_{1b}(0)=0,\, \dot{W}_{2b}(0)=0,\, \dot{W}_{1s}(0)=0,\, \dot{W}_{2s}(0)=0
\end{aligned} \tag{2.26}$$

The nonlinear-coupled equations of motion in time domain in Eq. (2.25) are then solved by using the finite difference method. For this purpose, first, Eq. (2.25) can be arranged in a matrix format as:

$$[M]\{\ddot{Q}\}+[K]\{Q\}+[F]=\{0\} \tag{2.27}$$

In this format, $\{\ddot{Q}\}$, $\{Q\}$ and $[F]$ denote acceleration, displacement and force vectors, respectively. By using the description of acceleration, it is defined as the derivative of velocity vector as a function of time. After that, the definition of derivative is used for velocity vector and Eq. (2.27) is transformed into a form as:

$$[M]\frac{\{\dot{Q}\}^{n+1}-\{\dot{Q}\}^{n}}{\Delta t}+[K]\{Q\}^{n+1}+\{F\}=\{0\} \tag{2.28}$$

After the definition of derivative is performed for $\{\dot{Q}\}^{n+1}$ once again, the rearranged equation has the following form in Eq. (2.29).

$$\left(\frac{1}{(\Delta t)^2}[M]+[K]\right)\{Q\}^{n+1}=\left(\frac{1}{\Delta t}[M]\right)\{\dot{Q}\}^{n}+\left(\frac{1}{(\Delta t)^2}[M]\right)\{Q\}^{n}-\{F\} \tag{2.29}$$

Finally, the equations of motion are reduced into a compact form in Eq. (2.30) that can be easily solved by LU decomposition as one of the methods for solution of linear equation systems. The coefficients – A_i, B_i, C_i, D_i, E_i and F_i – in Eq. (2.30) are given in App D.

$$
\begin{aligned}
A_1U^{n+1} + A_2V^{n+1} + A_3W_{1b}^{n+1} + A_4W_{2b}^{n+1} + A_5W_{1s}^{n+1} + A_6W_{2s}^{n+1} &= A_7 \\
B_1U^{n+1} + B_2V^{n+1} + B_3W_{1b}^{n+1} + B_4W_{2b}^{n+1} + B_5W_{1s}^{n+1} + B_6W_{2s}^{n+1} &= B_7 \\
C_1U^{n+1} + C_2V^{n+1} + C_3W_{1b}^{n+1} + C_4W_{2b}^{n+1} + C_5W_{1s}^{n+1} + C_6W_{2s}^{n+1} &= C_7 \\
D_1U^{n+1} + D_2V^{n+1} + D_3W_{1b}^{n+1} + D_4W_{2b}^{n+1} + D_5W_{1s}^{n+1} + D_6W_{2s}^{n+1} &= D_7 \\
E_1U^{n+1} + E_2V^{n+1} + E_3W_{1b}^{n+1} + E_4W_{2b}^{n+1} + E_5W_{1s}^{n+1} + E_6W_{2s}^{n+1} &= E_7 \\
F_1U^{n+1} + F_2V^{n+1} + F_3W_{1b}^{n+1} + F_4W_{2b}^{n+1} + F_5W_{1s}^{n+1} + F_6W_{2s}^{n+1} &= F_7
\end{aligned}
\tag{2.30}
$$

3. FINITE ELEMENT MODEL

The simply supported and clamped tapered rectangular sandwich plates with laminated face sheets are modelled using FEM by ANSYS finite element software. The plate is discretized using 28x28 eight nodded layered shell elements (Shell281) which have the geometric nonlinearity capability. Shell 281 has six degrees of freedom which are at each node. Three degrees of freedom is in translation while three is in rotation. These types of shell elements are not only typically described as geometrically planar elements, but also they are spatially 3D elements. Shell elements are very used to model thin and thick shell and plate structures which are subjected to bending.

The total number of elements, 784 is satisfactory and is chosen as based on the mesh sensitivity analysis. The individual laminas (laminated faces and core) are assumed to be perfectly bonded in the finite element model. The function in Eq. (2.1) is used to describe the variation of the thickness. However, it is impossible to define the function in Eq. (2.2) while creating a shell section. Because, the defined section function is read only for all of the laminas not certain laminas while defining lay-up. The air blast loading is also described as an another suitable function and apply as a pressure force on the plate area. Boundary conditions are created as no displacements for all simply supported edges while no displacements and no rotations for all clamped edges.

The large displacement transient analyses are performed for 10 ms with 200 steps to obtain the displacement-time and strain-time histories at certain points through the tapered direction. The finite element model and cross section of the tapered sandwich plate are illustrated in Figure 3.1 and Figure 3.2, respectively.

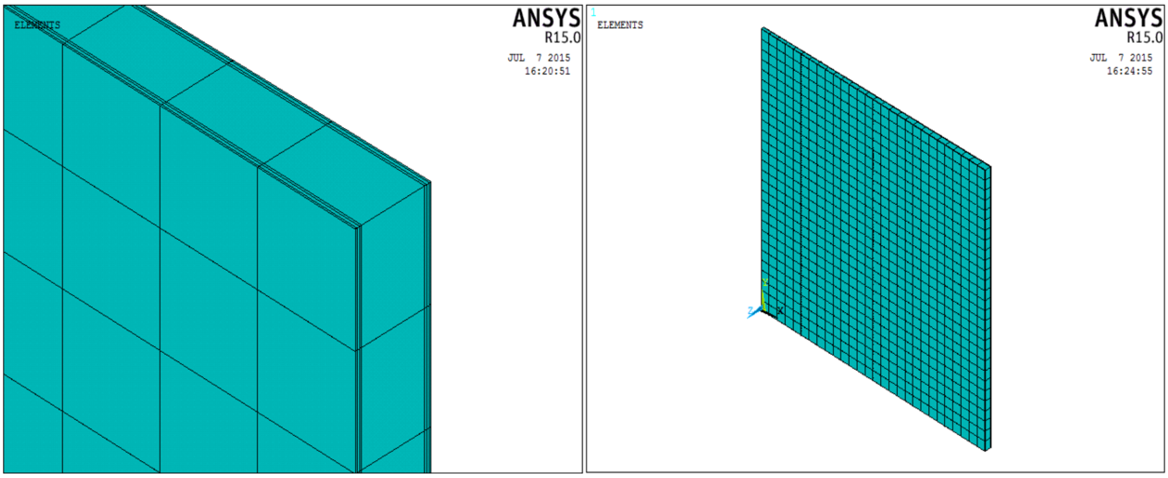

Figure 3.1 : Finite element model of the tapered sandwich plate.

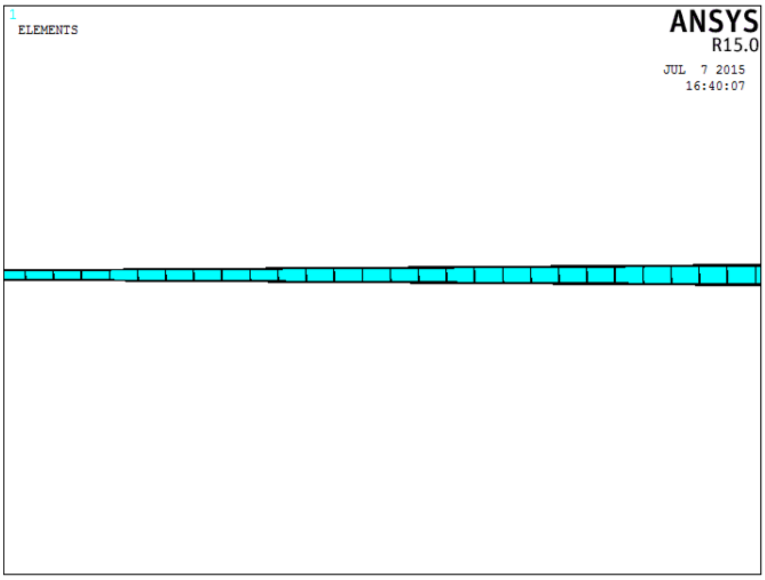

Figure 3.2 : Cross section of the tapered sandwich plate.

4. EXPERIMENTAL MODEL

The response of the composite sandwich tapered plate subjected to ait blast load has been investigated by simulating an environment and setting up a testing mechanism. The test section of this study can be divided into two parts:

- the manufacture and to determine the mechanical properties of the constituents
- the simulation

The first part contains manufacturing the tapered sandwich plates and coupons for mechanical properties and testing the coupons. The second part contains putting the experimental set-up together and performing air blast load tests.

In this study, blast load testing can be described as a two stage procedure:

- Blast load tests for transient pressure measurement on a model plate and defining and formularizing the distribution of pressure on the plate
- Air blast load testing on the real tapered sandwich plates for measuring strain and acceleration.

All test works are achieved by using the facilities of Composites & Structures Laboratory in Faculty of Aeronautics and Astronautics at Istanbul Technical University.

4.1 Manufacturing and Coupon Tests

4.1.1 Manufacturing the tapered sandwich plate

Fabricating a tapered sandwich plate begins with the decision of which types of materials will be used for faces and core of the sandwich plate. It is decided to use faces made of dry (0º/90º) fiber orientated carbon fabric cloth with resin MGS L285 / hardener MGS H285 and core made of polypropylene honeycomb.

First of all, four different rectangular two layered (0º/90º) carbon-epoxy panels are manufactured by the process of hand lay-up with the dimensions of approximately 450 mm x 900 mm. Hand lay-up is a basic method to fabricate composite components. The method depends on laying dry fabric layers by hand on a surface or into a mould and then applying resin to each dry ply until layup is complete. Then the curing process is started by pressurizing the component with the vacuum effect at room temperature or a higher temperature for a length of time.

For this study, all two layered (0º/90º) carbon-epoxy panels are cured for 24 hours nonstop at a temperature of 50 ºC. The vacuum table is used for the curing process which can be used for both pressurizing and heating at the same time. The epoxy matrix is composed of the mentioned resin and hardener above concerning parts by weight 100:40 (resin:hardener). The carbon epoxy panels are laid between plastic bags and the peel ply for both sides. Peel ply is a synthetic cloth which will make both surfaces of the panels perfectly smooth after peeling of it at the end of the curing. The peel plies absorb epoxy more than enough and also prevent bubble formations. Moreover, they create a texture on panels which improves adhesion while the honeycomb core is stuck to sandwich faces. One of four fabricated carbon-epoxy panels is shown in Figure 4.1.

Figure 4.1 : The fabricated carbon-epoxy panel.

The required top and bottom faces of the tapered sandwich plate which are 400 mm x 400 mm are cut from the fabricated carbon-epoxy panels. Two of four panels which are coded as *F1*, *F2*, *F3* and *F4*, will have selected for the faces after the coupon tests. In this study, the configuration of a tapered sandwich plate which has faces with constant thickness and a tapered core is only considered because of the limitation to fabricate a tapered laminated faces.

400 mm x 400 mm sandwich faces and specimens for obtaining material properties of carbon-epoxy are cut from each panel. So, the material properties of the selected faces will be directly obtained, because the specimens for the coupon tests are exactly cut from same panels as faces. A desktop CNC machine that has the capability of 3 dimensional axes is used and the optimum placement for the parts are shown in Figure 4.2. It is confirmed in CAD drawing that each 450 mm x 900 mm panel is bountifully big to have a 400 mm x 400 mm face and lots of specimens.

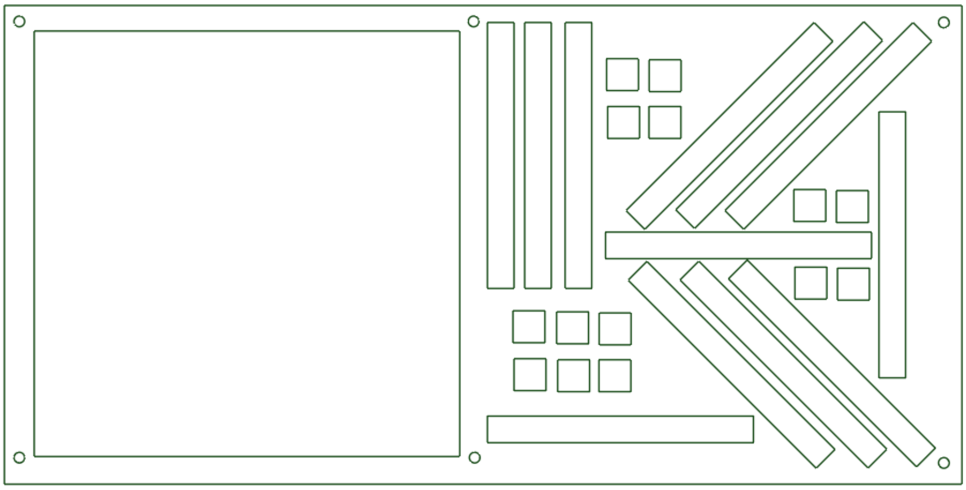

Figure 4.2 : CAD drawing of a carbon-epoxy panel for CNC cutting.

Manufacturing process of the sandwich core starts with cutting a 400 mm x 400 mm polypropylene honeycomb which has an initial thickness, 15 mm. Then, the linear tapering effect for thickness is formed along x-axis by using the desktop CNC machine and the writing G-Code. It will have been planned that minimum thickness is 8 mm at x=0 and maximum thickness is 12 mm at x=a. So, the thickness will be 10 mm at x=a/2 and β will be planned to be 0.5. The exact thickness values can be a bit smaller instead of planned ones. A view from the fabrication of the tapered polypropylene honeycomb is shown in Figure 4.3.

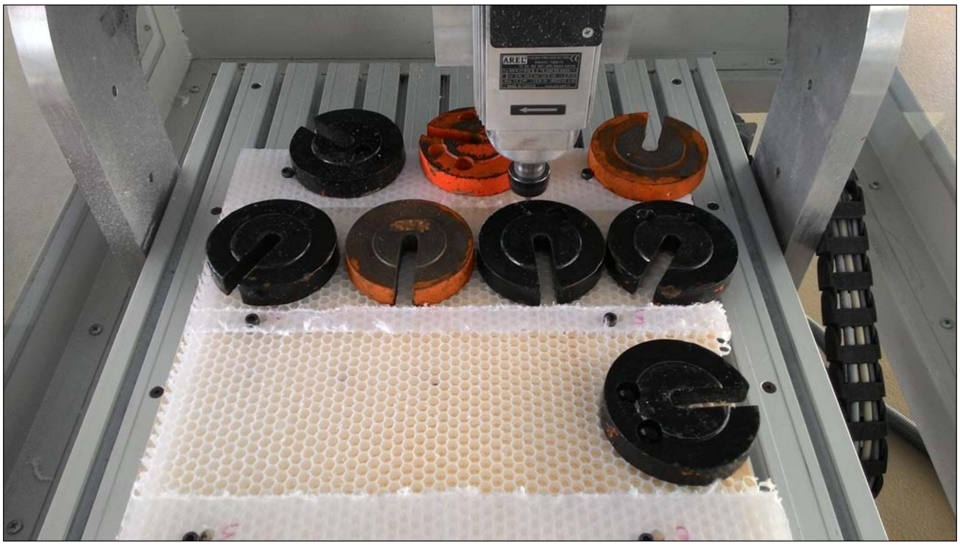

Figure 4.3 : A view from the fabrication of the tapered honeycomb.

After selection of two faces from suitable carbon-epoxy panels and finishing the CNC procedure of the tapered core, the tapered core is stuck to each selected face one by one with a very thin resin layer as an adhesive. Then, the bonded core and face are pressurized by the vacuum effect of the vacuum table at room temperature for 12 hours. Finally, the tapered sandwich plate is ready for the air blast test, after the holes are drilled in the plate for the screws to fasten the plate to the frames.

4.1.2 Coupon tests

Mechanical properties for the constituents of the manufactured tapered sandwich plate are needed to be obtained by the coupon tests. Because, the strain-time data which are recorded during the blast load tests can only be compared with the theoretical data if the mechanical properties are used in theoretical calculations. Therefore, necessary coupon tests are determined as:

- Density testing
- Tensile testing
- Shear testing

These tests have been done by the guidance of ASTM International standards which are Refs. [43,44,45], respectively. The material properties obtained by the tests will have belonged to carbon-epoxy face sheets of the tapered sandwich plate. The laboratory do not have any facilities for the core to determine material properties of a honeycomb material. The brochure of the supplier [46] of polypropylene honeycomb will be used for the properties of the core.

Figure 4.4 shows the cutting process of specimens according to dimensions given in ASTM standards [43,44,45]. The desktop CNC is used and the optimum placement of the face and specimens on the panels is taken in consideration in Figure 4.2.

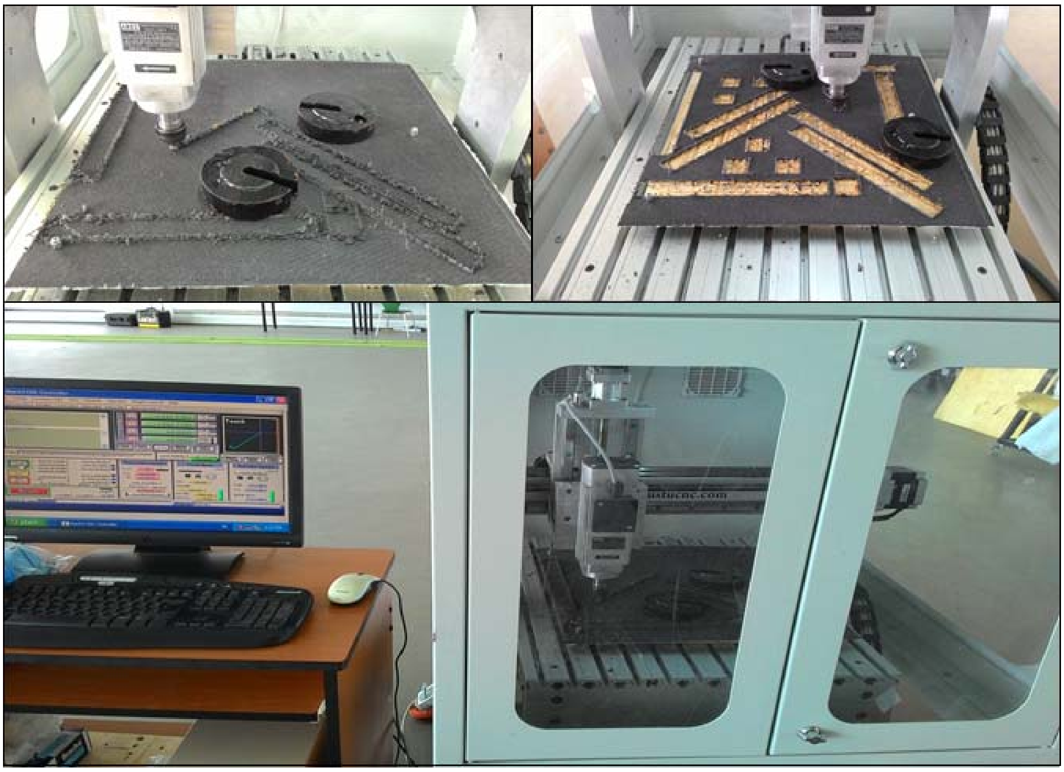

Figure 4.4 : The views from cutting specimens.

The specimens for the tests are entitled code names and the results of the tests are shown with these code names. The first capital describes the type of the coupon test. These are *D* for the density testing, *T* for the tensile testing and *S* for the shear testing. The middle characterization of the specimen name describes the panel number which the specimen is cut in. It can be *F1*, *F2*, *F3* or *F4* as stated in fabricating process. The last number of specimen name describes the specimen number for related panel. For example, the name of the first numbered specimen for tensile testing which is cut from panel *F3* is "*T-F3-1*". Figure 4.5 shows the specimens of tensile, shear and density testing. Tensile and shear specimens are in the shape of rectangle with the dimensions of 250 mm x 25 mm. The difference is that shear specimens are cut with an angle of 45º as seen in Figure 4.2. Density specimens have a square shape and the dimensions are 30 mm x 30 mm.

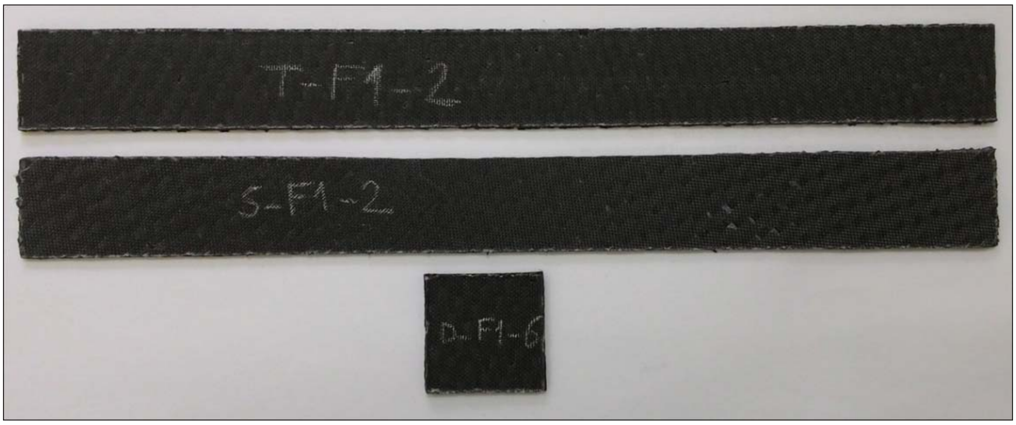

Figure 4.5 : The coupon test specimens.

To find the density of fabricated carbon-epoxy, a method that is based on immersing the specimen with a wire system in liquid and then comparing the mass in the air and in liquid is used according to ASTM D792-13 [43]. The water is preferred for the liquid and the temperature of water in vessel must be known exactly. The schematic overview of experimental set-up is illustrated in Figure 4.6.

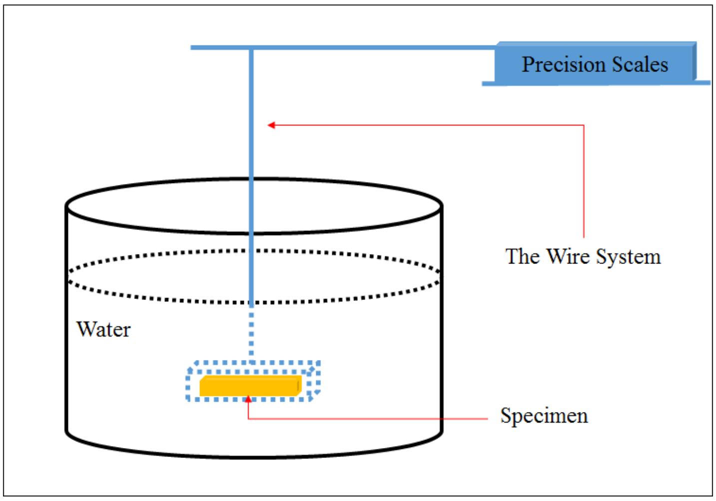

Figure 4.6 : The schematic view of density test set-up.

Eq. (4.1) is used for the calculations after all specimens are measured. ρ_S is the density of specimen. ρ_W is the density of water at the measured temperature. The expression, "*sp gr*" defines specific gravity of the specimen. *M* is apparent mass of specimen in air without wire. *N* is apparent mass of specimen completely immersed in water with the wire partially immersed in water. *P* is apparent mass partially immersed wire without the specimen. During the measurement, the wire system alone and with specimen in the water are not allowed to touch the ground of water filled vessel. They must be hanged in the water like Figure 4.6. Table 4.1 expresses the results of density testing in detail.

$$\rho_S = sp\,gr\,x\,\rho_W \quad ;where \quad sp\,gr = \frac{M}{(\mathrm{M} + P - N)} \tag{4.1}$$

Table 4.1 : The results of density testing.

Water Temp. (ºC)	ρ_W (kg/m^3)	Specimen	sp gr	ρ_S (kg/m^3)
21.5	997.88	D-F1-1	1.3445	1341.7
21.5	997.88	D-F1-2	1.3423	1339.5
21.5	997.88	D-F1-3	1.3305	1327.7
21.5	997.88	D-F1-4	1.3796	1376.7
21.5	997.88	D-F1-5	1.3333	1330.5
21.7	997.84	D-F2-1	1.3415	1338.6
21.7	997.84	D-F2-2	1.3471	1344.2
21.7	997.84	D-F2-3	1.3694	1366.4
21.7	997.84	D-F2-4	1.3670	1364.0
21.7	997.84	D-F2-5	1.3417	1338.8
21	997.99	D-F3-1	1.4022	1399.4
21	997.99	D-F3-2	1.3830	1380.2
21	997.99	D-F3-3	1.3663	1363.6
21	997.99	D-F3-4	1.3608	1358.1
21	997.99	D-F3-5	1.3551	1352.4
21	997.99	D-F4-1	1.3519	1349.1
21	997.99	D-F4-2	1.3482	1345.5
21	997.99	D-F4-3	1.3519	1349.1
21	997.99	D-F4-4	1.3363	1333.6
21	997.99	D-F4-5	1.3393	1336.6

Tensile properties are determined according to ASTM D3039/D3039M-14 [44]. MTS universal test machine is used as the general facility to force the tensile specimens, to measure the tensile load by the load cell and to save the load data. Strain is measured by strain gauges which are coded as Vishay C2A-06-0125LT-350. It is [0º-90º] rosette typed strain gauge and separately oriented to measure normal and transverse strains at the same time. Strain gauges are installed to the centre of each specimen at one side sensitively by the installation procedure given by Vishay. Strain data are collected by a data acquisition (DAQ) device called VTI EX1629 with a sampling rate of 20 Hz. Each coupon is compressed between test machine's grips and emery cloth is used as the interface between the grip and coupon. Test speed is arranged as 2 mm/min. The width and thickness of each specimen at three point in the gage length are measured sensitively and the average values of them are used for obtaining cross-sectional area of each coupon to calculate tensile stress. The views from a tensile test is shown in Figure 4.7.

Figure 4.7 : The views from the tensile test.

Tensile stress (σ_i) is calculated by obtained test load in Eq. (4.2) and then is used with strain data to find Young's modulus. P_i is i^{th} load data and A is the average cross-sectional area. If P_i is the maximum force before failure, σ_i is defined as ultimate tensile strength (σ_T).

$$\sigma_i = \frac{P_i}{A} \tag{4.2}$$

Young's modulus (E) is described as the slope of stress-strain curve in elastic non-damaged stress-strain region as Eq. (4.3). $\Delta\varepsilon_l$ is difference between the two longitudinal strain points. Generally, 1000 με and 3000 με are approximately used as start and end point, respectively. So, $\Delta\varepsilon_l$ becomes nearly 2000 με according to strain data. $\Delta\sigma$ is difference in applied tensile stress between the two strain points. In this study, longitudinal (E_1) and lateral modulus (E_2) are accepted as having the same value because of using (0º/90º) bidirectional carbon fabric cloth. Poisson's ratio (v) is calculated by Eq. (4.4). Two longitudinal strain points are selected like about 1000 με and 3000 με. The transverse strain values are also used for this points to find difference between these strain points.

$$E = \frac{\Delta \sigma}{\Delta \varepsilon_l} \tag{4.3}$$

$$\nu = -\frac{\Delta \varepsilon_t}{\Delta \varepsilon_l} \tag{4.4}$$

Table 4.2 : The results of tensile test.

Specimen	Ultimate Tensile Strength (MPa)	Young's Modulus (GPa)	Poisson's Ratio
T-F1-1	504.7	38.12	0.02
T-F1-3	509.0	37.70	0.15
T-F2-1	461.1	36.95	0.12
T-F2-3	536.4	37.46	0.04
T-F3-1	536.3	51.11	0.09
T-F3-4	511.0	49.84	0.15
T-F4-2	533.2	53.20	0.08
T-F4-4	558.0	52.36	0.07

Tensile properties of randomly selected coupons from four carbon-epoxy panels are given in Table 4.2. Failure modes in gage length for tensile coupons are shown in Figure 4.8.

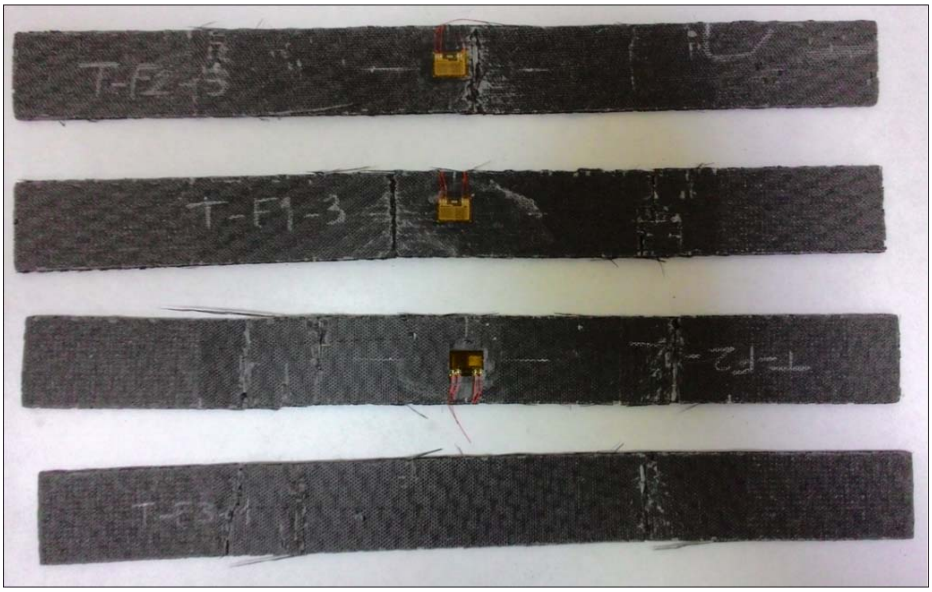

Figure 4.8 : Examples of failure for tensile coupons.

Shear properties are obtained by using ASTM D3518/D3518M-13 [45]. This test method is a special standard for determining in-plane shear response of polymer matrix composite materials which is limited to a continuous fiber reinforced composite ±45 laminate. This standard is exactly right one for the coupons which are cut from (0º/90º) fiber orientated carbon-epoxy panels with an angle of 45º. The procedure of the shear testing is the same as tensile test above and is performed like a ±45 laminate coupon in accordance with ASTM D3039/D3039M-14 [44]. The difference is about the calculations to find shear properties.

Shear stress (τ_{12i}) is calculated by obtained test load in Eq. (4.5) and then is used with longitudinal and lateral strain data to find the shear modulus. P_i is i^{th} load data and A is the average cross-sectional area. If P_i is the maximum force at or below 5% shear strain, τ_{12i} is defined as maximum shear stress or shear strength. Generally, a ±45 laminate coupon has the capability of high elongation without failure, so the maximum force is determined as the one at 5% shear strain.

$$\tau_{12i} = \frac{P_i}{2A} \tag{4.5}$$

Shear strain at i^{th} data point is obtained with Eq. (4.6) by using longitudinal (ε_l) and lateral strain (ε_t) which are collected by a [0º-90º] rosette typed strain gauge.

$$\gamma_{12i} = \varepsilon_{li} - \varepsilon_{ti} \tag{4.6}$$

Shear modulus (G_{12}) is described as the slope of shear stress- shear strain curve in the linear region as Eq. (4.7). $\Delta\gamma_{12}$ is difference between the two shear strain points. Generally, 2000 µε and 6000 µε are approximately used as start and end point, respectively. So, $\Delta\gamma_{12}$ becomes nearly 4000 µε according to shear strain data. $\Delta\tau_{12}$ is difference in applied shear stress between the two shear strain points.

$$G_{12} = \frac{\Delta\tau_{12}}{\Delta\gamma_{12}} \tag{4.7}$$

Shear properties of randomly selected coupons from four carbon-epoxy panels are given in Table 4.3.

Table 4.3 : The results of shear test.

Specimen	Shear Strength (MPa)	Shear Modulus (GPa)
S-F1-2	36.9	2.76
S-F1-3	26.3	1.61
S-F2-1	44.2	3.14
S-F2-4	37.5	2.48
S-F3-1	25.8	1.79
S-F3-4	27.8	2.05
S-F4-2	27.2	1.98
S-F4-4	27.6	1.97

4.1.3 A conclusion for the fabrication and material properties

The tapered sandwich plate is decided to fabricate from cut faces which are belongs to *F3* and *F4* carbon-epoxy panels as a result of coupon tests,. Because, material properties of *F3* and *F4* show consistency between each other to fabricate a symmetrically laminated tapered sandwich plate. Moreover, Young's modulus of *F1* and *F2* panels are approximately smaller 25% than *F3* and *F4* and there is a dispersion between results of *F1* and *F2* which can be effects of problems in hand lay-up manufacturing or curing process. The conclusive material and dimensional properties for the faces of the fabricated sandwich plate are resulted in Table 4.4 by averaging results of *F3* and *F4*.

Table 4.4 : The neccessary properties of the tapered sandwich plate.

Sandwich Face of 2 Layer Carbon-Epoxy with (0/90º) Fiber Orientation Angle					
E_1 ; E_2 (GPa)	ν_{12}	G_{12} (GPa)	ρ (kg/m^3)	h (mm)	
51.63	0.098	1.95	1356.8	1.06	
PP 8-80 Type Tapered Sandwich Core of Polypropylene Honeycomb with 8 mm Cell Size					
G_{12} (MPa)	G_{23} (MPa)	G_{13} (MPa)	ρ (kg/m^3)	h_0 (mm)	β
12.8	17.3	17.3	80	7.53	0.495

Properties of polypropylene honeycomb from the brochure of the supplier [46] and dimensional properties as a result of given tapered effect are also shown in Table 4.4. The compressive modulus of the honeycomb is also given in [46] as 97 MPa. In-plane shear modulus of polypropylene honeycomb had been obtained experimentally by the guidance of DIN 53294 standard [47] according to Ref. [46]. Out-of-plane shear modulus are calculated according to an analytical method adapted for core materials which have tubular or honeycomb cells [48]. G_{13} and G_{23} equal to each other and are expressed theoretically as Eq. (4.8) if the core is made of tubular core materials [48]. Out-of-plane shear modulus are also shown in Table 4.4.

$( )_*$ in Eq. (4.8) denotes the property for the basic material which is polypropylene in this study. Young's modulus for polypropylene is taken as 600 MPa. Poisson's ratio is taken as 0.4 which is also used for polypropylene honeycomb. e is the wall's thickness of tubes and is taken as 0.3 mm. R is the radius of tubes which is 4 mm.

$$G_{23} = G_{13} = \frac{2eG_*}{\sqrt{3}\left(R+e\right)} \; ; where \quad G_* = \frac{E_*}{2\left(1+\nu_*\right)} \tag{4.8}$$

The tapered sandwich plate is fabricated with the dimensions of 400 mm x 400 mm, but the actual effected size subjected to air blast is 300 mm x 300 mm to clamp the plate with a frame of 50 mm width at each edge. So, in Table 4.4, h_0 and β are represented as the expressions for the actual plate of 300 mm x 300 mm.

4.2 Introduction to Air Blast Load Test

The air blast load test can be carried out on a tapered composite sandwich plate as a two stage procedure. First, transient pressure measurement on a plexiglass model plate and defining the distribution of pressure on the plate have been done. Then, strain measurement has been performed for the actual tapered plate. Measurement of acceleration on the plate are additionally included for obtaining displacement. The overview of experimental set-up is shown in Figure 4.9. After the pressure is measured with plexiglass model plate, the fabricated tapered sandwich plate is replaced between the special metallic frames instead of plexiglass model for the measurement of strain and acceleration values.

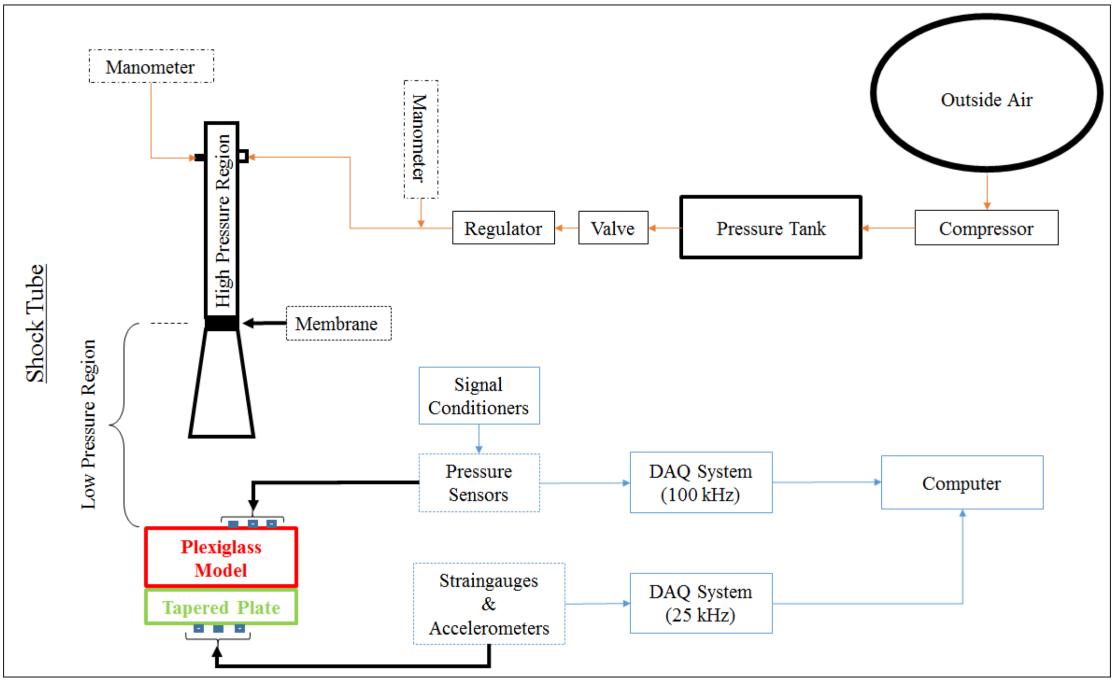

Figure 4.9 : The overview of air blast test method.

This procedure is preferred because of the type of pressure sensors that were used. PCB 111A26 ICP quartz miniature pressure sensors (Figure 4.10) are used to collect pressure data. Signal conditioner (PCB 480C02) for each sensor is also needed for the voltage supply. Three pressure sensors and three signal conditioners are used in the tests. Each pressure sensor is connected to its signal conditioner with a low noise 10 ft long 10-32 to BNC coaxial cable. On the other hand, each signal conditioner is connected to DAQ device with a low noise 10 ft long BNC to BNC coaxial cable. ICP sensors are very preferable for low budget and durability under the effect of burst overpressure. Installation of this sensor on a plate is needed a special mounting hole that must be drilled by the guidance of sensor's operation manual. The installation surface should be also flat not tapered. To avoid the stress concentrations around these holes on the fabricated plate, the conducted testing procedure is more feasible if the burst pressure is approximately the same value at each air blast test.

Figure 4.10 : The pressure sensor with signal conditioner and cables.

Membranes are thin structures and are used in shock tube tests. Its function is to separate the shock tube into two parts: the high pressure part and low pressure part as it is seen in Figure 4.9. The membrane keeps the air in the high pressure part until it is ruptured. When the membrane is ruptured, the pressurized air passes through the low pressure part with a very high speed. After that, the air hits the plate, because the plate acts like a barrier for the high speed air.

In this study, selection of the membrane material is very important. The burst pressure that is obtained by the rupture of membrane, must be nearly the same at each burst test. Because, the measurement of pressure values and the measurement of strain values are seperated from each other and they are not measured at the same time.

Membranes made of brass, rubber, polycarbonate and glass-epoxy can be used. The problem is that these materials have high strength. So, these kind of membranes everytime need a controlled damage in the middle of the membrane for rupturing. The burst pressure value is changed according the rate of controlled damage and it is not predictable. In this study, the membrane made of Mylar® polyester film is preferred (Figure 4.11).

Figure 4.11 : Mylar® polyester film and the shape of membrane.

After doing a number of burst tests by using the polyester film membrane with a thickness of 0.125 mm, the burst pressure is approximately same consistently when it is measured by the manometer. Moreover, when the number of 0.125 mm polyester film membranes is increased, it is achieved that approximate burst pressure is increased linearly in Figure 4.12. Because, the thickness for the membrane is increased. The significant point is that Mylar® polyester membrane does not need to a controlled damage for burst. Figure 4.13 shows the rupture for different number of polyester membranes. One Mylar® polyester film membrane with a thickness of 0.19 mm is used for all air blast tests in this study. This membrane provides approximately 600 kPa (6 bar) burst pressure for each test.

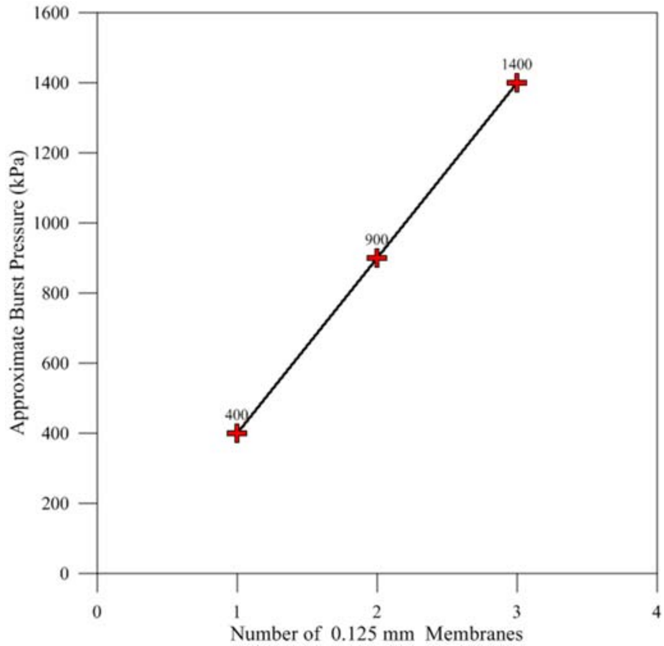

Figure 4.12 : Number of membranes versus burst pressure.

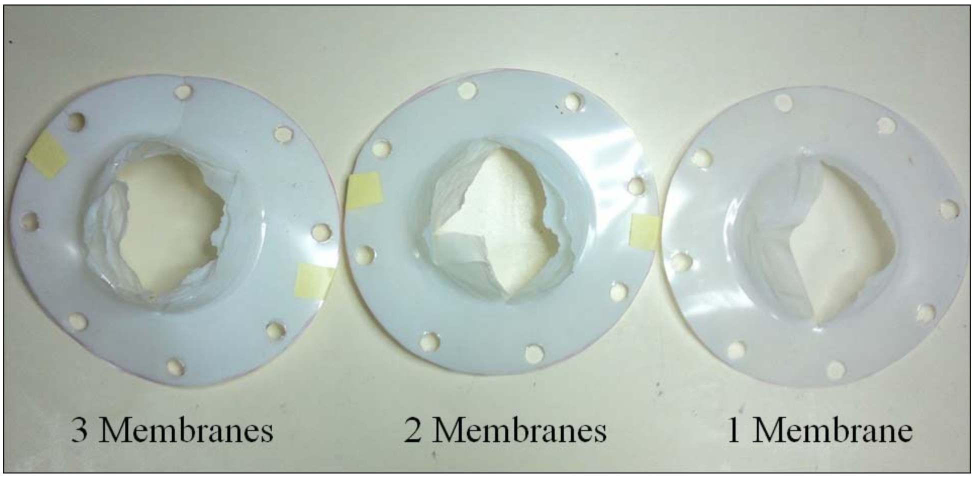

Figure 4.13 : The rupture of polyester film membranes.

The air compressor is used for storing the pressurized air from outside air into pressure tank. The compressor can pump the air up to 40 bar into pressure tank. The pressure tank has the capacity about 500 litres of pressurized air. The air compressor and the pressure tank are shown in Figure 4.14. The valve, the regulator and the manometer before the shock tube which have been schematically shown in Figure 4.9 are also shown in the right figure after the exit of pressure tank in Figure 4.14. The connection between the regulator and the shock tube is provided by a pressure resistant hose. The hose is about 10 meter long and resistant up to 256 bar.

Figure 4.14 : The air compressor and the pressure tank.

Strain is measured by strain gauges which are coded as Vishay C2A-06-062LT-350. It is [0º-90º] rosette typed strain gauge too like the ones used in the coupon tests, but these are smaller to increase the point measurement for certain points of the tapered sandwich plate. Brüel&Kjaer 4516-001 piezoelectric accelerometers are used for measuring acceleration. They have the capability of having a measuring range of ±1000 g and the installation is very easy by just mounting with adhesive. Signal conditioners for the pressure sensors are used for the voltage supply of accelerometers too.

IMC C-Series CS-7008-N DAQ device is used for the pressure measurement. It has 8 channels and it's 100 kHz maximum sampling rate is used for obtaining data. So, 100 number of pressure samples can be obtained in one millisecond. DAQ device for the strain measurement is the model EX1629 of VTI Instruments. It has been used for the coupon tests before. There are 48 channels on the board of this high performance strain gauge instrument, but it can be also used as a universal DAQ device. The sampling rate of 25 kHz are obtained by using up to 16 channels on the same analog board and without noise filter. If the channels are not limited to 16 maximum, the DAQ system is capable of supporting a sampling rate of 10 kHz maximum. The number of channels used for this study is suitable for obtaining 25 kHz sampling rate. Both DAQ devices need a laptop to control the device and to set up tests with their drivers and graphical user interfaces inside the laptop. Figure 4.15 shows CS-7008-N in the above figure and EX1629 below.

Figure 4.15 : DAQ devices.

Before measuring pressure distribution and obtaining strain and displacement values subjected to air blast load, the shock tube configuration is decided by comparing four types of low pressure part. The distance is fixed a length of nearly 1 m. from the membrane to model plate or tapered sandwich plate. This distance is actually low pressure region and can be configured as Figure 4.16 by using nothing or using additional parts. All four configuration are examined and the configuration of number 2 is decided. Because, it has the best performance to have the uniform distibution on the model plate while having a significant peak pressure at the same time for the length of 1 m. of low pressure region.

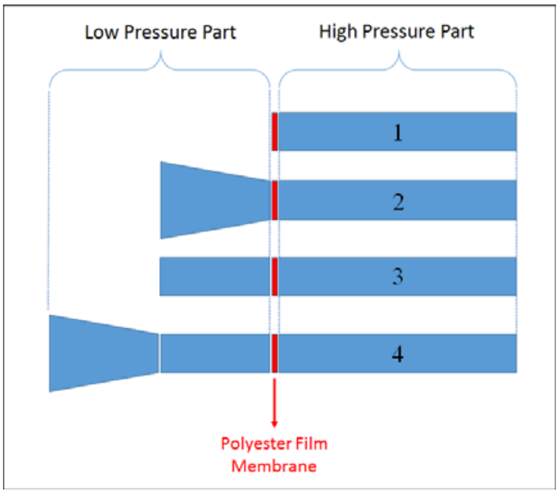

Figure 4.16 : Considered configurations for the shock tube.

4.3 Measurement of Pressure Distribution

A practical method is used to obtain the pressure data on different locations of the model plate as shown in Figure 4.17. After the pressure data is obtained on the quarter of the model for point 1 (P1), point 2 (P2) and point 3 (P3) and afterwards for P1, point 4 (P4) and point 5 (P5), the plexiglass plate is rotated three times for 90º and is fixed again. So, the pressure values at 17 locations on the plexiglass plate can be obtained by drilling 5 holes and using only 3 pressure sensors.

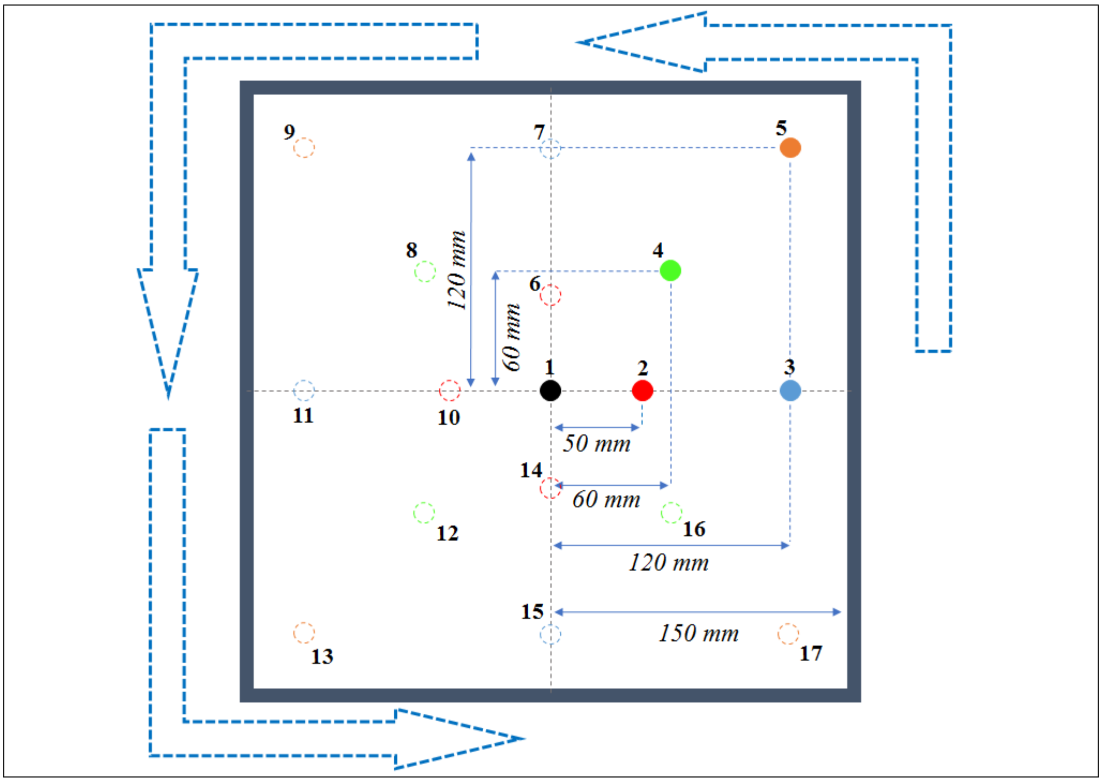

Figure 4.17 : Certain points for the pressure sensors.

General views of test set-up for pressure measurement are shown in Figure 4.18. Specially drilled locations for the pressure sensors and steel top/bottom frames are shown in Figure 4.19. The flat plexiglass plate is thick enough to install the sensors and has a 19 mm thickness.

Figure 4.18 : General views of the air blast test for the pressure distrubiton.

The model plate is attached to two steel frames with 12 bolts and nuts. 6 of them are also attached to mounting steel beams of shock tube system. Two steel frames and plexiglass model are also attached to each other with 24 smaller bolts and nuts to increase the clamped effect for all edges. Each steel frame is two of a kind and has about 7 mm thickness and 50 mm width along each edge.

Pressure data during the tests are collected by IMC C-Series CS-7008-N DAQ device with a sampling rate of 100 kHz and recommended device filter type called AAF.

Figure 4.19 : Pressure sensors and steel frames for fixing the model.

Figure 4.20 and Figure 4.21 show the results of eight tests to obtain the pressure distribution on a 300 mm x 300 mm plate. Pressure-time history at P1 is compared with the values obtained by the other two pressure sensors at the other two locations. These certain locations are also shown in Figure 4.17.

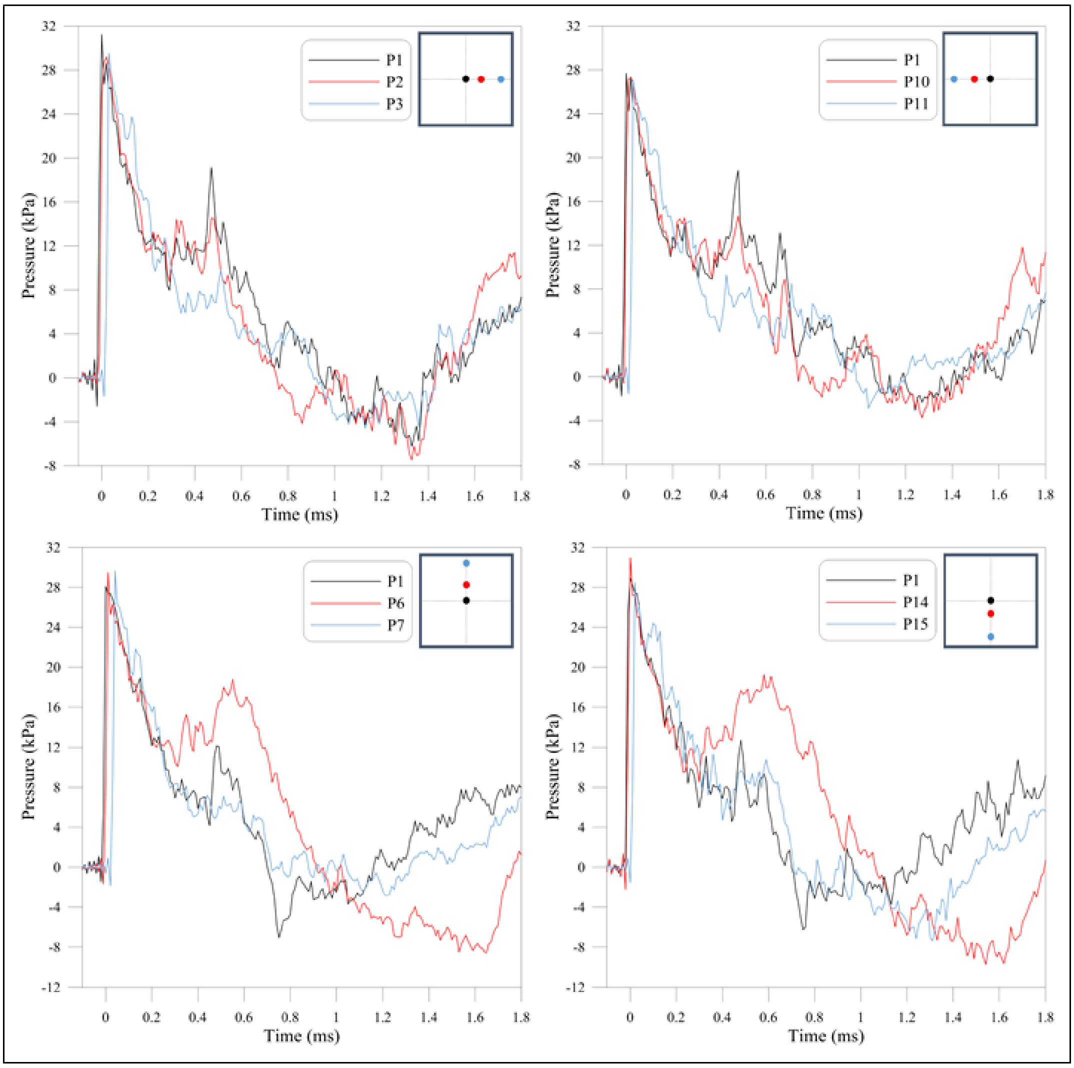

Figure 4.20 : Pressure-time histories at certain locations: part 1.

Peak pressure values at all certain locations are very close to the pressure value at P1 (a/2; b/2) when Figure 4.20 and Figure 4.21 are analysed. Each pressure-time history also has approximate value for positive phase duration described in Figure 1.3. This can lead to an assumption for the uniform pressure distribution.

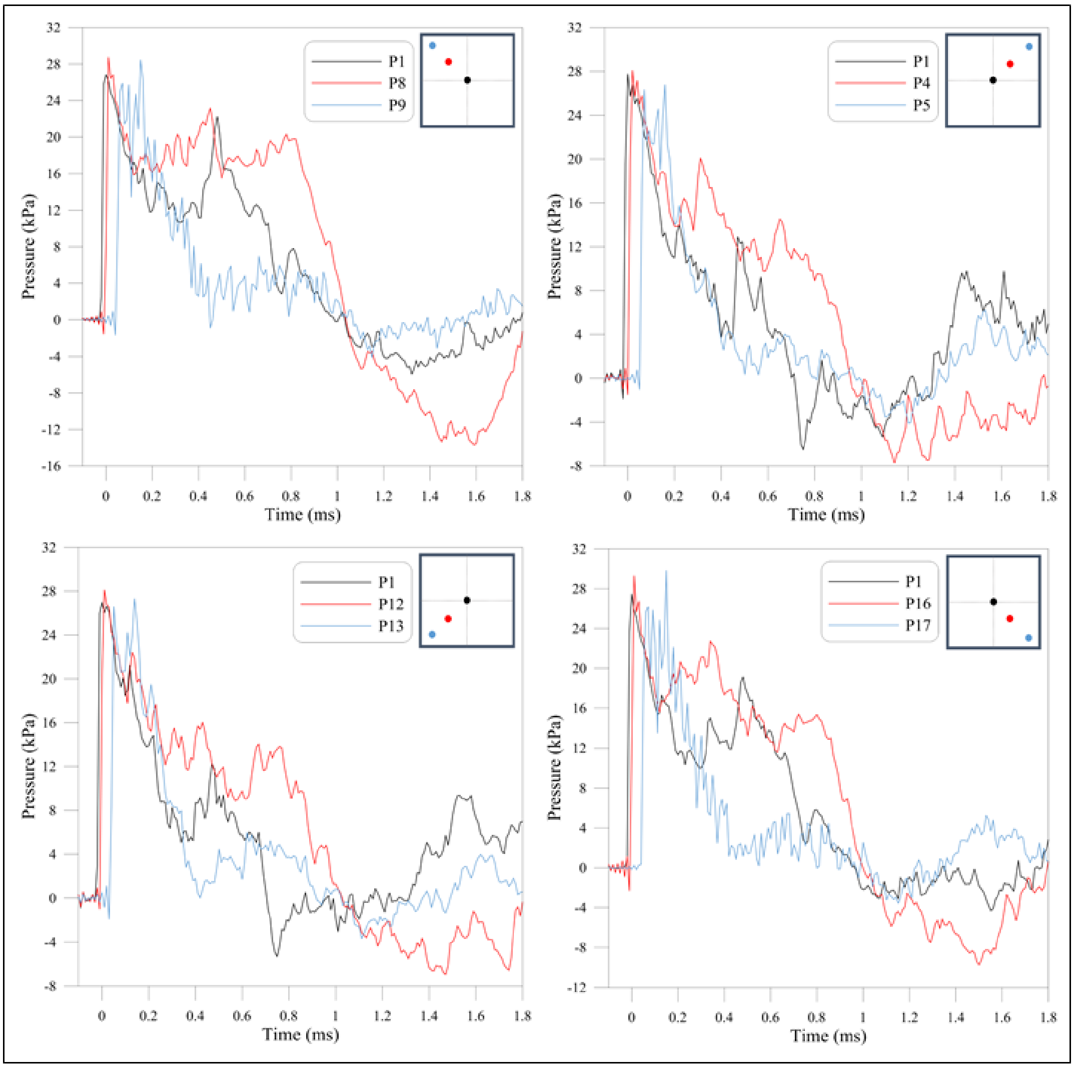

Figure 4.21 : Pressure-time histories at certain locations: part 2.

When the polyester film membrane is burst for each test, the pressure sensor at P1 measures peak pressure values close to each other as shown in Figure 4.22. Except for the value of first test that has a measured magnitude of 31.19 kPa, all peak pressure values range in an interval between 26.9 kPa and 28.9 kPa.

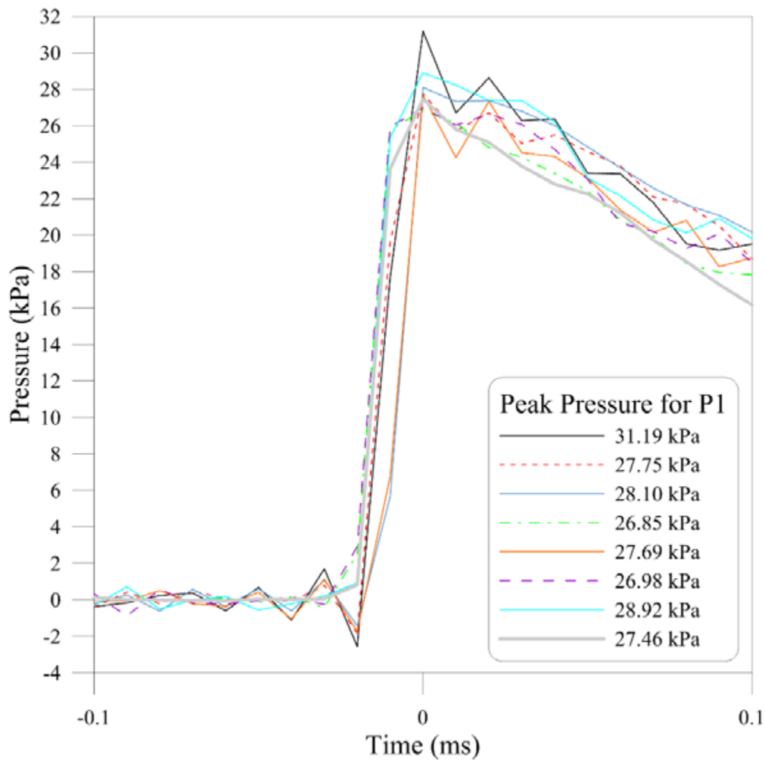

Figure 4.22 : The magnitudes for peak pressure at P1.

To formularize the pressure distribution on the plate surface according to pressure measurement results above and the definition of typical blast wave curve in Figure 1.3, Friedlander's waveform can be defined with a function of time. It is assumed that the plate is placed enough away from the source of the blast. So, the pressure distribution because of the blast loading is assumed to be uniform on the plate and subjects in the z direction only. This leads to $q_z \neq 0$ and $q_x = q_y = 0$ in Eq. (2.19). On the other hand, the consideration of only linear elastic material behaviour is a significant point for the distance and intensity of the blast load source.

Friedlander's equation can express the typical air blast load as shown in Eq. (4.9) and the load can vary exponentially only in time. The blast load is expanded in Fourier series and only the first term is chosen. p_m is the peak pressure, t_p is positive phase duration, and φ is a waveform parameter.

$$p(x,y,t) = p_m \left(1 - \frac{t}{t_p}\right) e^{-\frac{\varphi t}{t_p}} \tag{4.9}$$

The peak pressure and positive phase duration of the pressure curves can be easily obtained by using data of Figure 4.21 and Figure 4.22. The waveform parameter of each curve must be calculated by replacing p_m and t_p in Eq. (4.9). Then, the data point for negative peak pressure is selected in negative phase duration of each curve and is replaced in Eq. (4.9) too. Finally, the only unknown, φ is calculated for each curve. Table 4.5 shows the unknowns of Friedlander's function for each curve and the average of each parameter.

Table 4.5 : Detailed results of pressure measurement.

Test ID	Point ID	P_m (kPa)	t_p (ms)	φ
1	P1	31.19	0.93	0.54
	P2	29.18	0.73	0.64
	P3	29.51	0.87	0.50
2	P1	27.75	0.71	0.66
	P4	28.08	0.93	0.28
	P5	26.75	0.90	0.42
3	P1	28.10	0.70	0.89
	P6	29.46	0.90	0.57
	P7	29.63	0.68	1.27
4	P1	26.85	0.98	0.33
	P8	28.72	1.02	0.10
	P9	28.44	0.99	0.10
5	P1	27.69	1.06	0.38
	P10	27.18	1.06	0.30
	P11	26.96	0.95	1.02
6	P1	26.98	0.70	0.95
	P12	28.12	1.01	0.42
	P13	27.31	0.97	0.10
7	P1	28.92	0.70	0.97
	P14	30.95	1.06	0.25
	P15	28.46	0.69	0.66
8	P1	27.46	0.96	0.84
	P16	29.27	0.98	0.30
	P17	29.80	0.95	0.32
Average		*28.45*	*0.89*	*0.53*

The pressure-time history is obtained in Figure 4.23 by using Friedlander's function and the mean value of magnitudes in Table 4.5 as a result of experimental studies about pressure distribution.

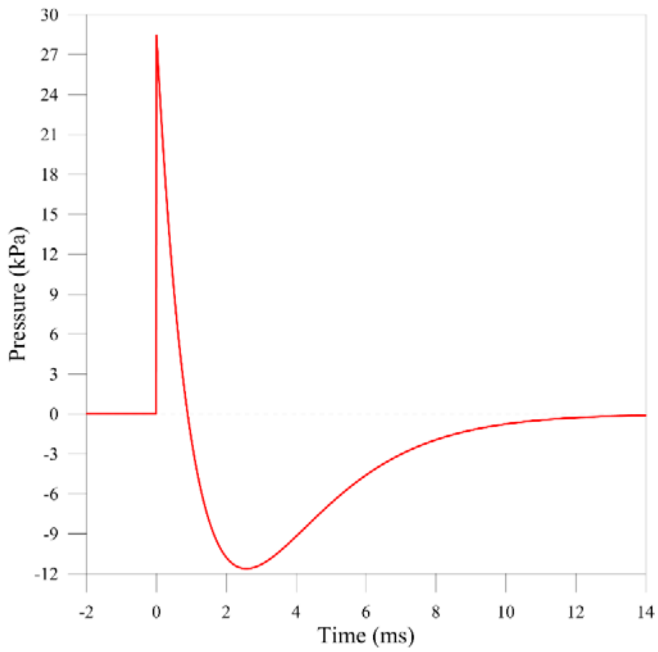

Figure 4.23 : The conclusive blast wave curve.

4.4 Measurement of Strain and Acceleration

After the tests about pressure distribution are finished, the real tapered sandwich plate is mounted instead of plexiglass model. A pair of different frames is used to clamp the tapered plate. Because, using a pair of frames with constant thickness like for plexiglass model is not suitable for fixing a tapered plate. Tapered sandwich plate can be forced with initial local loads. This can lead to wrong strain values. The easy solution is to design one sided tapered frames which have a consistent tapering ratio with the taper ratio of sandwich plate. The pair of one sided tapered frames are manufactured by an advanced CNC machine by using a service procurement. The pair of frames for the tapered plate is made of aluminium, because it is softer than steel for a milling process. The schematic side view of aluminium frames with the tapered sandwich plate is illustrated in Figure 4.24.

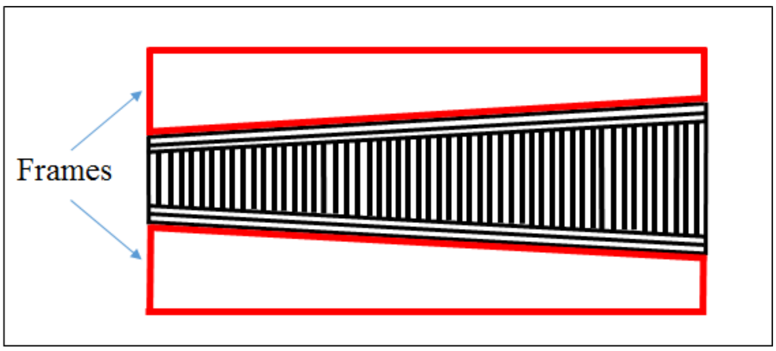

Figure 4.24 : The schematic side view of frames for the tapered sandwich plate.

The general views of test set-up for strain and acceleration measurement are shown in Figure 4.25. The fabricated clamped tapered sandwich plate is attached to shock tube system with aluminium tapered frames which is mentioned above. The measurement data during the tests are collected by the DAQ model EX1629 of VTI Instruments with a sampling rate of 25 kHz.

Figure 4.25 : General views of the tapered sandwich plate just before subjecting to air blast load.

The tapered sandwich plate which is clamped with the pair of special frames is shown with a close view in Figure 4.26. The figure is also focused on the [0º-90º] rosette typed strain gauges called Vishay C2A-06-062LT-350 which are installed at certain points on the top surface of the tapered sandwich plate. Three of these certain locations are point A (3a/14, b/2), point C (a/2, b/2) and point B (11a/14, b/2) through the tapered *x* direction. The fourth strain gauge is installed at point D (a/4, b/4). The strain gauges are installed with suitable orientations, so that the strains, ε_x and ε_y at certain locations are collected by 8 channels of DAQ device which has 32 channels. Two Brüel&Kjaer accelerometers are mounted on point C and point D next to strain gauges of these points as seen in Figure 4.26. They are connected to signal conditioners for power supply and to DAQ device.

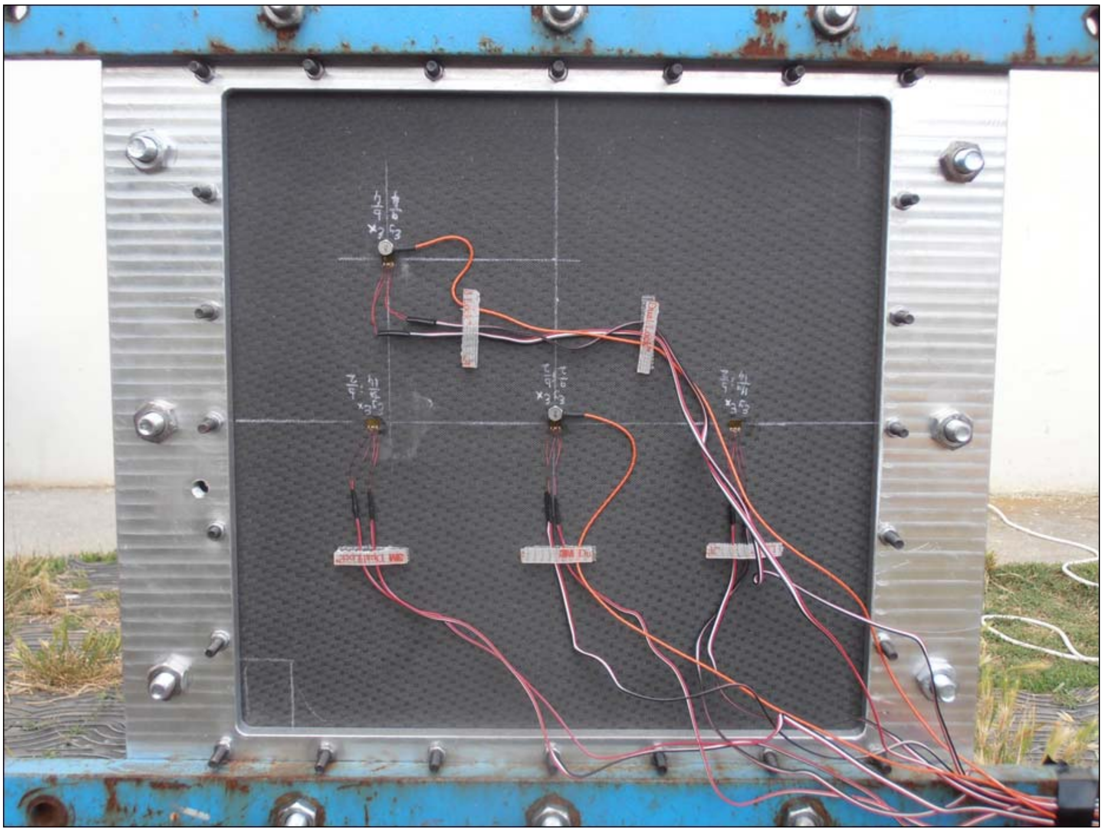

Figure 4.26 : Strain gauges and accelerometers on the top surface of tapered sandwich plate.

Figure 4.27 shows the strain values of four repeated tests at x direction and compares the strain-time histories of point A, point C and point B. The peak values of strain-time histories for certain points at each repeated test are very close to each other, so that it verifies the consistency of two stage procedure of air blast test and the pressure measurement with the plexi glass model. As another significant point, these measured strain values must be considered as top strain of the plate at certain points while comparing with theoretical and FEM results. Strain at point C has higher peak values than the ones at point A and point B. Moreover, strain gauge installed on thinner part of the tapered plate (point A) measured higher strain peak values than that of on the thicker part (point B).

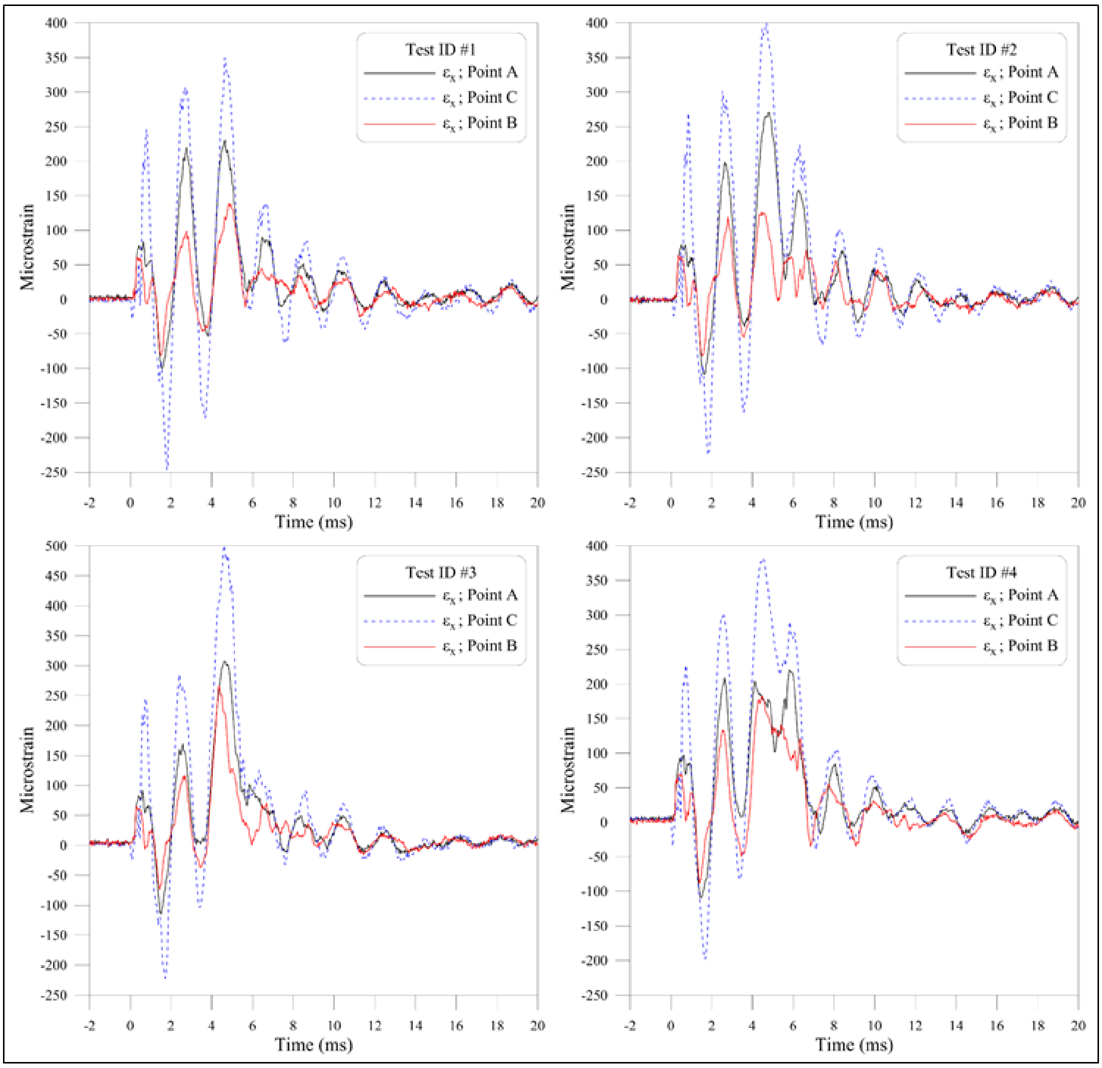

Figure 4.27 : The experimental strain-time histories along the tapered direction.

Strains at x and y directions at point D are compared with the ones at point C in consideration of the data belong to one of four tests in Figure 4.28. The values at point C are much higher than those of at point D as expected. The peak values for ε_x and ε_y are very close to each other at point D in comparison to those at point C.

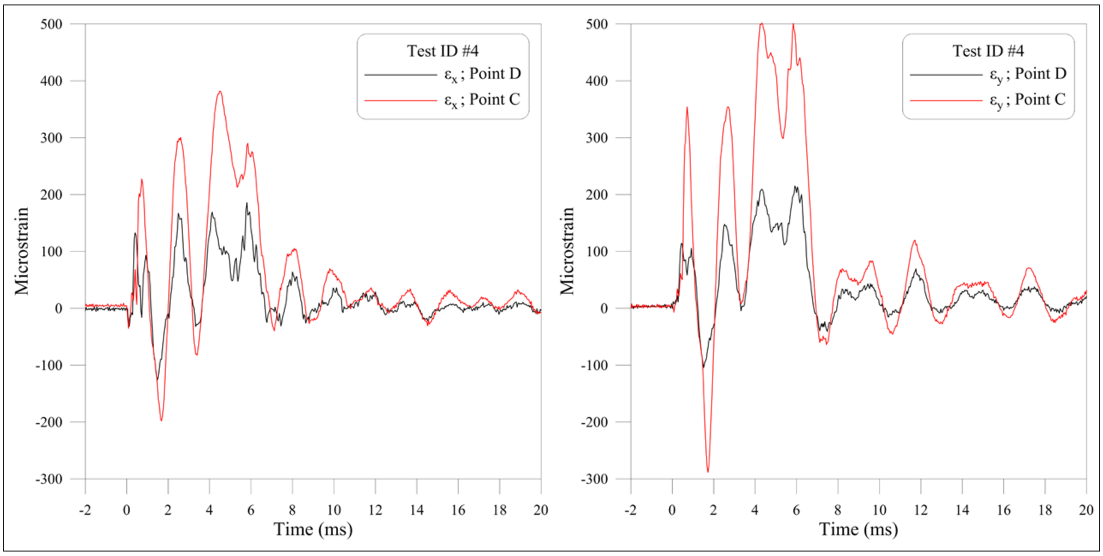

Figure 4.28 : The comprasion of strain values at point D and point C.

5. NUMERICAL RESULTS

The nonlinear dynamic behaviour of simply supported and clamped tapered sandwich composite plates are investigated respectively using the closed form solution by writing a numerical parametric computer program. Theoretical results for an imaginary design of a simply supported tapered sandwich plate are compared with only FEM results. On the other hand, experiments for a fabricated clamped tapered sandwich plate subjected to created and measured air blast load had been expressed in previous chapter. Those experimental results are compared with theoretical results for the fabricated plate and with FEM results for the quasi form of the fabricated plate.

5.1 Simply Supported Tapered Sandwich Plate with Multi-Layered Faces

The pressure distribution because of the blast loading, $p(x,y,t)$ is assumed to be uniform on the simply supported plate. The measured parameters shown in Eq. (4.9) are obtained as p_m=28.45 kPa, t_p=0.00089 s and φ=0.53 according to Table 4.5. Only square shaped plates are considered and the dimensions are taken as a=b=300 mm which are compatible with the model plate for the pressure distribution. Both shear correction factors are taken as 5/6 that is proposed by Goens [49].

Experimental results for a simply supported tapered plate are not available, because it is not possible to fix the fabricated plate under simply supported boundary conditions. So, theoretical results are compared with only FEM results.

A more complex fully tapered design than the fabricated one is considered to show the feasibility of the theoretical method. A composite sandwich plate, that has a tapered honeycomb core and symmetrically placed tapered hybrid face sheets which are made of three symmetrical layers, is designed (Figure 2.1). So, n equals 3 in the stiffness matrices of tapered sandwich plate given in Eq. (2.15).

The design configuration is set up by using mechanical properties of the constituents given in Table 5.1 [50,51]. E_1 and E_2 are Young's modulus, G_{12} is shear modulus, ν_{12} is Poisson's ratio and ρ is defined as the density of the material in the table. Out-of-plane shear modulus (G_{23}, G_{13}) for the honeycomb core are taken as 0.04 GPa. The acronyms in Table 5.1 – BG, UC and BB – are called bidirectional 0°-90° glass/epoxy, unidirectional 0° carbon/epoxy and bidirectional 0°-90° basalt/epoxy layers, respectively. The stacking sequence of face sheets is configured as $[UCBGBB]_S$. The fiber orientations of layers are remained as they are.

Table 5.1 : Material properties of the constituents.

	Bidirectional Glass/Epoxy (BG)	Unidirectional Carbon/Epoxy (UC)	Bidirectional Basalt/Epoxy (BB)	Honeycomb Core
E_1 (GPa)	23.37	135.14	23.5	0.0296
E_2 (GPa)	23.37	9.24	23.5	0.0145
ν_{12}	0.115	0.318	0.11	0.3
G_{12} (GPa)	5.23	6.27	9.04	0.014
ρ (kg/m^3)	1910	1620	2320	32
h (mm)	0.22	0.13	0.16	5.0

The taper ratios for the plate are chosen as β=0.2 and β=1.2 to understand the effect of taper ratio on the dynamic response. The thicknesses for the core and layers in Table 5.1 describe the values at the center of the plate so that the weight of the plate is kept constant according to taper ratios for all tapered configurations. The displacement-time histories at the mid-plane and strain-time histories at the mid-plane, top and bottom surfaces are obtained for certain locations that are point A (3a/14, b/2), point C (a/2, b/2) and point B (11a/14, b/2) through the tapered direction as seen in Figure 2.1.

Figure 5.1 and Figure 5.2 show the displacement-time histories of the $[UCBGBB]_S$ tapered laminated sandwich plate for β=0.2 and β=1.2, respectively. There is a good agreement between displacement-time histories obtained by closed form solution and FEM for both taper ratios. It is also noticed that increasing taper ratio do not change the rate of agreement, but the fact remains that the first positive peak for ANSYS result at point B has an higher value than theoretical result when increasing the taper ratio for six times. Apart from that, theoretical positive and negative peak results are higher than FEM results. The maximum deflection occurs at point C for both taper ratios as expected. Deflections at the point A and the point B obtained by using closed form solution and FEM do not have the same displacement-time histories and peak values. It is because of the effect of tapering.

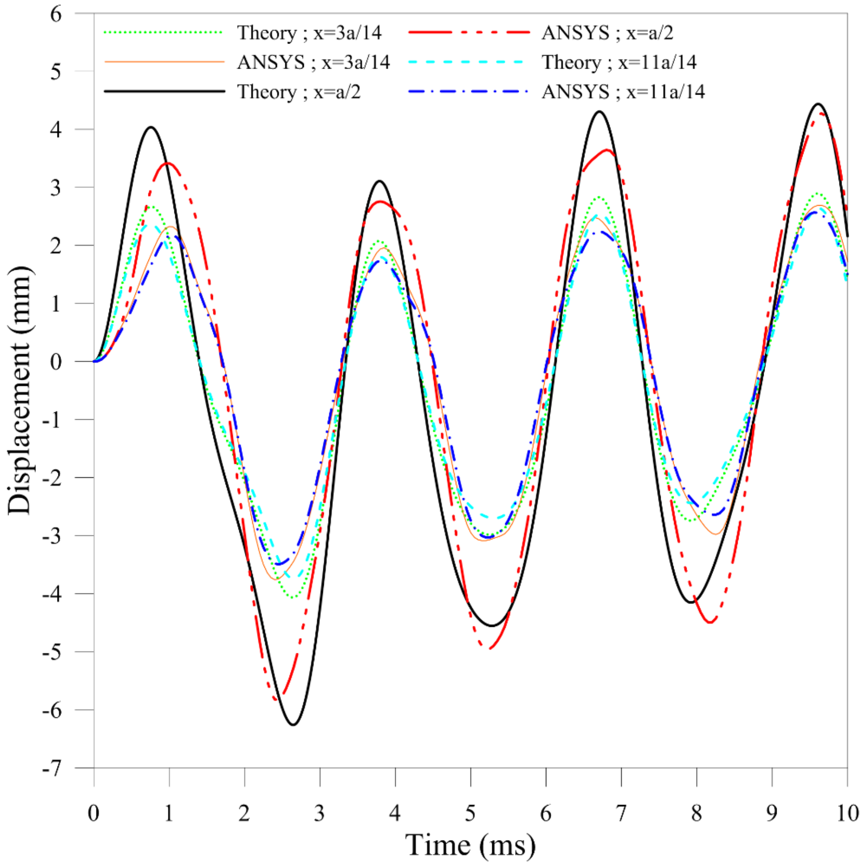

Figure 5.1 : The displacement-time histories for [UCBGBB]s and β=0.2.

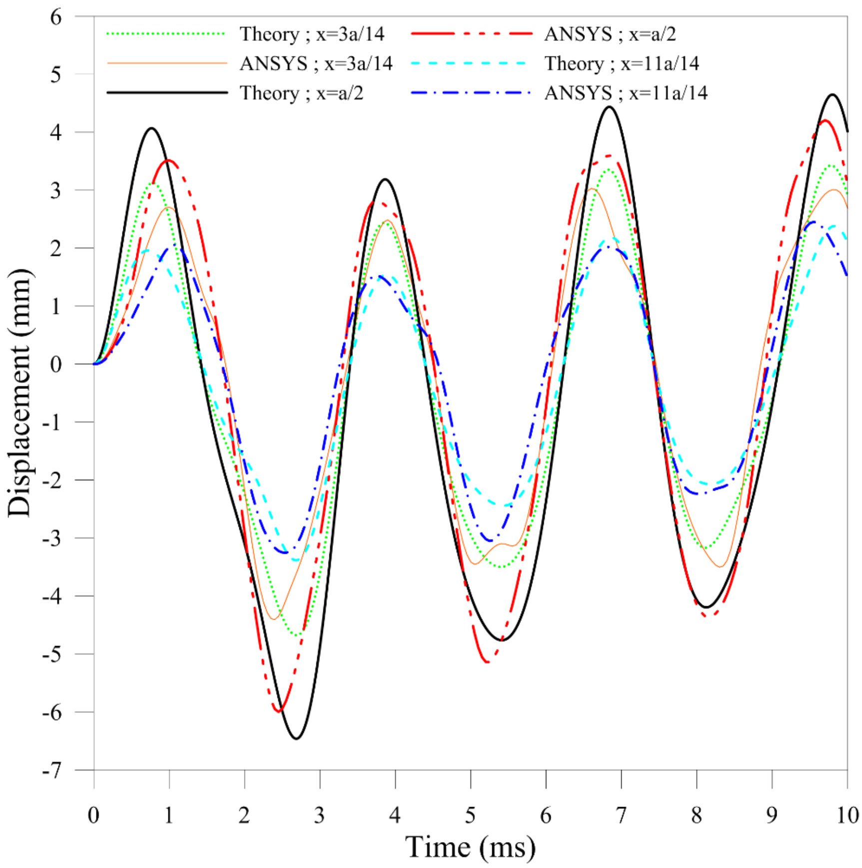

Figure 5.2 : The displacement-time histories for [UCBGBB]s and β=1.2.

The strain-time (ε_x) histories of the [UCBGBB]s plate at the middle plane of certain points mentioned above are obtained and shown in Figures 5.3-5.5 for both β=0.2 and β=1.2. These membrane strains are always positive and histories have good agreement. Likewise, strain-time histories at the top surface of these points are shown in Figures 5.6-5.8. Strain-time histories at the bottom surface of certain points are shown in Figures 5.9-5.11. Bottom surface of the tapered sandwich plate is where uniform blast pressure has an interaction with the plate. The strain-time histories obtained on the top and bottom surfaces also have a good agreement especially for the thinner parts of the plate and for the first peaks of histories.

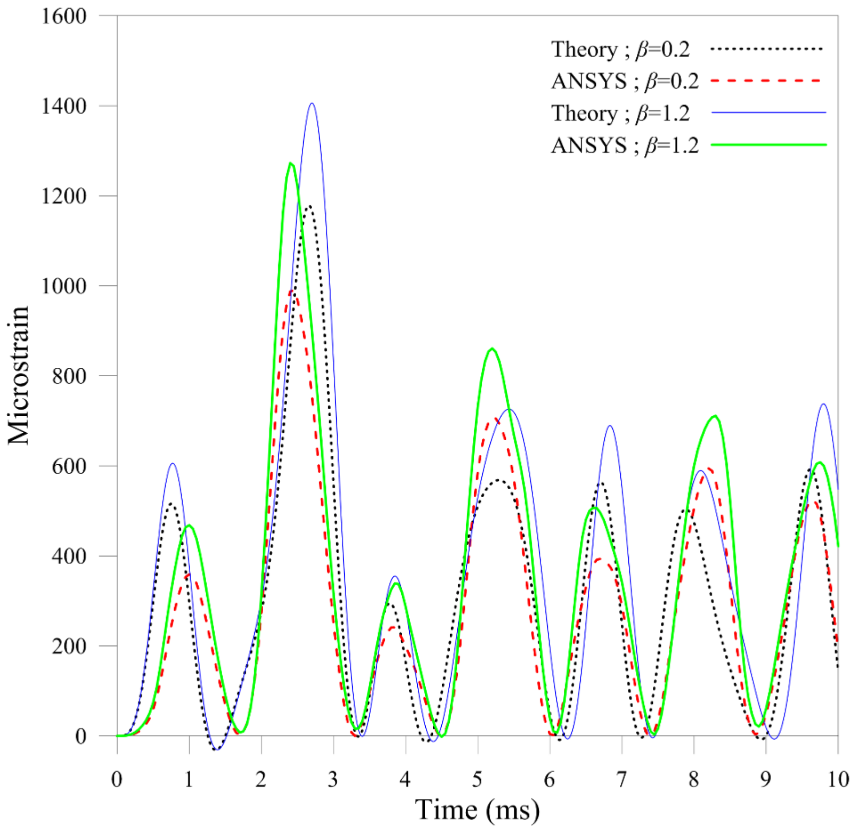

Figure 5.3 : The strain-time histories at point A on the middle plane of [UCBGBB]s.

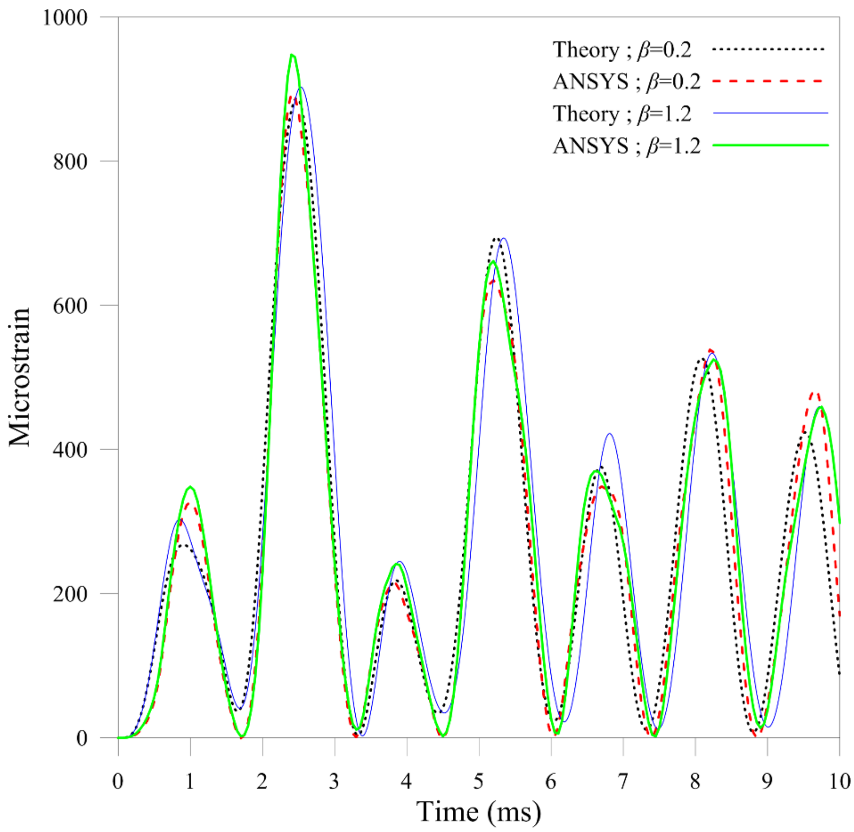

Figure 5.4 : The strain-time histories at point C on the middle plane of [UCBGBB]s.

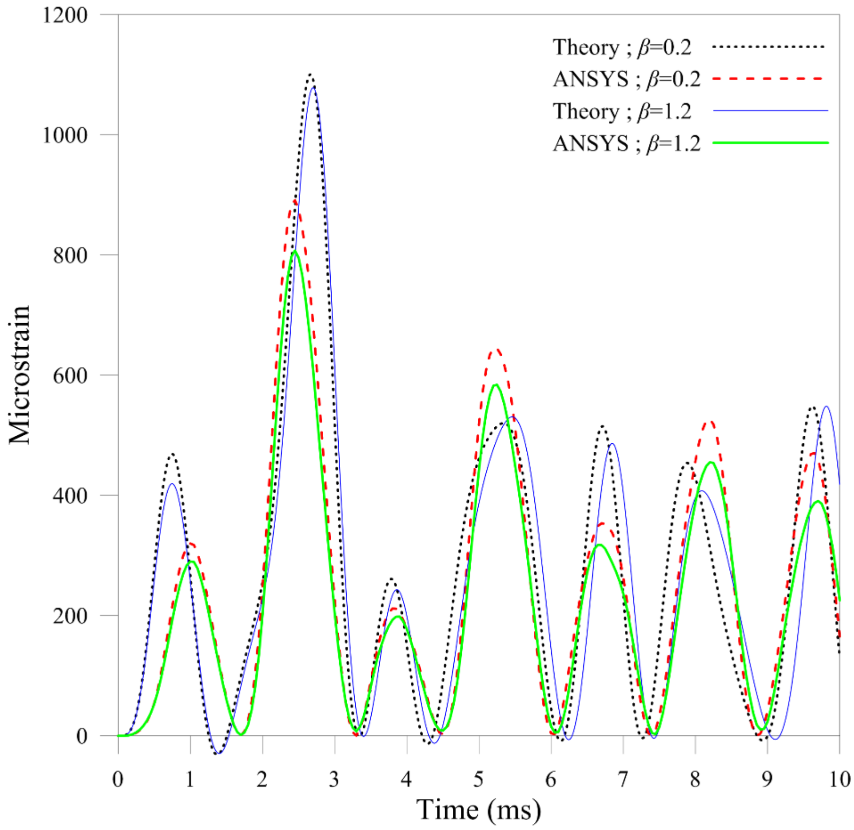

Figure 5.5 : The strain-time histories at point B on the middle plane of [UCBGBB]s.

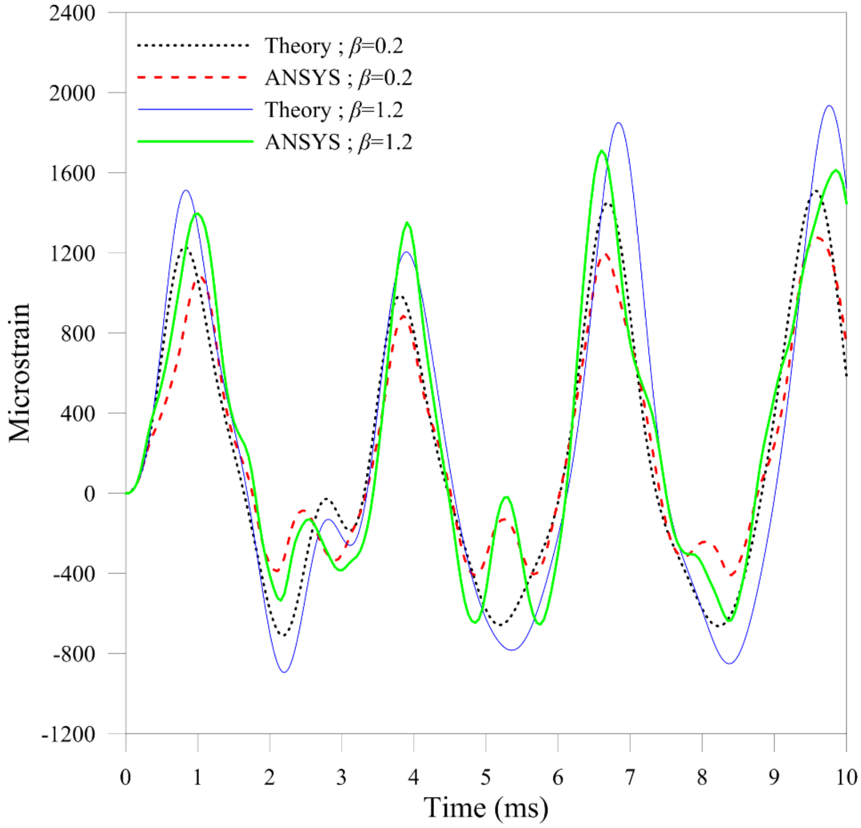

Figure 5.6 : The strain-time histories at point A on the top surface of [UCBGBB]s.

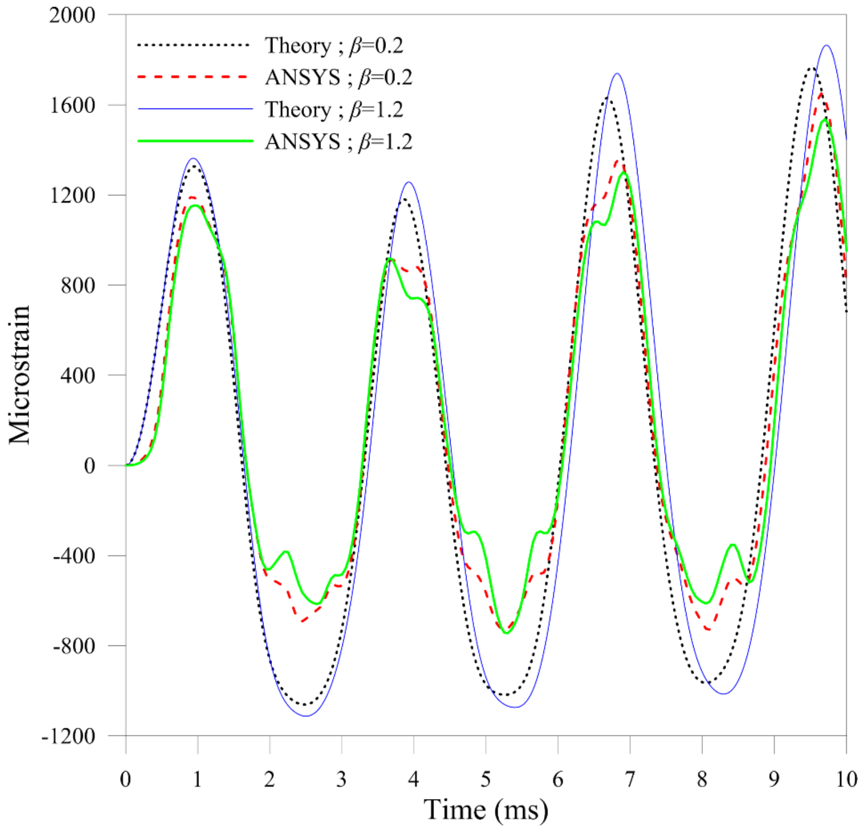

Figure 5.7 : The strain-time histories at point C on the top surface of [UCBGBB]s.

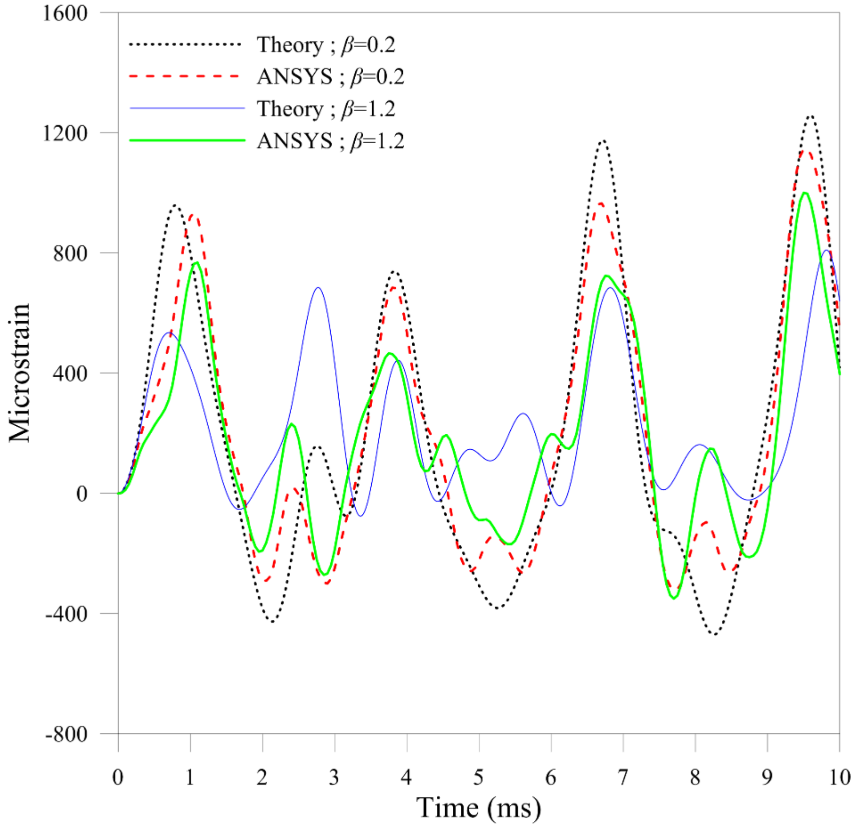

Figure 5.8 : The strain-time histories at point B on the top surface of [UCBGBB]s.

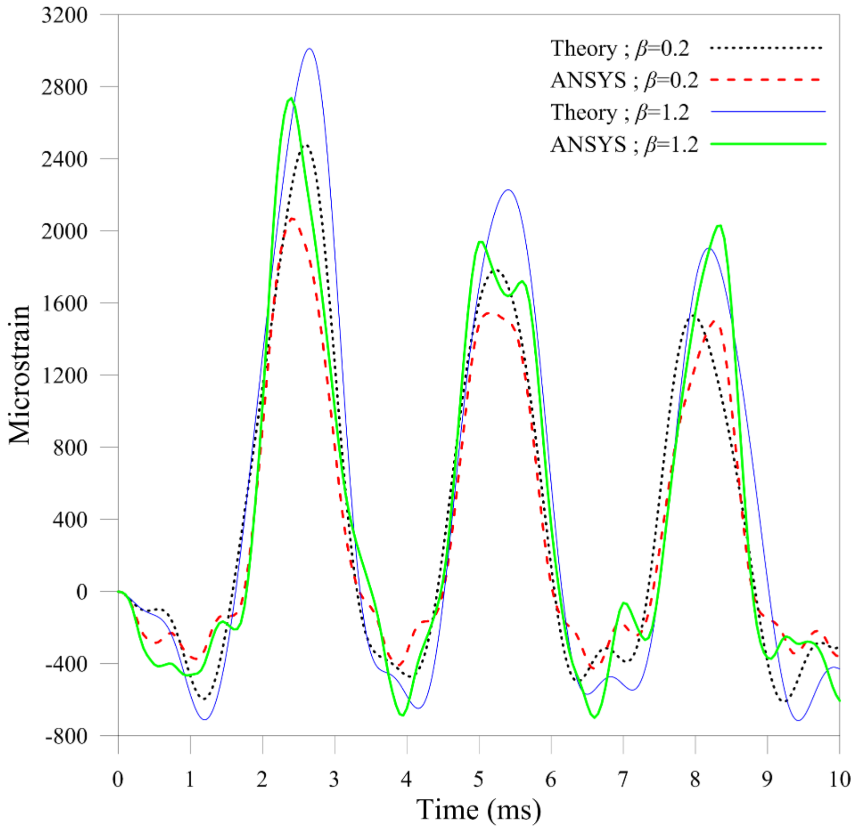

Figure 5.9 : The strain-time histories at point A on the bottom surface of [UCBGBB]s.

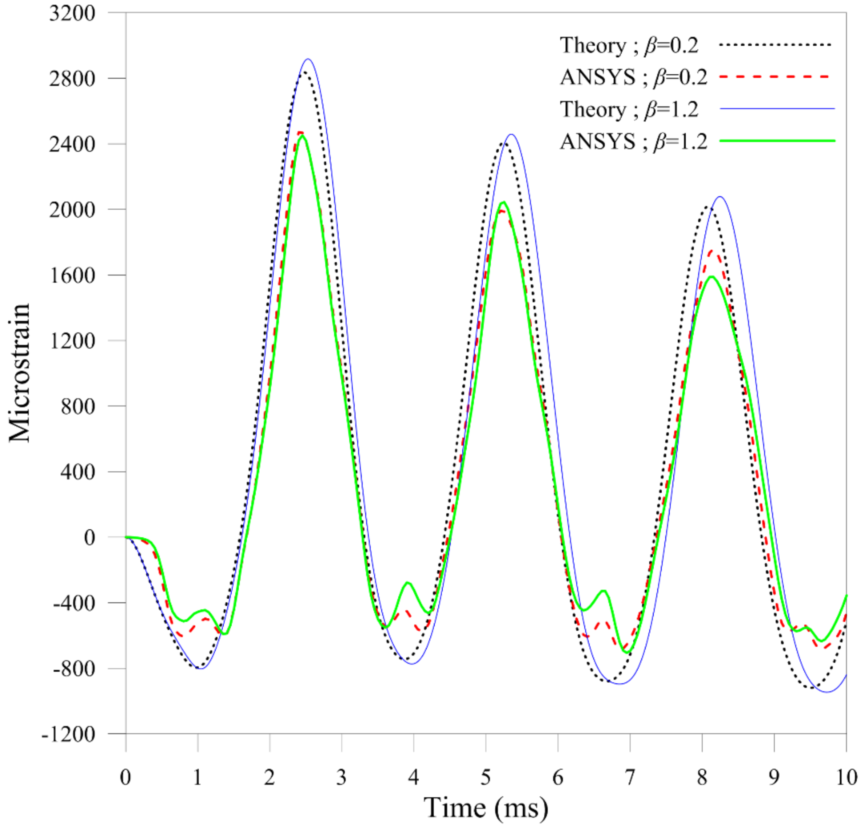

Figure 5.10 : The strain-time histories at point C on the bottom surface of [UCBGBB]s.

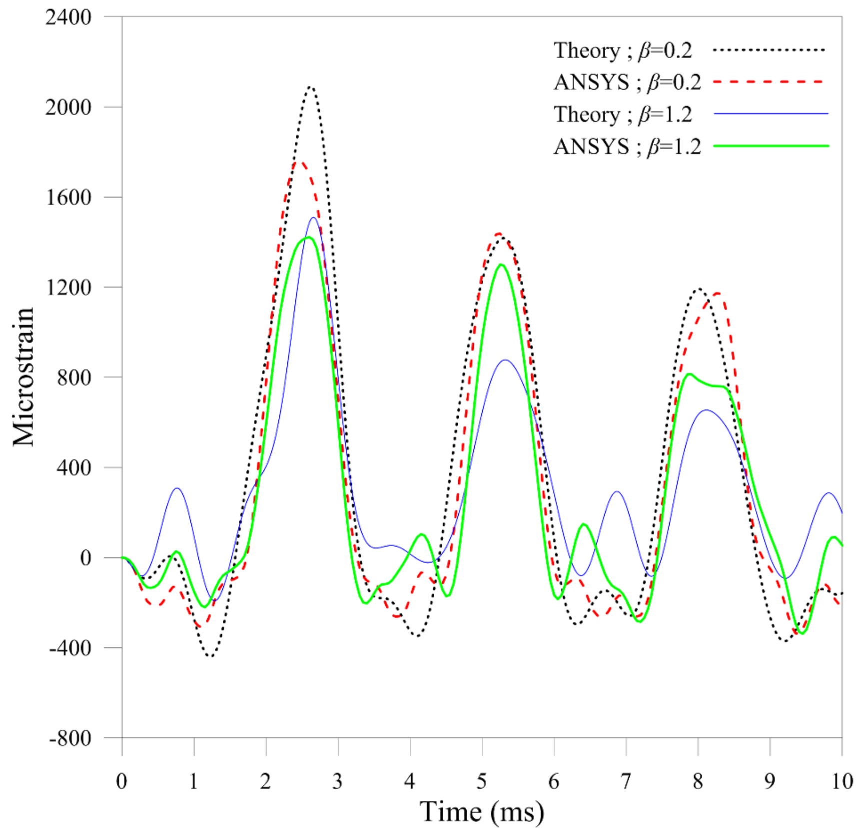

Figure 5.11 : The strain-time histories at point B on the bottom surface of [UCBGBB]s.

Another configuration of [UCBGBB]s tapered sandwich plate is also analysed to understand the effect of fiber orientations. Displacement-time histories of the selected points for β=1.2 and for the case of [90/±45/±45]s are shown in Figure 5.12. Changing fiber orientation angles effects the displacement-time histories. Smaller peak values of displacements are also obtained using either theory or ANSYS for the [UCBGBB]s plate with [90/±45/±45]s. Again, a good agreement is found between displacement-time histories obtained using two methods for [UCBGBB]s plate with [90/±45/±45]s.

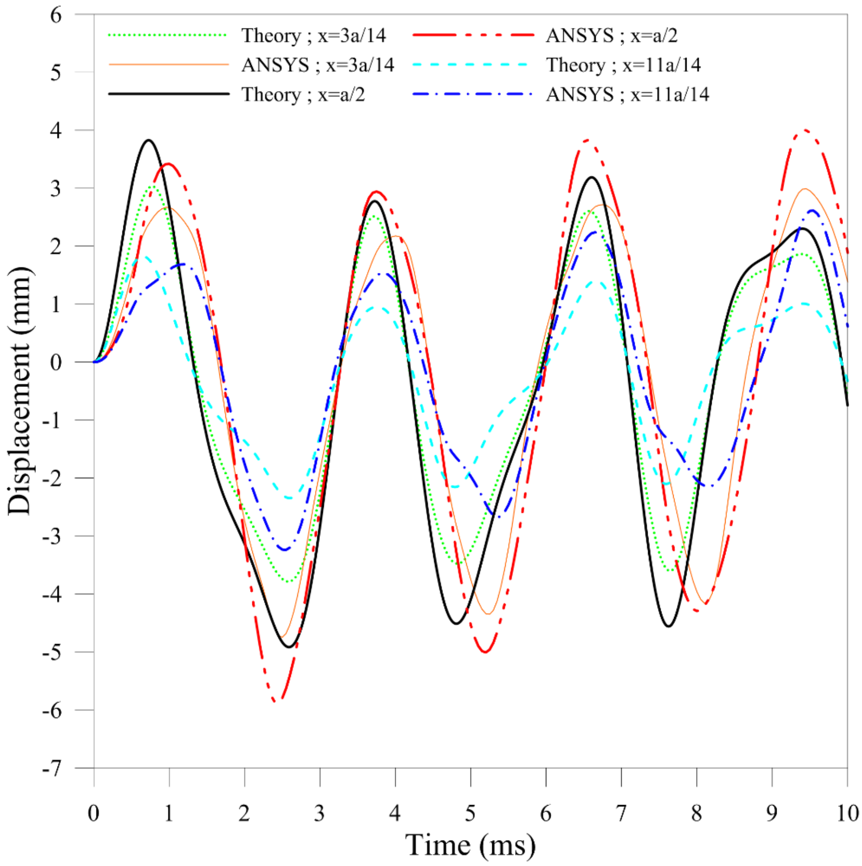

Figure 5.12 : The displacement-time histories of [UCBGBB]s for [90/±45/±45]s and β=1.2.

The strain-time histories at the top and bottom surface of point A, point C and point B for [90/±45/±45]s and β=1.2 are also shown in Figures 5.13-5.15, respectively. There is a very good agreement for point C, but the rate of agreement between theory and FEM is decreased for point A and point B of [90/±45/±45]s.

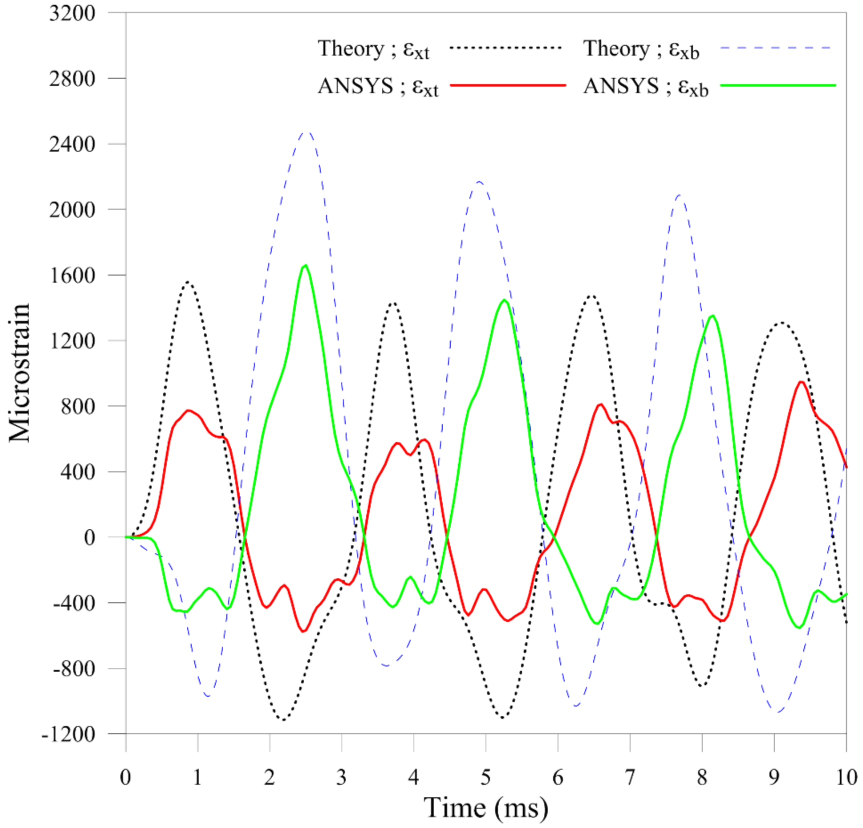

Figure 5.13 : The strain-time histories at point A on the top and bottom surfaces of [UCBGBB]s for [90/±45/±45]s and β=1.2.

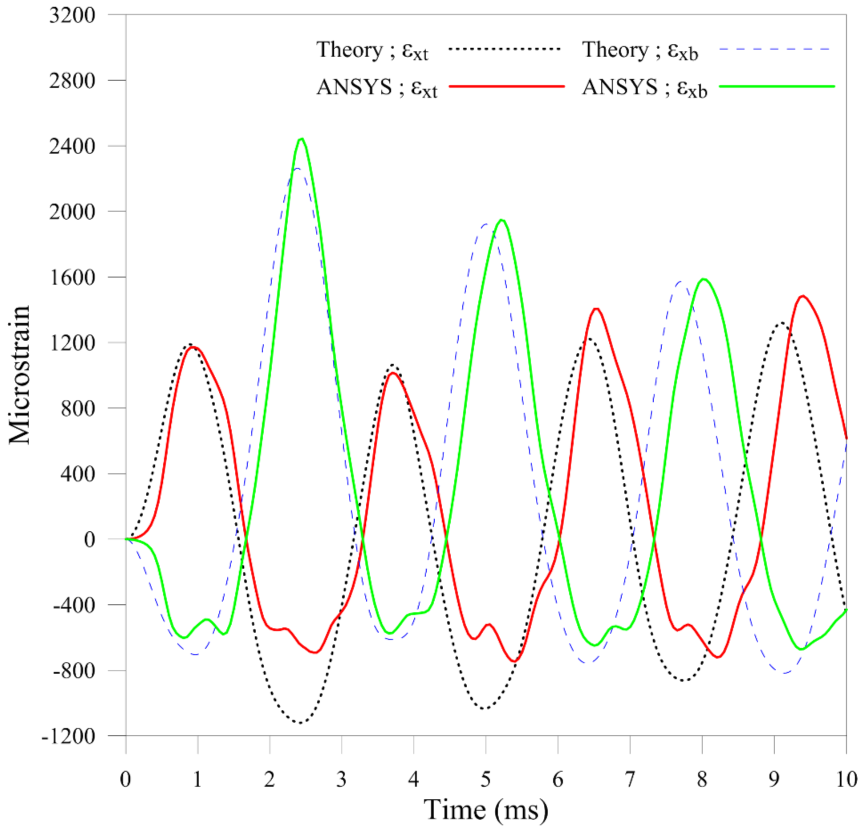

Figure 5.14 : The strain-time histories at point C on the top and bottom surfaces of [UCBGBB]s for [90/±45/±45]s and β=1.2.

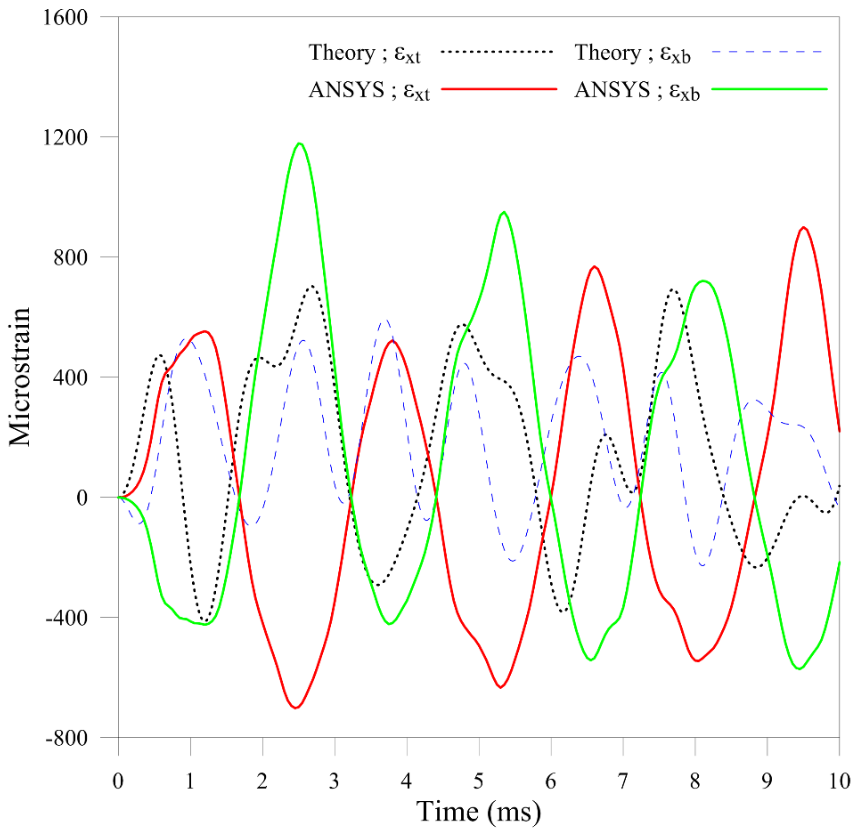

Figure 5.15 : The strain-time histories at point B on the top and bottom surfaces of [UCBGBB]s for [90/±45/±45]s and β=1.2.

5.2 Clamped Tapered Sandwich Plate

The application of clamped tapered sandwich plate subjected to air blast load is investigated by comparing experimental method with FEM and theoretical method. The fabricated tapered sandwich plate described above is used. The material and physical properties of this plate have been showed in Table 4.4.

The pressure distribution because of the blast loading, $p(x,y,t)$ is assumed to be uniform on the clamped plate. The same measured parameters are used for defining the blast loading as for simply supported tapered sandwich plate. Only square shaped plates are considered and the dimensions are taken as a=b=300 mm. Both shear correction factors are taken as 5/6 that is proposed by Goens [49].

Theoretical displacement-time and strain histories are obtained for both the tapered sandwich plate that has non-tapered faces and a tapered core (Condition 1- C1) and the fully tapered sandwich plate that has tapered faces and tapered core (Condition 2- C2). The thickness for the layers in Table 4.4 is rearranged for the plate of C2. The thickness for the plate of C1 is used for the thickness of plate C2 at the center of the plate so that the weight of the plate is still kept constant.

FEM results by ANSYS finite element software are obtained for only C2. Experimental strain-time histories are measured for C1 and has been also showed before for 20 ms in Figures 4.27-4.28. Displacement-time histories of experimental results are obtained from measured acceleration-time histories by numerical analysis with the technique of trapezoidal rule.

Figure 5.16 compares displacement-time histories of certain points under the conditions of C1 and C2. It is noticed that there are very small differences between C1 and C2. This situation is applicable for strain-time histories too. This can be the result of having small taper ratio. So, changing sandwich faces from constant thickness to tapered thickness does not effect too much while keeping the weight constant. Figure 5.16 also shows that deflections at the point A and the point B obtained by using closed form solution do not have the same displacement-time histories and peak values as expected.

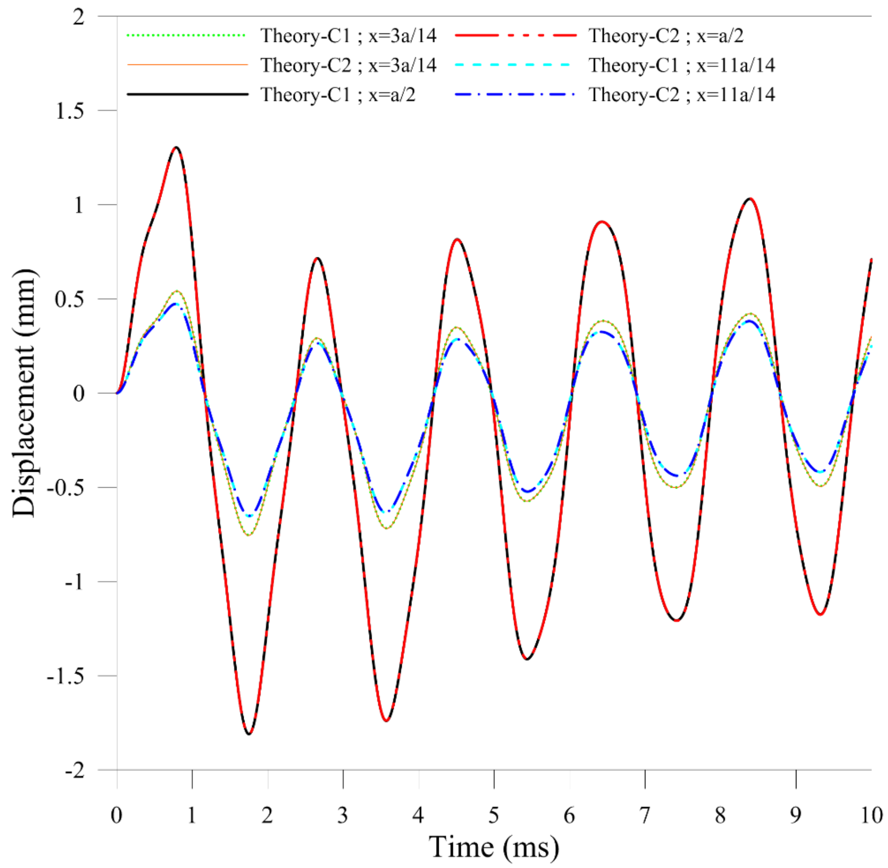

Figure 5.16 : The displacement-time histories at certain points of fabricated tapered plate for the theory of C1 and C2.

Displacement-time histories of theory and FEM for certain points are compared in Figure 5.17 for 10 ms. There is a good agreement between displacement-time histories obtained by closed form solution and FEM. The maximum deflection occurs at point C for both taper ratios as expected. FEM positive and negative peak results are higher than theoretical results for point A and B and not for point C. The rate of agreement for the frequency of displacement-time histories are better than the one for simply supported tapered plate.

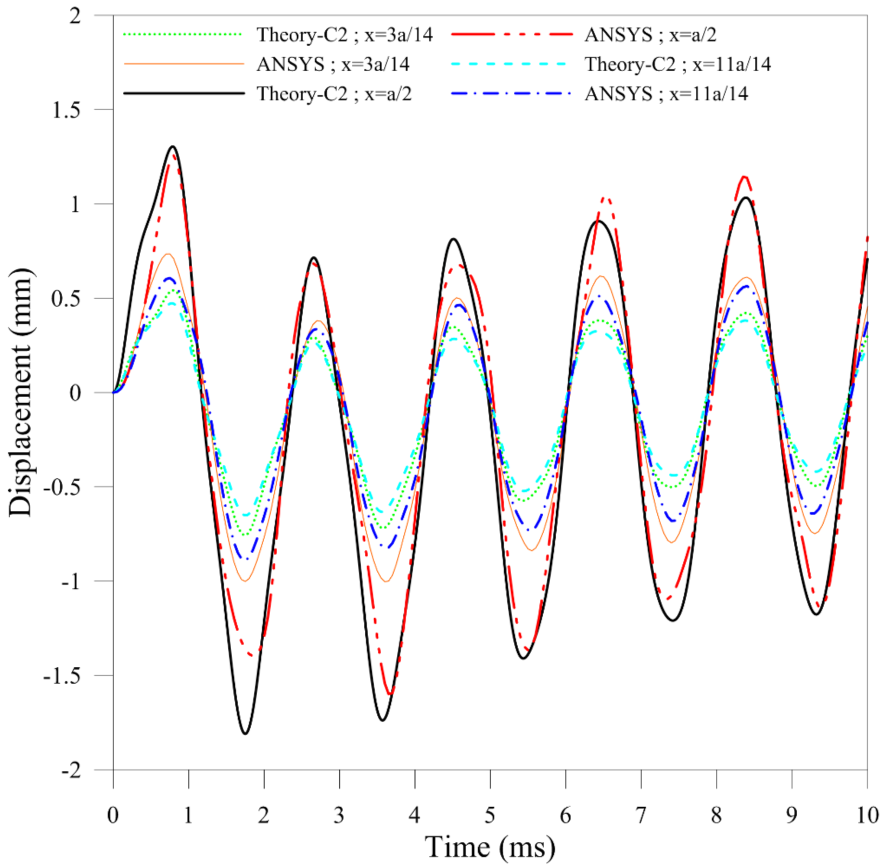

Figure 5.17 : The comparison of displacement-time histories at certain points of fabricated tapered plate for the theory of C2 and FEM.

The strain-time (ε_x) histories of the fabricated clamped tapered sandwich plate at the top surface of point A and point B are obtained for 3 ms and shown in Figures 5.18-5.19, respectively. The strain-time histories at point C and point D are also shown for 3 ms in Figures 5.20-5.21. In these figures, strain-time histories of four test results are compared with the theory of C1 and FEM except for point D. Two test results are shown for point D in Figure 5.21. The agreement between experimental and theoretical studies are very good for the first peak of strain-time histories at point A and point B which are the thinner and thicker part of the plate. The correlation with ANSYS results are also good for the first peak of strain-time histories at point A. There is a good agreement for point C between strain-time histories of experiments and ANSYS results too, although theoretical results do not have enough agreement with the others. In spite of this, the magnitude of strain for the first peak obtained by theory at point C is very close to the others.

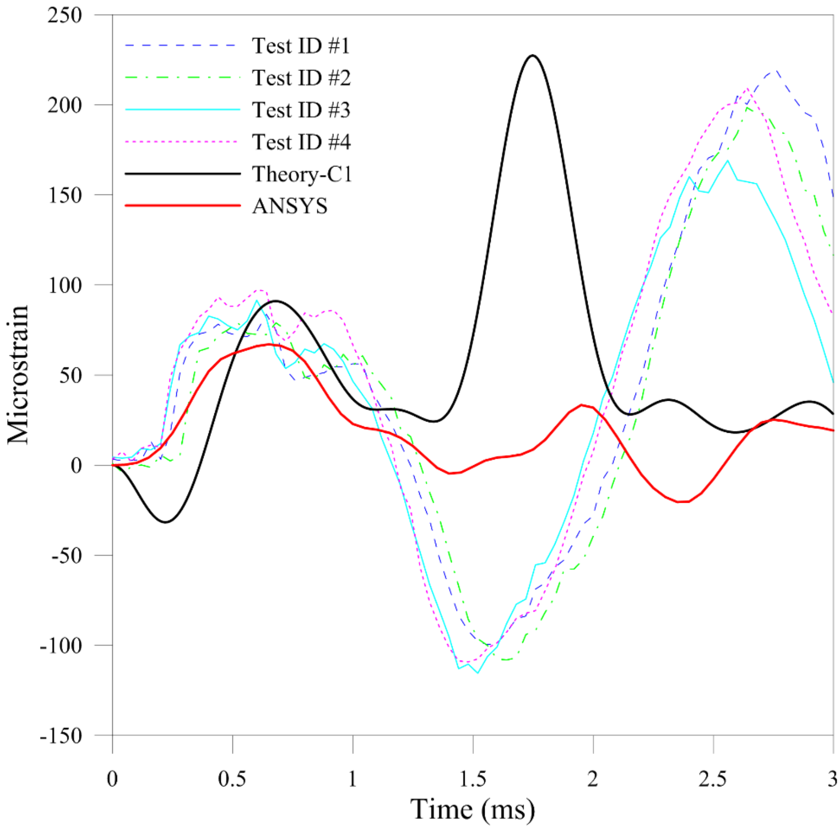

Figure 5.18 : The strain-time histories at point A on the top surface of fabricated tapered plate.

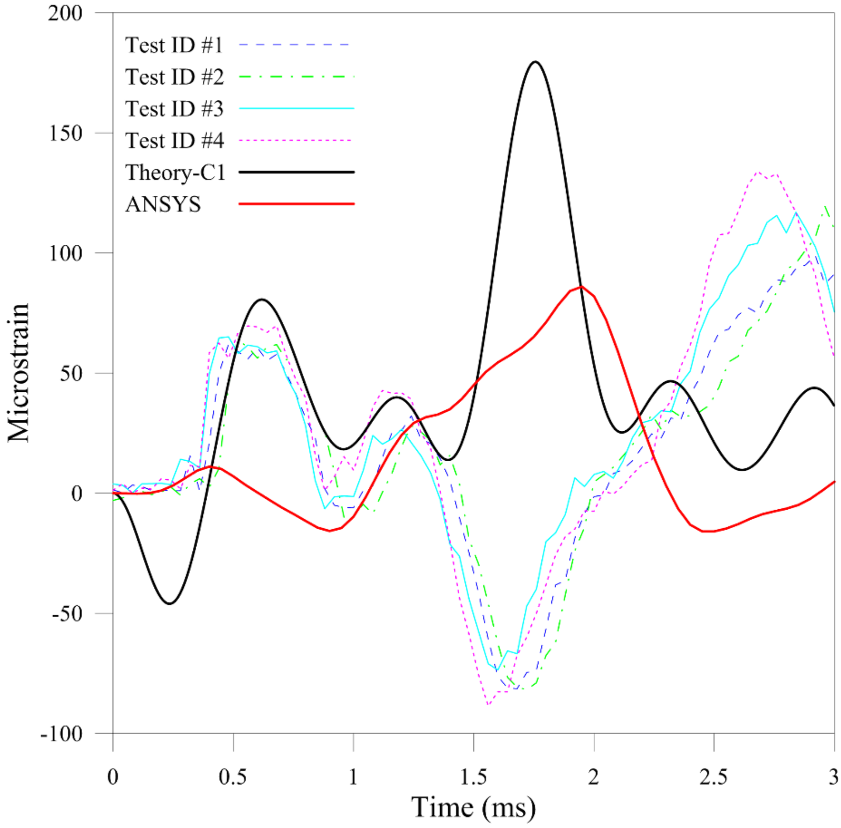

Figure 5.19 : The strain-time histories at point B on the top surface of fabricated tapered plate.

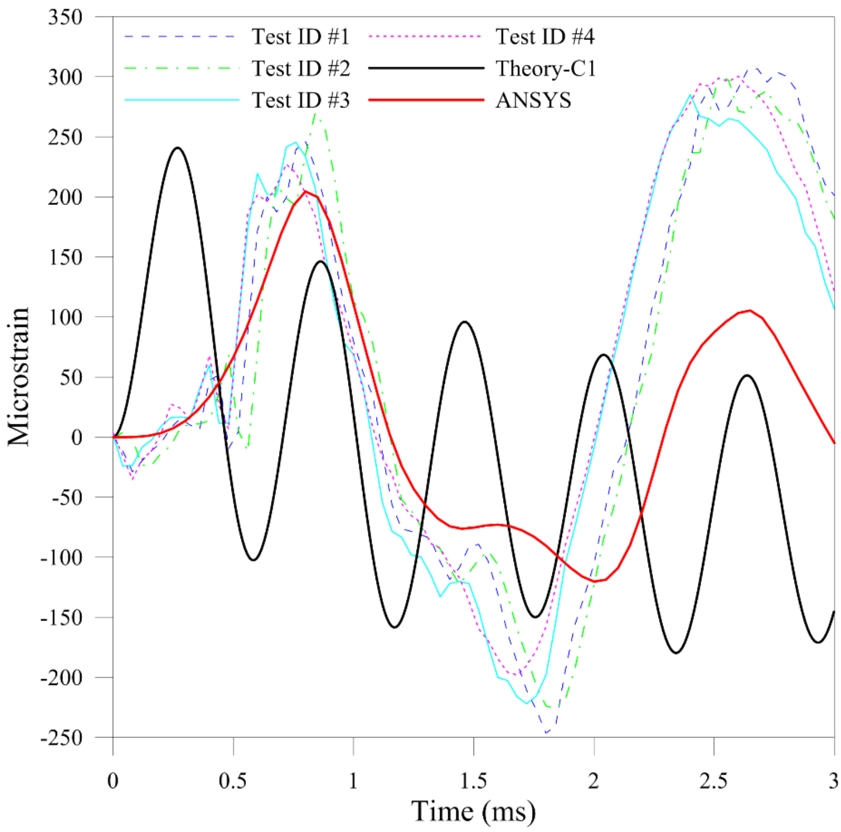

Figure 5.20 : The strain-time histories at point C on the top surface of fabricated tapered plate.

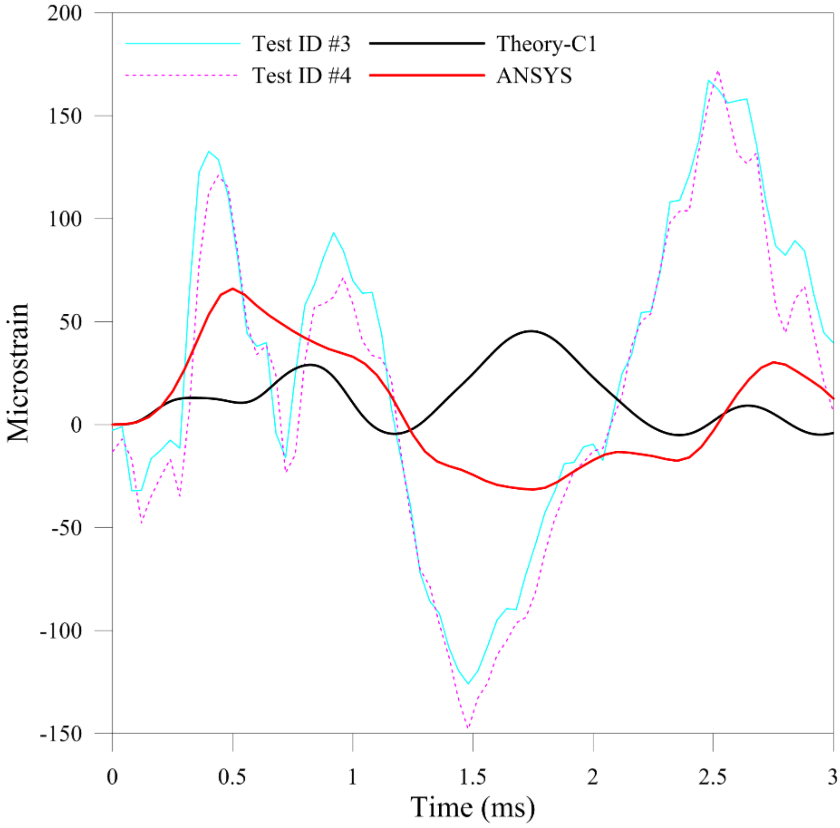

Figure 5.21 : The strain-time histories at point D on the top surface of fabricated tapered plate.

The displacement-time histories at point C and point D of fabricated clamped tapered sandwich plate are shown in Figures 5.22-5.23. The technique of trapezoidal rule is respectively applied for obtaining velocity-time and displacement-time histories by using measured acceleration-time histories with accelerometers. The agreement with test results are good especially for the first peak. The less better agreement at negative side of histories can be because of the starting of damping effects for test results.

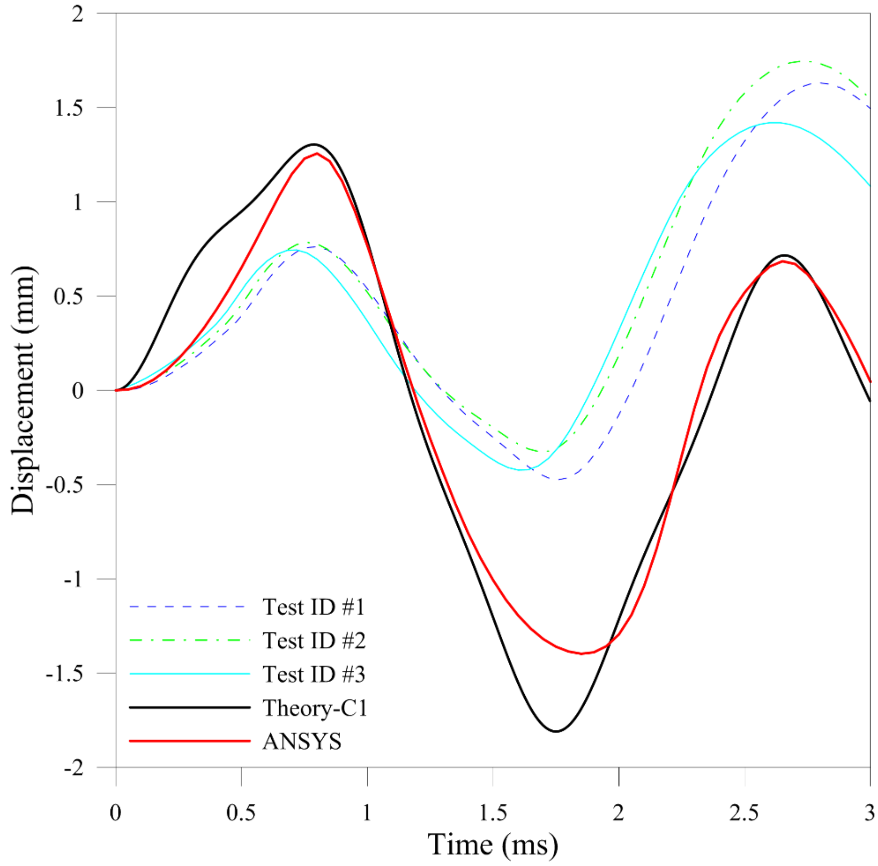

Figure 5.22 : The displacement-time histories at point C of fabricated tapered plate.

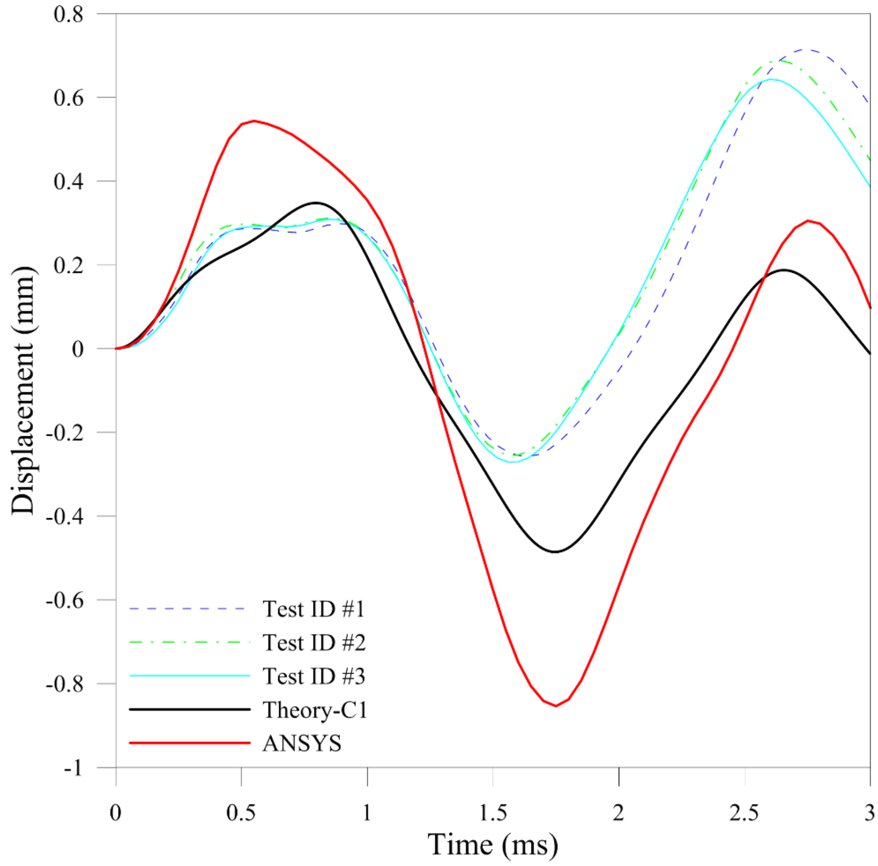

Figure 5.23 : The displacement-time histories at point D of fabricated tapered plate.

6. CONCLUSIONS AND FUTURE WORK

The effects of the varying thickness on laminated sandwich plate designs are analysed transiently by using sandwich plate theory with a closed form solution and are compared with the results of FEM and an experimental method. A sandwich plate theory for plates with constant thickness and one-layered face sheets found in the literature is developed to analyse the tapered sandwich plates with multi-layered face sheets. ANSYS commercial software is used to obtain finite element results. The experimental studies are based on simulating a air blast environment and setting up a shock tube testing mechanism. Fabrication of the tapered sandwich plate and the coupon tests for obtaining material properties of the constituents are also involved in the study before doing shock tube tests. Simply supported and clamped boundary conditions for all edges of the plates are considered in this study. Experimental results are included in the study for only clamped boundary conditions.

Simply supported tapered sandwich plate designs with two different taper ratios are compared with each other to understand the effect of variable thickness. Moreover, the fiber orientations for laminates of hybrid faces are changed to show the parametric quantity of this study. The deflection and strains at middle, top and bottom surfaces are obtained along the tapered direction for both theory and FEM. The analyses indicate that there is a good correlation between the results obtained by using present method and FEM.

The design of manufactured clamped tapered sandwich plate with the actual taper ratio subjected to the air blast load is investigated theoretically, numerically and experimentally. The deflection and strains at the top surface are obtained along the tapered direction for the theory, FEM and the experiments. Pressure values on a model plate and strain and acceleration at certain points on the fabricated tapered sandwich plate are measured and stored into a DAQ device. The technique of trapezoidal rule is applied for obtaining displacement-time histories by using measured acceleration-time histories with accelerometers. There is a good correlation between the results of theory and FEM with the experiments when displacement-time and strain-time histories for a short duration which contains the first peaks of histories are obtained. For longer duration, the effect of damping and the insufficient stability of testing mechanism make the agreement with the experimental results worse. The undamping results of clamped plate for theory and ANSYS have still good agreement as the results of simply supported plate.

The closed form solution presented here costs much lower computer time compared to the FEM. On the other hand, while the type of tapered plate called C1 in this study can only be solved by theory, ANSYS shell modelling is not avaiable for applying different thickness functions for laminas. Using 3D finite element modelling for C1 is a great waste of time for not only solving but also 3D modelling and meshing. The experimental studies are a troublesome process anyway which have a long period of time. However, the testing process is strongly needful for the validation of the theory. The code is once validated with the test, then the theory can be carried out the desired design of plates. Because, it is very easy to change design parameters for the theory. The method present here can be used in preliminary design of sandwich and laminated plates with variable thickness.

The experimental model presented here can reduce the period of time and the cost in comparison with conventional tests by using the mentioned two stage procedure. The present model do not need pressure measurement for each desired composite plate if one of the factors, which are the burst pressure, the distance to the plate, the length and the width of plate, is not changed. Moreover, the used pressure sensors are cheaper and do not have the risk of failure problems because of the burst effect. Polyester film membranes used in this study are also very practical and cheap for the blast testing.

The present theoretical method is very capable of predicting the nonlinear dynamic response of the tapered sandwich plate with multi-layered faces. The thickness variation is taken as a linear function of coordinate axis in this study. However, the thickness variation could be taken as the second or third degree functions of coordinate axis. The blast pressure is uniformly distributed on the tapered plate. Tapered sandwich plates could be more functional under the effect of non-uniform pressure distribution. The thicker part of the tapered plate could be subjected to higher pressure load while the thinner part is subjected to lower pressure load.

Either face sheet or core materials may behave nonlinearly. In some cases, the structural damping can also be important for the engineering structures. The tapered sandwich plates subjected to different types dynamic loadings such as other external pressure pulses can be compared with eachother. These are not investigated in the current study and will be the subject of future studies.

REFERENCES

[1] **Jeon, J.S. and Hong, C.S.** (1992). Analysis of tapered sandwich structures with anisotropic composite faces, *Computers & Structures*, *44*, 597–608.

[2] **Pinckney, R.L.** (1973). Helicopter rotor blades, In: *Applications of composite materials* (STP 524, pp. 108-133), ASTM Publications, Tallahassee, FL, United States.

[3] **FAA-H-8083-31** (2012). Aviation maintenance technician handbook-airframe: volume 1, *US Department of Transportation*, Oklahoma City, OK, United States.

[4] **Kuczma, S.K. and Vizzini, A.J.** (1999). Failure of sandwich to laminate tapered composite structures, *AIAA Journal*, *37*, 227–231.

[5] **Kinney, G.F., and Graham, K.J.** (1985). *Explosive shock in air*. The Macmillan Company, New York City, NY, United States.

[6] **Kazancı, Z. and Mecitoğlu, Z.** (2006). Nonlinear damped vibrations of a laminated composite plate subjected to blast load, *AIAA Journal*, *44*, 2002–2008.

[7] **Kazancı, Z. and Mecitoğlu, Z.** (2008). Nonlinear dynamic behavior of simply supported laminated composite plates subjected to blast load, *Journal of Sound and Vibration*, *317*, 883–897.

[8] **Upadhyay, A.K., Pandey, R. and Shukla, K.K.** (2011). Nonlinear dynamic response of laminated composite plates subjected to pulse loading, *Communications in Nonlinear Science and Numerical Simulation*, *16*, 4530–4544.

[9] **Türkmen, H.S. and Mecitoğlu, Z.** (1999). Dynamic response of a stiffened laminated composite plate subjected to blast load, *Journal of Sound and Vibration*, *221*, 371–389.

[10] **Louca, L.A. and Pan, Y.G.** (1998). Response of stiffened and unstiffened plates subjected to blast loading, *Engineering Structures*, *20*, 1079–1086.

[11] **Amabili, M.** (2004). Nonlinear vibrations of rectangular plates with different boundary conditions: theory and experiments, *Computers & Structures*, *82*, 2587–2605.

[12] **Amabili, M.** (2006). Theory and experiments for large-amplitude vibrations of rectangular plates with geometric imperfections, *Journal of Sound and Vibration*, *291*, 539–565.

[13] **Chen, J., Dawe, D.J. and Wang, S.** (2000). Nonlinear transient analysis of rectangular composite laminated plates, *Composite Structures*, *49*, 129–139.

[14] **Şenyer, M. and Kazancı, Z.** (2012). Nonlinear dynamic analysis of a laminated hybrid composite plate subjected to time-dependent external pulses, *Acta Mechanica Solida Sinica*, *25*, 586–597.

[15] **Baştürk, S., Uyanık, H. and Kazancı, Z.** (2014). An analytical model for predicting the deflection of laminated basalt composite plates under dynamic loads, *Composite Structures*, *116*, 273–285.

[16] **Baştürk, S., Uyanık, H. and Kazancı, Z.** (2014). Nonlinear damped vibrations of a hybrid laminated composite plate subjected to blast load, *Procedia Engineering*, *88*, 18–25.

[17] **Kazancı, Z.** (2011). Dynamic response of composite sandwich plates subjected to time-dependent pressure pulses, *International Journal of Non-Linear Mechanics*, *46*, 807–817.

[18] **Hause, T. and Librescu, L.** (2005). Dynamic response of anisotropic sandwich flat panels to explosive pressure pulses, *International Journal of Impact Engineering*, 2005, *31*, 607–628.

[19] **Librescu, L., Oh, S.Y. and Hohe, J.** (2004). Linear and non-linear dynamic response of sandwich panels to blast loading, *Composite Part B: Engineering*, *35*, 673–683.

[20] **Yang, Y., Fallah, A.S., Saunders, M. and Louca, L.A.** (2011). On the dynamic response of sandwich panels with different core set-ups subject to global and local blast loads, *Engineering Structures, 33*, 2781–2793.

[21] **Nayak, A.K., Shenoi, R.A. and Moy, S.S.J.** (2004). Transient response of composite sandwich plates, *Composite Structures*, *64*, 249–267.

[22] **Nayak, A.K., Shenoi, R.A. and Moy, S.S.J.** (2006). Dynamic response of composite sandwich plates subjected to initial stresses, *Composite Part A: Applied Science and Manufacturing*, *37*, 1189–1205.

[23] **Balkan, D. and Mecitoğlu, Z. (2014).** Nonlinear dynamic behaviour of viscoelastic sandwich composite plates under non-uniform blast load: theory and experiment, *International Journal of Impact Engineering*, *72*, 85–104.

[24] **He, K., Hoa, S.V. and Ganesan, R.** (2000). The study of tapered laminated composite structures: a review, *Composite Science and Technology*, *60*, 2643–2657.

[25] **Barton, O.Jr.** (1999). Fundamental frequency of tapered plates by the method of eigensensitivity analysis, *Ocean Engineering*, *26*, 565–573.

[26] **Nallim, L.G. and Grossi, R.O.** (2001). Natural frequencies of edge restrained tapered isotropic and orthotropic rectangular plates with a central free hole, *Applied Acoustics*, *62*, 289–305.

[27] **Kukreti, A.R., Farsa, J. and Bert, C.W.** (1992). Fundamental frequency of tapered plates by differential quadrature, *Journal of Engineering Mechanics*, *118*, 1221–1238.

[28] **Malekzadeh, P. and Karami, G. (2008).** Large amplitude flexural vibration analysis of tapered plates with edges elastically restrained against rotation using DQM, *Engineering Structures*, *30*, 2850–2858.

[29] **Civalek, O.** (2009). Fundamental frequency of isotropic and orthotropic rectangular plates with linearly varying thickness by discrete singular convolution method, *Applied Mathematical Modelling*, *33*, 3825–3835.

[30] **Nguyen, C.H., Chandrashekhara, K. and Birman, V.** (2011). Enhanced static response of sandwich panels with honeycomb cores through the use of stepped facings, *Journal of Sandwich Structures and Materials*, *13*, 237–260.

[31] **Vel, S.S., Caccese, V. and Zhao, H.** (2005). Elastic coupling effects in tapered sandwich panels with laminated anisotropic composite facings, *Journal of Composite Materials*, *39*, 2161–2183.

[32] **Rabinovitch, O. and Frostig, Y.** (2001). High-order analysis of unidirectional sandwich panels with flat and generally curved faces and a soft core, *Journal of Sandwich Structures and Materials*, *3*, 89–116.

[33] **Paydar, N. and Libove, L.** (1988) Bending of sandwich plates of variable thickness, *Journal of Applied Mechanics*, *55*, 419–424.

[34] **Wang, Q.** (1998). A method for static analysis of variable thickness sandwich plates, *Composite Structures*, *42*, 239–243.

[35] **Ganesan, R. and Liu, D.Y.** (2008). Progressive failure and post-buckling response of tapered composite plates under uni-axial compression, *Composite Structures*, *82*, 159–176.

[36] **Rasul, S.A.E. and Ganesan, R.** (2013). Compressive response of tapered curved composite plates based on a nine-node composite shell element, *Composite Structures*, *96*, 8–16.

[37] **Mustapha, S. and Ye, L.** (2015). Propagation behaviour of guided waves in tapered sandwich structures and debonding identification using time reversal, *Wave Motion*, *57*, 154–170.

[38] **Ramalingeswara Rao, S. and Ganesan, N.** (1995). Dynamic response of tapered composite beams using higher order shear deformation theory, *Journal of Sound and Vibration*, *187*, 737–756.

[39] **Susler, S., Turkmen, H.S. and Kazancı, Z.** (2012). The nonlinear dynamic behaviour of tapered laminated plates subjected to blast loading, *Shock and Vibration*, *19*, 1235–1255.

[40] **Susler, S., Kazancı, Z. and Turkmen, H.S.** (2011). Analysis of laminated plates with parabolic thickness variation, *The 13th International Conference on Civil Structural and Environmental Engineering Computing (CC2011)*, Chania, Crete, Greece, September 6–9.

[41] **Riber, H.J.** (1997). Non-linear analytical solutions for laterally loaded sandwich plates, *Composite Structures*, *39*, 63–83.

[42] **Kazancı, Z.** (2006). Anlık basınç yükü etkisi altındaki katmanlı kompozit bir plağın lineer olmayan dinamik davranışı, *PhD Thesis,* ITU, Istanbul.

[43] **ASTM D792-13** (2013). Standard test methods for density and specific gravity (relative density) of plastics by displacement, *ASTM International*, West Conshohocken, PA, United States.

[44] **ASTM D3039/D3039M-14** (2014). Standard test methods for tensile properties of polymer matrix composite materials, *ASTM International*, West Conshohocken, PA, United States.

[45] **ASTM D3518/D3518M-13** (2013). Standard test methods for in-plane shear response of polymer matrix composite materials by tensile test of a ±45º laminate, *ASTM International*, West Conshohocken, PA, United States.

[46] **Polypropylene honeycomb core** (n.d.). In *CEL Components S.r.l.*. Date retrieved: 08.09.2014, address: http://www.honeycombpanels.eu/96/technical-datasheets

[47] **DIN 53294** (1982). Testing of sandwiches: Shear test, *German National Standard*, Germany.

[48] **Meraghni, F., Desrumaux, F. and Benzeggagh, M.L.** (1999). Mechanical behaviour of cellular core for structural sandwich panels, *Composite: Part A*, *30*, 767–779.

[49] **Goens, E.** (1931). Uber die bestimmung des elastizitatsmodule von staben mit hilfe von biegungsschwingungen, *Annalen der Physik*, *11*, 649–678.

[50] **MIL-HDBK-17-2F** (2002). Composite materials handbook volume 2 polymer matrix composite materials properties, *US Department of Defence*, Fort Washington, PA, United States.

[51] **Baştürk, S., Süsler, S., Uyanık, H., Türkmen, H.S., Lopresto, V., Genna, S. and Kazancı, Z.** (2015). Experimental and numerical analysis of laminated basalt composite plate subjected to blast load, *The 20th International Conference on Composite Materials (ICCM20)*, Copenhagen, Denmark, July 19–24.

APPENDICES

APPENDIX A: The coefficients of the nonlinear-coupled equations of motion in time domain for a simply supported tapered sandwich plate that has both tapered faces and tapered core.

APPENDIX B: The coefficients of the nonlinear-coupled equations of motion in time domain for a clamped tapered sandwich plate that has both tapered faces and tapered core

APPENDIX C: The coefficients of the nonlinear-coupled equations of motion in time domain for a clamped tapered sandwich plate that has non-tapered faces and a tapered core

APPENDIX D: The coefficients of the linear equations of motion

APPENDIX A

All stiffness terms (A_{ij} and D_{ij}) in the coefficients below denote with the notation $(\ )_0^{t\_sand}$.

$$a_0 = \frac{ab^9\overline{m}}{1260},\ a_1 = \frac{b^7(2+\beta)(3a^2A_{66}+b^2A_{11}\pi^2)}{630a},\ a_2 = \frac{9a^4(A_{12}+A_{66})b^4(2+\beta)}{2\pi^6},$$

$$a_3 = 0,\ a_4 = 0,\ a_5 = 0,\ a_6 = 0,$$

$$a_7 = \frac{b^3(2+\beta)\left(A_{11}b^2(45+\pi^4)+a^2\left(90A_{66}-A_{12}(-45+\pi^4)\right)\right)}{480a^2\pi},\ a_8 = 0,$$

$$a_9 = \frac{b^3(2+\beta)\left(A_{11}b^2(45+\pi^4)+a^2\left(90A_{66}-A_{12}(-45+\pi^4)\right)\right)}{480a^2\pi},\ a_{10} = 0,$$

$$a_{11} = -\frac{2b^3\beta\left(121A_{11}b^2(45+\pi^4)+2a^2\left(1260A_{66}+A_{12}(-45+\pi^4)\right)\right)}{3375a^2\pi^3},$$

$$a_{12} = \frac{b^3(2+\beta)\left(A_{11}b^2(45+\pi^4)+a^2\left(90A_{66}-A_{12}(-45+\pi^4)\right)\right)}{240a^2\pi},$$

$$a_{13} = -\frac{2b^3\beta\left(121A_{11}b^2(45+\pi^4)+2a^2\left(1260A_{66}+A_{12}(-45+\pi^4)\right)\right)}{3375a^2\pi^3},$$

$$a_{14} = -\frac{2b^3\beta\left(121A_{11}b^2(45+\pi^4)+2a^2\left(1260A_{66}+A_{12}(-45+\pi^4)\right)\right)}{3375a^2\pi^3},\ a_{15} = 0,$$

$$a_{16} = -\frac{2b^3\beta\left(121A_{11}b^2(45+\pi^4)+2a^2\left(1260A_{66}+A_{12}(-45+\pi^4)\right)\right)}{3375a^2\pi^3},\ a_{17} = 0$$

$$b_0 = \frac{a^9b\overline{m}}{1260},\ b_1 = \frac{9a^4(A_{12}+A_{66})b^4(2+\beta)}{2\pi^6},\ b_2 = \frac{a^7(2+\beta)(3b^2A_{66}+a^2A_{22}\pi^2)}{630b},$$

$$b_3 = 0,\ b_4 = 0,\ b_5 = 0,\ b_6 = 0,$$

$$b_7 = \frac{a^3(2+\beta)\left(a^2A_{22}(45+\pi^4)+b^2\left(90A_{66}-A_{12}(-45+\pi^4)\right)\right)}{480b^2\pi},$$

$$b_8 = \frac{a^3(2+\beta)\left(a^2A_{22}(45+16\pi^4)+4b^2\left(90A_{66}+A_{12}(45-16\pi^4)\right)\right)}{7680b^2\pi},$$

$$b_9=\frac{a^3\left(2+\beta\right)\left(a^2A_{22}\left(45+\pi^4\right)+b^2\left(90A_{66}-A_{12}\left(-45+\pi^4\right)\right)\right)}{480b^2\pi},$$

$$b_{10}=\frac{a^3\left(2+\beta\right)\left(a^2A_{22}\left(45+16\pi^4\right)+4b^2\left(90A_{66}+A_{12}\left(45-16\pi^4\right)\right)\right)}{7680b^2\pi},$$

$$b_{11}=\frac{4a^3\beta\left(40a^2A_{22}\left(-91+9\pi^2\right)+b^2\left(A_{12}\left(7300-738\pi^2\right)+45A_{66}\left(-32+3\pi^2\right)\right)\right)}{243b^2\pi^3},$$

$$b_{12}=\frac{a^3\left(2+\beta\right)\left(a^2A_{22}\left(45+\pi^4\right)+b^2\left(90A_{66}-A_{12}\left(-45+\pi^4\right)\right)\right)}{240b^2\pi},$$

$$b_{13}=\frac{4a^3\beta\left(40a^2A_{22}\left(-91+9\pi^2\right)+b^2\left(A_{12}\left(7300-738\pi^2\right)+45A_{66}\left(-32+3\pi^2\right)\right)\right)}{243b^2\pi^3},$$

$$b_{14}=\frac{4a^3\beta\left(40a^2A_{22}\left(-91+9\pi^2\right)+b^2\left(A_{12}\left(7300-738\pi^2\right)+45A_{66}\left(-32+3\pi^2\right)\right)\right)}{243b^2\pi^3},$$

$$b_{15}=\frac{a^3\left(2+\beta\right)\left(a^2A_{22}\left(45+16\pi^4\right)+4b^2\left(90A_{66}+A_{12}\left(45-16\pi^4\right)\right)\right)}{3840b^2\pi},$$

$$b_{16}=\frac{4a^3\beta\left(40a^2A_{22}\left(-91+9\pi^2\right)+b^2\left(A_{12}\left(7300-738\pi^2\right)+45A_{66}\left(-32+3\pi^2\right)\right)\right)}{243b^2\pi^3},$$

$$b_{17}=0$$

$$c_0=\frac{1}{4}ab\overline{m},\ c_1=0,\ c_2=0,$$

$$c_3=\frac{\left(2+\beta\right)\pi^2}{16a^3b^3}\begin{pmatrix}-3\beta^2\left(b^4D_{11}+a^4D_{22}+2a^2b^2\left(D_{12}-2D_{66}\right)\right)+\\ \left(2+\beta\left(2+\beta\right)\right)\left(b^4D_{11}+a^4D_{22}+2a^2b^2\left(D_{12}+2D_{66}\right)\right)\pi^2\end{pmatrix},$$

$$c_4=\begin{pmatrix}\dfrac{16\beta^3\left(20b^4D_{11}+5a^4D_{22}+a^2b^2\left(25D_{12}+41D_{66}\right)\right)}{27a^3b^3}-\\ \dfrac{18\beta\left(2+\beta\left(2+\beta\right)\right)\left(4b^4D_{11}+a^4D_{22}+5a^2b^2\left(D_{12}+2D_{66}\right)\right)\pi^2}{27a^3b^3}\end{pmatrix},$$

$$c_5=0,\ c_6=0,\ c_7=\frac{b^3(2+\beta)(A_{11}b^2(45+\pi^4)+a^2(90A_{66}-A_{12}(-45+\pi^4)))}{240a^2\pi},$$

$$c_8=-\frac{2b^3\beta\left(121A_{11}b^2\left(45+\pi^4\right)+2a^2\left(1260A_{66}+A_{12}\left(-45+\pi^4\right)\right)\right)}{3375a^2\pi^3},$$

$$c_9 = \frac{b^3(2+\beta)(A_{11}b^2(45+\pi^4)+a^2(90A_{66}-A_{12}(-45+\pi^4)))}{240a^2\pi},$$

$$c_{10} = -\frac{2b^3\beta\left(121A_{11}b^2\left(45+\pi^4\right)+2a^2\left(1260A_{66}+A_{12}\left(-45+\pi^4\right)\right)\right)}{3375a^2\pi^3},$$

$$c_{11} = \frac{a^3(2+\beta)(a^2A_{22}(45+\pi^4)+b^2(90A_{66}-A_{12}(-45+\pi^4)))}{240b^2\pi},$$

$$c_{12} = \frac{4a^3\beta(40a^2A_{22}(-91+9\pi^2)+b^2(A_{12}(7300-738\pi^2)+45A_{66}(-32+3\pi^2)))}{243b^2\pi^3},$$

$$c_{13} = \frac{a^3(2+\beta)(a^2A_{22}(45+\pi^4)+b^2(90A_{66}-A_{12}(-45+\pi^4)))}{240b^2\pi},$$

$$c_{14} = \frac{4a^3\beta(40a^2A_{22}(-91+9\pi^2)+b^2(A_{12}(7300-738\pi^2)+45A_{66}(-32+3\pi^2)))}{243b^2\pi^3},$$

$$c_{15} = \frac{(9a^4A_{22}+2a^2(A_{12}+2A_{66})b^2+9A_{11}b^4)(2+\beta)\pi^4}{256a^3b^3},$$

$$c_{16} = -\frac{(1368a^4A_{22}+988a^2(A_{12}+2A_{66})b^2+14031A_{11}b^4)\beta\pi^2}{11025a^3b^3},$$

$$c_{17} = \frac{(9a^4A_{22}+2a^2(A_{12}+2A_{66})b^2+9A_{11}b^4)(2+\beta)\pi^4}{256a^3b^3},$$

$$c_{18} = -\frac{(1368a^4A_{22}+988a^2(A_{12}+2A_{66})b^2+14031A_{11}b^4)\beta\pi^2}{11025a^3b^3},$$

$$c_{19} = \frac{(9a^4A_{22}+5a^2(A_{12}+2A_{66})b^2+36A_{11}b^4)(2+\beta)\pi^4}{128a^3b^3},$$

$$c_{20} = \frac{3(9a^4A_{22}+2a^2(A_{12}+2A_{66})b^2+9A_{11}b^4)(2+\beta)\pi^4}{256a^3b^3},$$

$$c_{21} = \frac{(9a^4A_{22}+5a^2(A_{12}+2A_{66})b^2+36A_{11}b^4)(2+\beta)\pi^4}{128a^3b^3},$$

$$c_{22} = -\frac{(72a^4A_{22}+28a^2(A_{12}+2A_{66})b^2+369A_{11}b^4)\beta\pi^2}{300a^3b^3},$$

$$c_{23} = -\frac{(72a^4A_{22}+28a^2(A_{12}+2A_{66})b^2+369A_{11}b^4)\beta\pi^2}{300a^3b^3},$$

$$c_{24} = -\frac{(1368a^4A_{22}+988a^2(A_{12}+2A_{66})b^2+14031A_{11}b^4)\beta\pi^2}{3675a^3b^3},$$

$$c_{25} = \frac{3(9a^4A_{22}+2a^2(A_{12}+2A_{66})b^2+9A_{11}b^4)(2+\beta)\pi^4}{256a^3b^3},$$

$$c_{26}=\frac{(9a^4A_{22}+5a^2(A_{12}+2A_{66})b^2+36A_{11}b^4)(2+\beta)\pi^4}{128a^3b^3},$$

$$c_{27}=\frac{(9a^4A_{22}+5a^2(A_{12}+2A_{66})b^2+36A_{11}b^4)(2+\beta)\pi^4}{128a^3b^3},$$

$$c_{28}=-\frac{(72a^4A_{22}+28a^2(A_{12}+2A_{66})b^2+369A_{11}b^4)\beta\pi^2}{300a^3b^3},$$

$$c_{29}=-\frac{(1368a^4A_{22}+988a^2(A_{12}+2A_{66})b^2+14031A_{11}b^4)\beta\pi^2}{3675a^3b^3},$$

$$c_{30}=-\frac{(72a^4A_{22}+28a^2(A_{12}+2A_{66})b^2+369A_{11}b^4)\beta\pi^2}{300a^3b^3},$$

$$c_{31}=-\frac{(72a^4A_{22}+28a^2(A_{12}+2A_{66})b^2+369A_{11}b^4)\beta\pi^2}{150a^3b^3},$$

$$c_{32}=\frac{(9a^4A_{22}+5a^2(A_{12}+2A_{66})b^2+36A_{11}b^4)(2+\beta)\pi^4}{64a^3b^3},$$

$$c_{33}=-\frac{(72a^4A_{22}+28a^2(A_{12}+2A_{66})b^2+369A_{11}b^4)\beta\pi^2}{150a^3b^3},$$

$$c_{34}=\frac{(9a^4A_{22}+5a^2(A_{12}+2A_{66})b^2+36A_{11}b^4)(2+\beta)\pi^4}{64a^3b^3},\ c_{35}=-\frac{4abq_z}{\pi^2}$$

$$d_0=\frac{1}{4}ab\overline{m},\ d_1=0,\ d_2=0,$$

$$d_3=\frac{1}{27a^3b^3}\begin{pmatrix}16\beta^3\left(20b^4D_{11}+5a^4D_{22}+a^2b^2\left(25D_{12}+41D_{66}\right)\right)-\\ 18\beta\left(2+\beta\left(2+\beta\right)\right)\left(4b^4D_{11}+a^4D_{22}+5a^2b^2\left(D_{12}+2D_{66}\right)\right)\pi^2\end{pmatrix},$$

$$d_4=\frac{\left(2+\beta\right)\pi^2}{64a^3b^3}\begin{pmatrix}-3\beta^2\left(16b^4D_{11}+a^4D_{22}+8a^2b^2\left(D_{12}-2D_{66}\right)\right)+\\ 4\left(2+\beta\left(2+\beta\right)\right)\left(16b^4D_{11}+a^4D_{22}+8a^2b^2\left(D_{12}+2D_{66}\right)\right)\pi^2\end{pmatrix},$$

$$d_5=0,\ d_6=0,\ d_7=-\frac{2b^3\beta\left(121A_{11}b^2\left(45+\pi^4\right)+2a^2\left(1260A_{66}+A_{12}\left(-45+\pi^4\right)\right)\right)}{3375a^2\pi^3},$$

$$d_8=0,\ d_9=-\frac{2b^3\beta\left(121A_{11}b^2\left(45+\pi^4\right)+2a^2\left(1260A_{66}+A_{12}\left(-45+\pi^4\right)\right)\right)}{3375a^2\pi^3},\ d_{10}=0,$$

$$d_{11}=\frac{4a^3\beta\left(40a^2A_{22}\left(-91+9\pi^2\right)+b^2\left(A_{12}\left(7300-738\pi^2\right)+45A_{66}\left(-32+3\pi^2\right)\right)\right)}{243b^2\pi^3},$$

$$d_{12}=\frac{a^3\left(2+\beta\right)\left(a^2A_{22}\left(45+16\pi^4\right)+4b^2\left(90A_{66}+A_{12}\left(45-16\pi^4\right)\right)\right)}{3840b^2\pi},$$

$$d_{13}=\frac{4a^3\beta\left(40a^2A_{22}\left(-91+9\pi^2\right)+b^2\left(A_{12}\left(7300-738\pi^2\right)+45A_{66}\left(-32+3\pi^2\right)\right)\right)}{243b^2\pi^3},$$

$$d_{14}=\frac{a^3\left(2+\beta\right)\left(a^2A_{22}\left(45+16\pi^4\right)+4b^2\left(90A_{66}+A_{12}\left(45-16\pi^4\right)\right)\right)}{3840b^2\pi},$$

$$d_{15}=-\frac{\left(72a^4A_{22}+28a^2\left(A_{12}+2A_{66}\right)b^2+369A_{11}b^4\right)\beta\pi^2}{900a^3b^3},$$

$$d_{16}=\frac{\left(9a^4A_{22}+8a^2\left(A_{12}+2A_{66}\right)b^2+144A_{11}b^4\right)\left(2+\beta\right)\pi^4}{256a^3b^3},$$

$$d_{17}=-\frac{\left(72a^4A_{22}+28a^2\left(A_{12}+2A_{66}\right)b^2+369A_{11}b^4\right)\beta\pi^2}{900a^3b^3},$$

$$d_{18}=\frac{\left(9a^4A_{22}+8a^2\left(A_{12}+2A_{66}\right)b^2+144A_{11}b^4\right)\left(2+\beta\right)\pi^4}{256a^3b^3},$$

$$d_{19}=-\frac{\left(1368a^4A_{22}+988a^2\left(A_{12}+2A_{66}\right)b^2+14031A_{11}b^4\right)\beta\pi^2}{3675a^3b^3},$$

$$d_{20}=-\frac{\left(72a^4A_{22}+28a^2\left(A_{12}+2A_{66}\right)b^2+369A_{11}b^4\right)\beta\pi^2}{300a^3b^3},$$

$$d_{21}=-\frac{\left(1368a^4A_{22}+988a^2\left(A_{12}+2A_{66}\right)b^2+14031A_{11}b^4\right)\beta\pi^2}{3675a^3b^3},$$

$$d_{22}=\frac{\left(9a^4A_{22}+5a^2\left(A_{12}+2A_{66}\right)b^2+36A_{11}b^4\right)\left(2+\beta\right)\pi^4}{128a^3b^3},$$

$$d_{23}=\frac{\left(9a^4A_{22}+5a^2\left(A_{12}+2A_{66}\right)b^2+36A_{11}b^4\right)\left(2+\beta\right)\pi^4}{128a^3b^3},$$

$$d_{24}=\frac{3\left(9a^4A_{22}+8a^2\left(A_{12}+2A_{66}\right)b^2+144A_{11}b^4\right)\left(2+\beta\right)\pi^4}{256a^3b^3},$$

$$d_{25}=-\frac{\left(72a^4A_{22}+28a^2\left(A_{12}+2A_{66}\right)b^2+369A_{11}b^4\right)\beta\pi^2}{300a^3b^3},$$

$$d_{26}=-\frac{\left(1368a^4A_{22}+988a^2\left(A_{12}+2A_{66}\right)b^2+14031A_{11}b^4\right)\beta\pi^2}{3675a^3b^3},$$

$$d_{27}=-\frac{\left(1368a^4A_{22}+988a^2\left(A_{12}+2A_{66}\right)b^2+14031A_{11}b^4\right)\beta\pi^2}{3675a^3b^3},$$

$$d_{28}=\frac{\left(9a^4A_{22}+5a^2\left(A_{12}+2A_{66}\right)b^2+36A_{11}b^4\right)(2+\beta)\pi^4}{128a^3b^3},$$

$$d_{29}=\frac{3\left(9a^4A_{22}+8a^2\left(A_{12}+2A_{66}\right)b^2+144A_{11}b^4\right)(2+\beta)\pi^4}{256a^3b^3},$$

$$d_{30}=\frac{\left(9a^4A_{22}+5a^2\left(A_{12}+2A_{66}\right)b^2+36A_{11}b^4\right)(2+\beta)\pi^4}{128a^3b^3},$$

$$d_{31}=\frac{\left(9a^4A_{22}+5a^2\left(A_{12}+2A_{66}\right)b^2+36A_{11}b^4\right)(2+\beta)\pi^4}{64a^3b^3},$$

$$d_{32}=-\frac{2\left(1368a^4A_{22}+988a^2\left(A_{12}+2A_{66}\right)b^2+14031A_{11}b^4\right)\beta\pi^2}{3675a^3b^3},$$

$$d_{33}=\frac{\left(9a^4A_{22}+5a^2\left(A_{12}+2A_{66}\right)b^2+36A_{11}b^4\right)(2+\beta)\pi^4}{64a^3b^3},$$

$$d_{34}=-\frac{2\left(1368a^4A_{22}+988a^2\left(A_{12}+2A_{66}\right)b^2+14031A_{11}b^4\right)\beta\pi^2}{3675a^3b^3},\ d_{35}=0$$

$$e_0=\frac{1}{4}ab\bar{m},\ e_1=0,\ e_2=0,\ e_3=0,\ e_4=0,$$

$$e_5=\frac{(2+\beta)\left(a^2A_{44}k_{44}+b^2A_{55}k_{55}\right)\pi^2}{8ab},\ e_6=-\frac{2\beta\left(2a^2A_{44}k_{44}+5b^2A_{55}k_{55}\right)}{9ab},$$

$$e_7=\frac{b^3(2+\beta)\left(A_{11}b^2\left(45+\pi^4\right)+a^2\left(90A_{66}-A_{12}\left(-45+\pi^4\right)\right)\right)}{240a^2\pi},$$

$$e_8=-\frac{2b^3\beta\left(121A_{11}b^2\left(45+\pi^4\right)+2a^2\left(1260A_{66}+A_{12}\left(-45+\pi^4\right)\right)\right)}{3375a^2\pi^3},$$

$$e_9=\frac{b^3(2+\beta)\left(A_{11}b^2\left(45+\pi^4\right)+a^2\left(90A_{66}-A_{12}\left(-45+\pi^4\right)\right)\right)}{240a^2\pi},$$

$$e_{10}=-\frac{2b^3\beta\left(121A_{11}b^2\left(45+\pi^4\right)+2a^2\left(1260A_{66}+A_{12}\left(-45+\pi^4\right)\right)\right)}{3375a^2\pi^3},$$

$$e_{11}=\frac{a^3(2+\beta)\left(a^2A_{22}\left(45+\pi^4\right)+b^2\left(90A_{66}-A_{12}\left(-45+\pi^4\right)\right)\right)}{240b^2\pi},$$

$$e_{12}=\frac{4a^3\beta\left(40a^2A_{22}\left(-91+9\pi^2\right)+b^2\left(A_{12}\left(7300-738\pi^2\right)+45A_{66}\left(-32+3\pi^2\right)\right)\right)}{243b^2\pi^3},$$

$$e_{13} = \frac{a^3\left(2+\beta\right)\left(a^2 A_{22}\left(45+\pi^4\right)+b^2\left(90A_{66}-A_{12}\left(-45+\pi^4\right)\right)\right)}{240b^2\pi},$$

$$e_{14} = \frac{4a^3\beta\left(40a^2A_{22}\left(-91+9\pi^2\right)+b^2\left(A_{12}\left(7300-738\pi^2\right)+45A_{66}\left(-32+3\pi^2\right)\right)\right)}{243b^2\pi^3},$$

$$e_{15} = \frac{\left(9a^4A_{22}+2a^2\left(A_{12}+2A_{66}\right)b^2+9A_{11}b^4\right)\left(2+\beta\right)\pi^4}{256a^3b^3},$$

$$e_{16} = -\frac{\left(1368a^4A_{22}+988a^2\left(A_{12}+2A_{66}\right)b^2+14031A_{11}b^4\right)\beta\pi^2}{11025a^3b^3},$$

$$e_{17} = \frac{\left(9a^4A_{22}+2a^2\left(A_{12}+2A_{66}\right)b^2+9A_{11}b^4\right)\left(2+\beta\right)\pi^4}{256a^3b^3},$$

$$e_{18} = -\frac{\left(1368a^4A_{22}+988a^2\left(A_{12}+2A_{66}\right)b^2+14031A_{11}b^4\right)\beta\pi^2}{11025a^3b^3},$$

$$e_{19} = \frac{\left(9a^4A_{22}+5a^2\left(A_{12}+2A_{66}\right)b^2+36A_{11}b^4\right)\left(2+\beta\right)\pi^4}{128a^3b^3},$$

$$e_{20} = \frac{3\left(9a^4A_{22}+2a^2\left(A_{12}+2A_{66}\right)b^2+9A_{11}b^4\right)\left(2+\beta\right)\pi^4}{256a^3b^3},$$

$$e_{21} = \frac{\left(9a^4A_{22}+5a^2\left(A_{12}+2A_{66}\right)b^2+36A_{11}b^4\right)\left(2+\beta\right)\pi^4}{128a^3b^3},$$

$$e_{22} = -\frac{\left(72a^4A_{22}+28a^2\left(A_{12}+2A_{66}\right)b^2+369A_{11}b^4\right)\beta\pi^2}{300a^3b^3},$$

$$e_{23} = -\frac{\left(72a^4A_{22}+28a^2\left(A_{12}+2A_{66}\right)b^2+369A_{11}b^4\right)\beta\pi^2}{300a^3b^3},$$

$$e_{24} = -\frac{\left(1368a^4A_{22}+988a^2\left(A_{12}+2A_{66}\right)b^2+14031A_{11}b^4\right)\beta\pi^2}{3675a^3b^3},$$

$$e_{25} = \frac{3\left(9a^4A_{22}+2a^2\left(A_{12}+2A_{66}\right)b^2+9A_{11}b^4\right)\left(2+\beta\right)\pi^4}{256a^3b^3},$$

$$e_{26} = \frac{\left(9a^4A_{22}+5a^2\left(A_{12}+2A_{66}\right)b^2+36A_{11}b^4\right)\left(2+\beta\right)\pi^4}{128a^3b^3},$$

$$e_{27} = \frac{\left(9a^4A_{22}+5a^2\left(A_{12}+2A_{66}\right)b^2+36A_{11}b^4\right)\left(2+\beta\right)\pi^4}{128a^3b^3},$$

$$e_{28} = -\frac{\left(72a^4A_{22}+28a^2\left(A_{12}+2A_{66}\right)b^2+369A_{11}b^4\right)\beta\pi^2}{300a^3b^3},$$

$$e_{29} = -\frac{\left(1368a^4 A_{22} + 988a^2\left(A_{12} + 2A_{66}\right)b^2 + 14031A_{11}b^4\right)\beta\pi^2}{3675a^3b^3},$$

$$e_{30} = -\frac{\left(72a^4 A_{22} + 28a^2\left(A_{12} + 2A_{66}\right)b^2 + 369A_{11}b^4\right)\beta\pi^2}{300a^3b^3},$$

$$e_{31} = -\frac{\left(72a^4 A_{22} + 28a^2\left(A_{12} + 2A_{66}\right)b^2 + 369A_{11}b^4\right)\beta\pi^2}{150a^3b^3},$$

$$e_{32} = \frac{\left(9a^4 A_{22} + 5a^2\left(A_{12} + 2A_{66}\right)b^2 + 36A_{11}b^4\right)\left(2+\beta\right)\pi^4}{64a^3b^3},$$

$$e_{33} = -\frac{\left(72a^4 A_{22} + 28a^2\left(A_{12} + 2A_{66}\right)b^2 + 369A_{11}b^4\right)\beta\pi^2}{150a^3b^3},$$

$$e_{34} = \frac{\left(9a^4 A_{22} + 5a^2\left(A_{12} + 2A_{66}\right)b^2 + 36A_{11}b^4\right)\left(2+\beta\right)\pi^4}{64a^3b^3},\; e_{35} = -\frac{4abq_z}{\pi^2}$$

$$f_0 = \frac{1}{4}ab\overline{m},\; f_1 = 0,\; f_2 = 0,\; f_3 = 0,\; f_4 = 0,$$

$$f_5 = -\frac{2\beta\left(2a^2 A_{44}k_{44} + 5b^2 A_{55}k_{55}\right)}{9ab},\; f_6 = \frac{\left(2+\beta\right)\left(a^2 A_{44}k_{44} + 4b^2 A_{55}k_{55}\right)\pi^2}{8ab},$$

$$f_7 = -\frac{2b^3\beta\left(121A_{11}b^2\left(45+\pi^4\right) + 2a^2\left(1260A_{66} + A_{12}\left(-45+\pi^4\right)\right)\right)}{3375a^2\pi^3},\; f_8 = 0,$$

$$f_9 = -\frac{2b^3\beta\left(121A_{11}b^2\left(45+\pi^4\right) + 2a^2\left(1260A_{66} + A_{12}\left(-45+\pi^4\right)\right)\right)}{3375a^2\pi^3},\; f_{10} = 0,$$

$$f_{11} = \frac{4a^3\beta\left(40a^2A_{22}\left(-91+9\pi^2\right) + b^2\left(A_{12}\left(7300-738\pi^2\right) + 45A_{66}\left(-32+3\pi^2\right)\right)\right)}{243b^2\pi^3},$$

$$f_{12} = \frac{a^3\left(2+\beta\right)\left(a^2A_{22}\left(45+16\pi^4\right) + 4b^2\left(90A_{66} + A_{12}\left(45-16\pi^4\right)\right)\right)}{3840b^2\pi},$$

$$f_{13} = \frac{4a^3\beta\left(40a^2A_{22}\left(-91+9\pi^2\right) + b^2\left(A_{12}\left(7300-738\pi^2\right) + 45A_{66}\left(-32+3\pi^2\right)\right)\right)}{243b^2\pi^3},$$

$$f_{14} = \frac{a^3\left(2+\beta\right)\left(a^2A_{22}\left(45+16\pi^4\right) + 4b^2\left(90A_{66} + A_{12}\left(45-16\pi^4\right)\right)\right)}{3840b^2\pi},$$

$$f_{15} = \frac{\left(-72a^4 A_{22} + 28a^2\left(A_{12} + 2A_{66}\right)b^2 + 369A_{11}b^4\right)\beta\pi^2}{900a^3b^3},$$

$$f_{16} = \frac{\left(9a^4 A_{22} + 8a^2 \left(A_{12} + 2A_{66}\right) b^2 + 144 A_{11} b^4\right)\left(2+\beta\right)\pi^4}{256 a^3 b^3},$$

$$f_{17} = -\frac{\left(72a^4 A_{22} + 28a^2 \left(A_{12} + 2A_{66}\right) b^2 + 369 A_{11} b^4\right)\beta\pi^2}{900 a^3 b^3},$$

$$f_{18} = \frac{\left(9a^4 A_{22} + 8a^2 \left(A_{12} + 2A_{66}\right) b^2 + 144 A_{11} b^4\right)\left(2+\beta\right)\pi^4}{256 a^3 b^3},$$

$$f_{19} = -\frac{\left(1368a^4 A_{22} + 988a^2 \left(A_{12} + 2A_{66}\right) b^2 + 14031 A_{11} b^4\right)\beta\pi^2}{3675 a^3 b^3},$$

$$f_{20} = -\frac{\left(72a^4 A_{22} + 28a^2 \left(A_{12} + 2A_{66}\right) b^2 + 369 A_{11} b^4\right)\beta\pi^2}{300 a^3 b^3},$$

$$f_{21} = -\frac{\left(1368a^4 A_{22} + 988a^2 \left(A_{12} + 2A_{66}\right) b^2 + 14031 A_{11} b^4\right)\beta\pi^2}{3675 a^3 b^3},$$

$$f_{22} = \frac{\left(9a^4 A_{22} + 5a^2 \left(A_{12} + 2A_{66}\right) b^2 + 36 A_{11} b^4\right)\left(2+\beta\right)\pi^4}{128 a^3 b^3},$$

$$f_{23} = \frac{\left(9a^4 A_{22} + 5a^2 \left(A_{12} + 2A_{66}\right) b^2 + 36 A_{11} b^4\right)\left(2+\beta\right)\pi^4}{128 a^3 b^3},$$

$$f_{24} = \frac{3\left(9a^4 A_{22} + 8a^2 \left(A_{12} + 2A_{66}\right) b^2 + 144 A_{11} b^4\right)\left(2+\beta\right)\pi^4}{256 a^3 b^3},$$

$$f_{25} = -\frac{\left(72a^4 A_{22} + 28a^2 \left(A_{12} + 2A_{66}\right) b^2 + 369 A_{11} b^4\right)\beta\pi^2}{300 a^3 b^3},$$

$$f_{26} = -\frac{\left(1368a^4 A_{22} + 988a^2 \left(A_{12} + 2A_{66}\right) b^2 + 14031 A_{11} b^4\right)\beta\pi^2}{3675 a^3 b^3},$$

$$f_{27} = -\frac{\left(1368a^4 A_{22} + 988a^2 \left(A_{12} + 2A_{66}\right) b^2 + 14031 A_{11} b^4\right)\beta\pi^2}{3675 a^3 b^3},$$

$$f_{28} = \frac{\left(9a^4 A_{22} + 5a^2 \left(A_{12} + 2A_{66}\right) b^2 + 36 A_{11} b^4\right)\left(2+\beta\right)\pi^4}{128 a^3 b^3},$$

$$f_{29} = \frac{3\left(9a^4 A_{22} + 8a^2 \left(A_{12} + 2A_{66}\right) b^2 + 144 A_{11} b^4\right)\left(2+\beta\right)\pi^4}{256 a^3 b^3},$$

$$f_{30} = \frac{\left(9a^4 A_{22} + 5a^2 \left(A_{12} + 2A_{66}\right) b^2 + 36 A_{11} b^4\right)\left(2+\beta\right)\pi^4}{128 a^3 b^3},$$

$$f_{31} = \frac{\left(9a^4 A_{22} + 5a^2 \left(A_{12} + 2A_{66}\right) b^2 + 36 A_{11} b^4\right)\left(2+\beta\right)\pi^4}{64 a^3 b^3},$$

$$f_{32} = -\frac{2\left(1368a^4 A_{22} + 988a^2\left(A_{12} + 2A_{66}\right)b^2 + 14031A_{11}b^4\right)\beta\pi^2}{3675a^3b^3},$$

$$f_{33} = \frac{\left(9a^4 A_{22} + 5a^2\left(A_{12} + 2A_{66}\right)b^2 + 36A_{11}b^4\right)\left(2+\beta\right)\pi^4}{64a^3b^3},$$

$$f_{34} = -\frac{2\left(1368a^4 A_{22} + 988a^2\left(A_{12} + 2A_{66}\right)b^2 + 14031A_{11}b^4\right)\beta\pi^2}{3675a^3b^3},\ f_{35} = 0$$

APPENDIX B

All stiffness terms (A_{ij} and D_{ij}) in the coefficients below denote with the notation $(\ )_0^{t\_sand}$.

$$a_0 = \frac{a^{11} b \bar{m}}{18480},\ a_1 = \frac{a^9 (2+\beta)(33 b^2 A_{11} + a^2 A_{66} \pi^2)}{27720 b},$$

$$a_2 = \frac{a^5 (A_{12} + A_{66}) b^5 (2+\beta)(-15+\pi^2)^2}{8\pi^8},\ a_3 = 0,\ a_4 = 0,\ a_5 = 0,\ a_6 = 0,$$

$$a_7 = -\frac{5a^3 (2+\beta)\left(3a^2 (A_{12} - A_{66})(-63+4\pi^2) + A_{11} b^2 (-15+4\pi^2)\right)}{128 b \pi^2},$$

$$a_8 = -\frac{5a^3 (2+\beta)\left(7a^2 (A_{12} - A_{66})(-12455+912\pi^2) + 20 A_{11} b^2 (-40607+2640\pi^2)\right)}{221184 b \pi^2},$$

$$a_9 = -\frac{5a^3 (2+\beta)\left(3a^2 (A_{12} - A_{66})(-63+4\pi^2) + A_{11} b^2 (-15+4\pi^2)\right)}{128 b \pi^2},$$

$$a_{10} = -\frac{5a^3 (2+\beta)\left(7a^2 (A_{12} - A_{66})(-12455+912\pi^2) + 20 A_{11} b^2 (-40607+2640\pi^2)\right)}{221184 b \pi^2},$$

$$a_{11} = \frac{5a^3 \beta\left(5 A_{11} b^2 (-39935+4512\pi^2) + 14 a^2 \left(1355(-5A_{12} + 6A_{66}) + 84(8A_{12} - 9A_{66})\pi^2\right)\right)}{10368 b \pi^3},$$

$$a_{12} = -\frac{5a^3 (2+\beta)\left(3a^2 (A_{12} - A_{66})(-63+4\pi^2) + A_{11} b^2 (-15+4\pi^2)\right)}{64 b \pi^2},$$

$$a_{13} = \frac{5a^3 \beta\left(5 A_{11} b^2 (-39935+4512\pi^2) + 14 a^2 \left(1355(-5A_{12} + 6A_{66}) + 84(8A_{12} - 9A_{66})\pi^2\right)\right)}{10368 b \pi^3},$$

$$a_{14} = \frac{5a^3 \beta\left(5 A_{11} b^2 (-39935+4512\pi^2) + 14 a^2 \left(1355(-5A_{12} + 6A_{66}) + 84(8A_{12} - 9A_{66})\pi^2\right)\right)}{10368 b \pi^3},$$

$$a_{15} = -\frac{5a^3 (2+\beta)\left(7a^2 (A_{12} - A_{66})(-12455+912\pi^2) + 20 A_{11} b^2 (-40607+2640\pi^2)\right)}{110592 b \pi^2},$$

$$a_{16} = \frac{5a^3 \beta\left(5 A_{11} b^2 (-39935+4512\pi^2) + 14 a^2 \left(1355(-5A_{12} + 6A_{66}) + 84(8A_{12} - 9A_{66})\pi^2\right)\right)}{10368 b \pi^3},$$

$$a_{17} = 0$$

$$b_0=\frac{ab^{11}\overline{m}}{18480},\ b_1=\frac{a^5\left(A_{12}+A_{66}\right)b^5\left(2+\beta\right)\left(-15+\pi^2\right)^2}{8\pi^8},$$

$$b_2=\frac{b^9\left(2+\beta\right)\left(33a^2A_{22}+b^2A_{66}\pi^2\right)}{27720a},$$

$$b_3=0,\ b_4=0,\ b_5=0,\ b_6=0,$$

$$b_7=-\frac{5b^3\left(2+\beta\right)\left(3\left(A_{12}-A_{66}\right)b^2\left(-63+4\pi^2\right)+a^2A_{22}\left(-15+4\pi^2\right)\right)}{128a\pi^2},$$

$$b_8=-\frac{b^3\left(2+\beta\right)\left(15\left(12A_{12}-A_{66}\right)b^2\left(-63+4\pi^2\right)+7a^2A_{22}\left(-15+4\pi^2\right)\right)}{512a\pi^2},$$

$$b_9=-\frac{5b^3\left(2+\beta\right)\left(3\left(A_{12}-A_{66}\right)b^2\left(-63+4\pi^2\right)+a^2A_{22}\left(-15+4\pi^2\right)\right)}{128a\pi^2},$$

$$b_{10}=-\frac{b^3\left(2+\beta\right)\left(15\left(12A_{12}-A_{66}\right)b^2\left(-63+4\pi^2\right)+7a^2A_{22}\left(-15+4\pi^2\right)\right)}{512a\pi^2},$$

$$b_{11}=\frac{5b^3\beta\left(5\left(12A_{12}-17A_{66}\right)b^2\left(-63+4\pi^2\right)+14a^2A_{22}\left(-15+4\pi^2\right)\right)}{2048a\pi^3},$$

$$b_{12}=-\frac{5b^3\left(2+\beta\right)\left(3\left(A_{12}-A_{66}\right)b^2\left(-63+4\pi^2\right)+a^2A_{22}\left(-15+4\pi^2\right)\right)}{64a\pi^2},$$

$$b_{13}=\frac{5b^3\beta\left(5\left(12A_{12}-17A_{66}\right)b^2\left(-63+4\pi^2\right)+14a^2A_{22}\left(-15+4\pi^2\right)\right)}{2048a\pi^3},$$

$$b_{14}=\frac{5b^3\beta\left(5\left(12A_{12}-17A_{66}\right)b^2\left(-63+4\pi^2\right)+14a^2A_{22}\left(-15+4\pi^2\right)\right)}{2048a\pi^3},$$

$$b_{15}=-\frac{b^3\left(2+\beta\right)\left(15\left(12A_{12}-A_{66}\right)b^2\left(-63+4\pi^2\right)+7a^2A_{22}\left(-15+4\pi^2\right)\right)}{256a\pi^2},$$

$$b_{16}=\frac{5b^3\beta\left(5\left(12A_{12}-17A_{66}\right)b^2\left(-63+4\pi^2\right)+14a^2A_{22}\left(-15+4\pi^2\right)\right)}{2048a\pi^3},\ b_{17}=0$$

$$c_0 = \frac{9}{4} ab\overline{m}\,,\; c_1 = 0\,,\; c_2 = 0\,,$$

$$c_3 = \frac{(2+\beta)\pi^2}{4a^3b^3}\begin{pmatrix} -3\beta^2\left(-3b^4 D_{11} + 15a^4 D_{22} + 2a^2b^2\left(7D_{12} + 2D_{66}\right)\right) + \\ 4\left(2+\beta(2+\beta)\right)\left(3b^4 D_{11} + 3a^4 D_{22} + 2a^2b^2\left(D_{12} + 2D_{66}\right)\right)\pi^2 \end{pmatrix},$$

$$c_4 = \frac{\beta\pi}{72a^3b^3}\begin{pmatrix} \beta^2\left(1263b^4 D_{11} + 490a^4 D_{22} + 10a^2b^2\left(83D_{12} + 94D_{66}\right)\right) - \\ 24\left(3+\beta(3+\beta)\right)\left(39b^4 D_{11} + 10a^4 D_{22} + 14a^2b^2\left(D_{12} + 2D_{66}\right)\right)\pi^2 \end{pmatrix},$$

$$c_5 = 0\,,\; c_6 = 0\,,\; c_7 = -\frac{5a^3(2+\beta)\left(3a^2\left(A_{12} - A_{66}\right)\left(-63 + 4\pi^2\right) + A_{11}b^2\left(-15 + 4\pi^2\right)\right)}{64b\pi^2},$$

$$c_8 = \frac{5a^3\beta\left(5A_{11}b^2\left(-39935 + 4512\pi^2\right) + 14a^2\left(1355\left(-5A_{12} + 6A_{66}\right) + 84\left(8A_{12} - 9A_{66}\right)\pi^2\right)\right)}{10368b\pi^3},$$

$$c_9 = -\frac{5a^3(2+\beta)\left(3a^2\left(A_{12} - A_{66}\right)\left(-63 + 4\pi^2\right) + A_{11}b^2\left(-15 + 4\pi^2\right)\right)}{64b\pi^2},$$

$$c_{10} = \frac{5a^3\beta\left(5A_{11}b^2\left(-39935 + 4512\pi^2\right) + 14a^2\left(1355\left(-5A_{12} + 6A_{66}\right) + 84\left(8A_{12} - 9A_{66}\right)\pi^2\right)\right)}{10368b\pi^3},$$

$$c_{11} = \frac{5b^3(2+\beta)\left(a^2 A_{22}\left(15 - 4\pi^2\right) + 3\left(A_{12} - A_{66}\right)b^2\left(63 - 4\pi^2\right)\right)}{64a\pi^2},$$

$$c_{12} = \frac{5b^3\beta\left(5\left(12A_{12} - 17A_{66}\right)b^2\left(-63 + 4\pi^2\right) + 14a^2 A_{22}\left(-15 + 4\pi^2\right)\right)}{2048a\pi^3},$$

$$c_{13} = \frac{5b^3(2+\beta)\left(a^2 A_{22}\left(15 - 4\pi^2\right) + 3\left(A_{12} - A_{66}\right)b^2\left(63 - 4\pi^2\right)\right)}{64a\pi^2},$$

$$c_{14} = \frac{5b^3\beta\left(5\left(12A_{12} - 17A_{66}\right)b^2\left(-63 + 4\pi^2\right) + 14a^2 A_{22}\left(-15 + 4\pi^2\right)\right)}{2048a\pi^3},$$

$$c_{15} = \frac{5\left(21a^4 A_{22} + 10a^2\left(A_{12} + 2A_{66}\right)b^2 + 21A_{11}b^4\right)(2+\beta)\pi^4}{16a^3b^3},$$

$$c_{16} = -\frac{\left(660a^4 A_{22} + 995a^2\left(A_{12} + 2A_{66}\right)b^2 + 3633A_{11}b^4\right)\beta\pi^3}{448a^3b^3},$$

$$c_{17} = \frac{5\left(21a^4 A_{22} + 10a^2\left(A_{12} + 2A_{66}\right)b^2 + 21A_{11}b^4\right)(2+\beta)\pi^4}{16a^3b^3},$$

$$c_{18} = -\frac{\left(660a^4 A_{22} + 995a^2\left(A_{12} + 2A_{66}\right)b^2 + 3633A_{11}b^4\right)\beta\pi^3}{448a^3b^3},$$

$$c_{19}=\frac{7\left(27a^4A_{22}+35a^2\left(A_{12}+2A_{66}\right)b^2+90A_{11}b^4\right)(2+\beta)\pi^4}{32a^3b^3},$$

$$c_{20}=\frac{15\left(21a^4A_{22}+10a^2\left(A_{12}+2A_{66}\right)b^2+21A_{11}b^4\right)(2+\beta)\pi^4}{16a^3b^3},$$

$$c_{21}=\frac{7\left(27a^4A_{22}+35a^2\left(A_{12}+2A_{66}\right)b^2+90A_{11}b^4\right)(2+\beta)\pi^4}{32a^3b^3},$$

$$c_{22}=-\frac{21\left(108a^4A_{22}+85a^2\left(A_{12}+2A_{66}\right)b^2+395A_{11}b^4\right)\beta\pi^3}{320a^3b^3},$$

$$c_{23}=-\frac{21\left(108a^4A_{22}+85a^2\left(A_{12}+2A_{66}\right)b^2+395A_{11}b^4\right)\beta\pi^3}{320a^3b^3},$$

$$c_{24}=-\frac{3\left(660a^4A_{22}+995a^2\left(A_{12}+2A_{66}\right)b^2+3633A_{11}b^4\right)\beta\pi^3}{448a^3b^3},$$

$$c_{25}=\frac{15\left(21a^4A_{22}+10a^2\left(A_{12}+2A_{66}\right)b^2+21A_{11}b^4\right)(2+\beta)\pi^4}{16a^3b^3},$$

$$c_{26}=\frac{7\left(27a^4A_{22}+35a^2\left(A_{12}+2A_{66}\right)b^2+90A_{11}b^4\right)(2+\beta)\pi^4}{32a^3b^3},$$

$$c_{27}=\frac{7\left(27a^4A_{22}+35a^2\left(A_{12}+2A_{66}\right)b^2+90A_{11}b^4\right)(2+\beta)\pi^4}{32a^3b^3},$$

$$c_{28}=-\frac{21\left(108a^4A_{22}+85a^2\left(A_{12}+2A_{66}\right)b^2+395A_{11}b^4\right)\beta\pi^3}{320a^3b^3},$$

$$c_{29}=-\frac{3\left(660a^4A_{22}+995a^2\left(A_{12}+2A_{66}\right)b^2+3633A_{11}b^4\right)\beta\pi^3}{448a^3b^3},$$

$$c_{30}=-\frac{21\left(108a^4A_{22}+85a^2\left(A_{12}+2A_{66}\right)b^2+395A_{11}b^4\right)\beta\pi^3}{320a^3b^3},$$

$$c_{31}=-\frac{21\left(108a^4A_{22}+85a^2\left(A_{12}+2A_{66}\right)b^2+395A_{11}b^4\right)\beta\pi^3}{160a^3b^3},$$

$$c_{32}=\frac{7\left(27a^4A_{22}+35a^2\left(A_{12}+2A_{66}\right)b^2+90A_{11}b^4\right)(2+\beta)\pi^4}{16a^3b^3},$$

$$c_{33}=-\frac{21\left(108a^4A_{22}+85a^2\left(A_{12}+2A_{66}\right)b^2+395A_{11}b^4\right)\beta\pi^3}{160a^3b^3},$$

$$c_{34}=\frac{7\left(27a^4A_{22}+35a^2\left(A_{12}+2A_{66}\right)b^2+90A_{11}b^4\right)(2+\beta)\pi^4}{16a^3b^3},\ c_{35}=-abq_z$$

$$d_0 = \frac{15}{16} ab\overline{m}\,,\ d_1 = 0\,,\ d_2 = 0\,,$$

$$d_3 = \frac{\beta\pi}{72a^3b^3}\left(\begin{array}{l}\beta^2\left(1263b^4D_{11} + 490a^4D_{22} + 10a^2b^2\left(83D_{12} + 94D_{66}\right)\right) - \\ 24\left(3+\beta\left(3+\beta\right)\right)\left(39b^4D_{11} + 10a^4D_{22} + 14a^2b^2\left(D_{12} + 2D_{66}\right)\right)\pi^2\end{array}\right),$$

$$d_4 = \frac{\left(2+\beta\right)\pi^2}{192a^3b^3}\left(\begin{array}{l}-\beta^2\left(7008b^4D_{11} + 665a^4D_{22} + 40a^2b^2\left(73D_{12} + 110D_{66}\right)\right) + \\ 48\left(2+\beta\left(2+\beta\right)\right)\left(60b^4D_{11} + 5a^4D_{22} + 16a^2b^2\left(D_{12} + 2D_{66}\right)\right)\pi^2\end{array}\right),$$

$$d_5 = 0\,,\ d_6 = 0\,,$$

$$d_7 = \frac{5a^3\beta\left(5A_{11}b^2\left(-39935+4512\pi^2\right)+14a^2\left(1355\left(-5A_{12}+6A_{66}\right)+84\left(8A_{12}-9A_{66}\right)\pi^2\right)\right)}{10368b\pi^3},$$

$$d_8 = -\frac{5a^3\left(2+\beta\right)\left(7a^2\left(A_{12}-A_{66}\right)\left(-12455+912\pi^2\right)+20A_{11}b^2\left(-40607+2640\pi^2\right)\right)}{110592b\pi^2},$$

$$d_9 = \frac{5a^3\beta\left(5A_{11}b^2\left(-39935+4512\pi^2\right)+14a^2\left(1355\left(-5A_{12}+6A_{66}\right)+84\left(8A_{12}-9A_{66}\right)\pi^2\right)\right)}{10368b\pi^3},$$

$$d_{10} = -\frac{5a^3\left(2+\beta\right)\left(7a^2\left(A_{12}-A_{66}\right)\left(-12455+912\pi^2\right)+20A_{11}b^2\left(-40607+2640\pi^2\right)\right)}{110592b\pi^2},$$

$$d_{11} = \frac{5b^3\beta\left(5\left(12A_{12}-17A_{66}\right)b^2\left(-63+4\pi^2\right)+14a^2A_{22}\left(-15+4\pi^2\right)\right)}{2048a\pi^3},$$

$$d_{12} = \frac{b^3\left(2+\beta\right)\left(7a^2A_{22}\left(15-4\pi^2\right)+15\left(12A_{12}-A_{66}\right)b^2\left(63-4\pi^2\right)\right)}{256a\pi^2},$$

$$d_{13} = \frac{5b^3\beta\left(5\left(12A_{12}-17A_{66}\right)b^2\left(-63+4\pi^2\right)+14a^2A_{22}\left(-15+4\pi^2\right)\right)}{2048a\pi^3},$$

$$d_{14} = \frac{b^3\left(2+\beta\right)\left(7a^2A_{22}\left(15-4\pi^2\right)+15\left(12A_{12}-A_{66}\right)b^2\left(63-4\pi^2\right)\right)}{256a\pi^2},$$

$$d_{15} = -\frac{7\left(108a^4A_{22}+85a^2\left(A_{12}+2A_{66}\right)b^2+395A_{11}b^4\right)\beta\pi^3}{320a^3b^3},$$

$$d_{16} = \frac{3\left(99a^4A_{22}+200a^2\left(A_{12}+2A_{66}\right)b^2+3360A_{11}b^4\right)\left(2+\beta\right)\pi^4}{256a^3b^3},$$

$$d_{17} = -\frac{7\left(108a^4A_{22}+85a^2\left(A_{12}+2A_{66}\right)b^2+395A_{11}b^4\right)\beta\pi^3}{320a^3b^3},$$

$$d_{18} = \frac{3\left(99a^4 A_{22} + 200a^2 \left(A_{12} + 2A_{66}\right)b^2 + 3360A_{11}b^4\right)\left(2+\beta\right)\pi^4}{256a^3b^3},$$

$$d_{19} = -\frac{3\left(660a^4 A_{22} + 995a^2 \left(A_{12} + 2A_{66}\right)b^2 + 3633A_{11}b^4\right)\beta\pi^3}{448a^3b^3},$$

$$d_{20} = -\frac{21\left(108a^4 A_{22} + 85a^2 \left(A_{12} + 2A_{66}\right)b^2 + 395A_{11}b^4\right)\beta\pi^3}{320a^3b^3},$$

$$d_{21} = -\frac{3\left(660a^4 A_{22} + 995a^2 \left(A_{12} + 2A_{66}\right)b^2 + 3633A_{11}b^4\right)\beta\pi^3}{448a^3b^3},$$

$$d_{22} = \frac{7\left(27a^4 A_{22} + 35a^2 \left(A_{12} + 2A_{66}\right)b^2 + 90A_{11}b^4\right)\left(2+\beta\right)\pi^4}{32a^3b^3},$$

$$d_{23} = \frac{7\left(27a^4 A_{22} + 35a^2 \left(A_{12} + 2A_{66}\right)b^2 + 90A_{11}b^4\right)\left(2+\beta\right)\pi^4}{32a^3b^3},$$

$$d_{24} = \frac{9\left(99a^4 A_{22} + 200a^2 \left(A_{12} + 2A_{66}\right)b^2 + 3360A_{11}b^4\right)\left(2+\beta\right)\pi^4}{256a^3b^3},$$

$$d_{25} = -\frac{21\left(108a^4 A_{22} + 85a^2 \left(A_{12} + 2A_{66}\right)b^2 + 395A_{11}b^4\right)\beta\pi^3}{320a^3b^3},$$

$$d_{26} = -\frac{3\left(660a^4 A_{22} + 995a^2 \left(A_{12} + 2A_{66}\right)b^2 + 3633A_{11}b^4\right)\beta\pi^3}{448a^3b^3},$$

$$d_{27} = -\frac{3\left(660a^4 A_{22} + 995a^2 \left(A_{12} + 2A_{66}\right)b^2 + 3633A_{11}b^4\right)\beta\pi^3}{448a^3b^3},$$

$$d_{28} = \frac{7\left(27a^4 A_{22} + 35a^2 \left(A_{12} + 2A_{66}\right)b^2 + 90A_{11}b^4\right)\left(2+\beta\right)\pi^4}{32a^3b^3},$$

$$d_{29} = \frac{9\left(99a^4 A_{22} + 200a^2 \left(A_{12} + 2A_{66}\right)b^2 + 3360A_{11}b^4\right)\left(2+\beta\right)\pi^4}{256a^3b^3},$$

$$d_{30} = \frac{7\left(27a^4 A_{22} + 35a^2 \left(A_{12} + 2A_{66}\right)b^2 + 90A_{11}b^4\right)\left(2+\beta\right)\pi^4}{32a^3b^3},$$

$$d_{31} = \frac{7\left(27a^4 A_{22} + 35a^2 \left(A_{12} + 2A_{66}\right)b^2 + 90A_{11}b^4\right)\left(2+\beta\right)\pi^4}{16a^3b^3},$$

$$d_{32} = -\frac{3\left(660a^4 A_{22} + 995a^2 \left(A_{12} + 2A_{66}\right)b^2 + 3633A_{11}b^4\right)\beta\pi^3}{224a^3b^3},$$

$$d_{33} = \frac{7\left(27a^4 A_{22} + 35a^2\left(A_{12} + 2A_{66}\right)b^2 + 90A_{11}b^4\right)\left(2+\beta\right)\pi^4}{16a^3b^3},$$

$$d_{34} = -\frac{3\left(660a^4 A_{22} + 995a^2\left(A_{12} + 2A_{66}\right)b^2 + 3633A_{11}b^4\right)\beta\pi^3}{224a^3b^3},\ d_{35} = 0$$

$$e_0 = \frac{9}{4}ab\overline{m},\ e_1 = 0,\ e_2 = 0,\ e_3 = 0,\ e_4 = 0,$$

$$e_5 = \frac{3\left(2+\beta\right)\left(a^2 A_{44}k_{44} + b^2 A_{55}k_{55}\right)\pi^2}{2ab},\ e_6 = -\frac{\beta\left(10a^2 A_{44}k_{44} + 21b^2 A_{55}k_{55}\right)\pi}{12ab},$$

$$e_7 = -\frac{5a^3\left(2+\beta\right)\left(3a^2\left(A_{12} - A_{66}\right)\left(-63 + 4\pi^2\right) + A_{11}b^2\left(-15 + 4\pi^2\right)\right)}{64b\pi^2},$$

$$e_8 = \frac{5a^3\beta\left(5A_{11}b^2\left(-39935 + 4512\pi^2\right) + 14a^2\left(1355\left(-5A_{12} + 6A_{66}\right) + 84\left(8A_{12} - 9A_{66}\right)\pi^2\right)\right)}{10368b\pi^3},$$

$$e_9 = -\frac{5a^3\left(2+\beta\right)\left(3a^2\left(A_{12} - A_{66}\right)\left(-63 + 4\pi^2\right) + A_{11}b^2\left(-15 + 4\pi^2\right)\right)}{64b\pi^2},$$

$$e_{10} = \frac{5a^3\beta\left(5A_{11}b^2\left(-39935 + 4512\pi^2\right) + 14a^2\left(1355\left(-5A_{12} + 6A_{66}\right) + 84\left(8A_{12} - 9A_{66}\right)\pi^2\right)\right)}{10368b\pi^3},$$

$$e_{11} = \frac{5b^3\left(2+\beta\right)\left(a^2 A_{22}\left(15 - 4\pi^2\right) + 3\left(A_{12} - A_{66}\right)b^2\left(63 - 4\pi^2\right)\right)}{64a\pi^2},$$

$$e_{12} = \frac{5b^3\beta\left(5\left(12A_{12} - 17A_{66}\right)b^2\left(-63 + 4\pi^2\right) + 14a^2 A_{22}\left(-15 + 4\pi^2\right)\right)}{2048a\pi^3},$$

$$e_{13} = \frac{5b^3\left(2+\beta\right)\left(a^2 A_{22}\left(15 - 4\pi^2\right) + 3\left(A_{12} - A_{66}\right)b^2\left(63 - 4\pi^2\right)\right)}{64a\pi^2},$$

$$e_{14} = \frac{5b^3\beta\left(5\left(12A_{12} - 17A_{66}\right)b^2\left(-63 + 4\pi^2\right) + 14a^2 A_{22}\left(-15 + 4\pi^2\right)\right)}{2048a\pi^3},$$

$$e_{15} = \frac{5\left(21a^4 A_{22} + 10a^2\left(A_{12} + 2A_{66}\right)b^2 + 21A_{11}b^4\right)\left(2+\beta\right)\pi^4}{16a^3b^3},$$

$$e_{16} = -\frac{\left(660a^4 A_{22} + 995a^2\left(A_{12} + 2A_{66}\right)b^2 + 3633A_{11}b^4\right)\beta\pi^3}{448a^3b^3},$$

$$e_{17} = \frac{5\left(21a^4 A_{22} + 10a^2\left(A_{12} + 2A_{66}\right)b^2 + 21A_{11}b^4\right)\left(2+\beta\right)\pi^4}{16a^3b^3},$$

$$e_{18} = -\frac{\left(660a^4 A_{22} + 995a^2\left(A_{12} + 2A_{66}\right)b^2 + 3633A_{11}b^4\right)\beta\pi^3}{448a^3b^3},$$

$$e_{19} = \frac{7\left(27a^4 A_{22} + 35a^2\left(A_{12} + 2A_{66}\right)b^2 + 90A_{11}b^4\right)\left(2+\beta\right)\pi^4}{32a^3b^3},$$

$$e_{20} = \frac{15\left(21a^4 A_{22} + 10a^2\left(A_{12} + 2A_{66}\right)b^2 + 21A_{11}b^4\right)\beta\pi^4}{16a^3b^3},$$

$$e_{21} = \frac{7\left(27a^4 A_{22} + 35a^2\left(A_{12} + 2A_{66}\right)b^2 + 90A_{11}b^4\right)\left(2+\beta\right)\pi^4}{32a^3b^3},$$

$$e_{22} = -\frac{21\left(108a^4 A_{22} + 85a^2\left(A_{12} + 2A_{66}\right)b^2 + 395A_{11}b^4\right)\beta\pi^3}{320a^3b^3},$$

$$e_{23} = -\frac{21\left(108a^4 A_{22} + 85a^2\left(A_{12} + 2A_{66}\right)b^2 + 395A_{11}b^4\right)\beta\pi^3}{320a^3b^3},$$

$$e_{24} = -\frac{3\left(660a^4 A_{22} + 995a^2\left(A_{12} + 2A_{66}\right)b^2 + 3633A_{11}b^4\right)\beta\pi^3}{448a^3b^3},$$

$$e_{25} = \frac{15\left(21a^4 A_{22} + 10a^2\left(A_{12} + 2A_{66}\right)b^2 + 21A_{11}b^4\right)\left(2+\beta\right)\pi^4}{16a^3b^3},$$

$$e_{26} = \frac{7\left(27a^4 A_{22} + 35a^2\left(A_{12} + 2A_{66}\right)b^2 + 90A_{11}b^4\right)\left(2+\beta\right)\pi^4}{32a^3b^3},$$

$$e_{27} = \frac{7\left(27a^4 A_{22} + 35a^2\left(A_{12} + 2A_{66}\right)b^2 + 90A_{11}b^4\right)\left(2+\beta\right)\pi^4}{32a^3b^3},$$

$$e_{28} = -\frac{21\left(108a^4 A_{22} + 85a^2\left(A_{12} + 2A_{66}\right)b^2 + 395A_{11}b^4\right)\beta\pi^3}{320a^3b^3},$$

$$e_{29} = -\frac{3\left(660a^4 A_{22} + 995a^2\left(A_{12} + 2A_{66}\right)b^2 + 3633A_{11}b^4\right)\beta\pi^3}{448a^3b^3},$$

$$e_{30} = -\frac{21\left(108a^4 A_{22} + 85a^2\left(A_{12} + 2A_{66}\right)b^2 + 395A_{11}b^4\right)\beta\pi^3}{320a^3b^3},$$

$$e_{31} = -\frac{21\left(108a^4 A_{22} + 85a^2\left(A_{12} + 2A_{66}\right)b^2 + 395A_{11}b^4\right)\beta\pi^3}{160a^3b^3},$$

$$e_{32} = \frac{7\left(27a^4 A_{22} + 35a^2\left(A_{12} + 2A_{66}\right)b^2 + 90A_{11}b^4\right)\left(2+\beta\right)\pi^4}{16a^3b^3},$$

$$e_{33} = -\frac{21\left(108a^4 A_{22} + 85a^2\left(A_{12} + 2A_{66}\right)b^2 + 395A_{11}b^4\right)\beta\pi^3}{160a^3b^3},$$

$$e_{34} = \frac{7\left(27a^4 A_{22} + 35a^2\left(A_{12} + 2A_{66}\right)b^2 + 90A_{11}b^4\right)\left(2+\beta\right)\pi^4}{16a^3b^3},\ e_{35} = -abq_z$$

$$f_0 = \frac{15}{16}ab\overline{m},\ f_1 = 0,\ f_2 = 0,\ f_3 = 0,\ f_4 = 0,$$

$$f_5 = -\frac{\beta\left(10a^2 A_{44}k_{44} + 21b^2 A_{55}k_{55}\right)\pi}{12ab},\ f_6 = \frac{\left(2+\beta\right)\left(5a^2 A_{44}k_{44} + 24b^2 A_{55}k_{55}\right)\pi^2}{8ab},$$

$$f_7 = \frac{5a^3\beta\left(5A_{11}b^2\left(-39935 + 4512\pi^2\right) + 14a^2\left(1355\left(-5A_{12} + 6A_{66}\right) + 84\left(8A_{12} - 9A_{66}\right)\pi^2\right)\right)}{10368b\pi^3},$$

$$f_8 = -\frac{5a^3\left(2+\beta\right)\left(7a^2\left(A_{12} - A_{66}\right)\left(-12455 + 912\pi^2\right) + 20A_{11}b^2\left(-40607 + 2640\pi^2\right)\right)}{110592b\pi^2},$$

$$f_9 = \frac{5a^3\beta\left(5A_{11}b^2\left(-39935 + 4512\pi^2\right) + 14a^2\left(1355\left(-5A_{12} + 6A_{66}\right) + 84\left(8A_{12} - 9A_{66}\right)\pi^2\right)\right)}{10368b\pi^3},$$

$$f_{10} = -\frac{5a^3\left(2+\beta\right)\left(7a^2\left(A_{12} - A_{66}\right)\left(-12455 + 912\pi^2\right) + 20A_{11}b^2\left(-40607 + 2640\pi^2\right)\right)}{110592b\pi^2},$$

$$f_{11} = \frac{5b^3\beta\left(5\left(12A_{12} - 17A_{66}\right)b^2\left(-63 + 4\pi^2\right) + 14a^2 A_{22}\left(-15 + 4\pi^2\right)\right)}{2048a\pi^3},$$

$$f_{12} = \frac{b^3\left(2+\beta\right)\left(7a^2 A_{22}\left(15 - 4\pi^2\right) + 15\left(12A_{12} - A_{66}\right)b^2\left(63 - 4\pi^2\right)\right)}{256a\pi^2},$$

$$f_{13} = \frac{5b^3\beta\left(5\left(12A_{12} - 17A_{66}\right)b^2\left(-63 + 4\pi^2\right) + 14a^2 A_{22}\left(-15 + 4\pi^2\right)\right)}{2048a\pi^3},$$

$$f_{14} = \frac{b^3\left(2+\beta\right)\left(7a^2 A_{22}\left(15 - 4\pi^2\right) + 15\left(12A_{12} - A_{66}\right)b^2\left(63 - 4\pi^2\right)\right)}{256a\pi^2},$$

$$f_{15} = -\frac{7\left(108a^4 A_{22} + 85a^2\left(A_{12} + 2A_{66}\right)b^2 + 395A_{11}b^4\right)\beta\pi^3}{320a^3b^3},$$

$$f_{16} = \frac{3\left(99a^4 A_{22} + 200a^2\left(A_{12} + 2A_{66}\right)b^2 + 3360A_{11}b^4\right)\left(2+\beta\right)\pi^4}{256a^3b^3},$$

$$f_{17} = -\frac{7\left(108a^4 A_{22} + 85a^2\left(A_{12} + 2A_{66}\right)b^2 + 395A_{11}b^4\right)\beta\pi^3}{320a^3b^3},$$

$$f_{18}=\frac{3\left(99a^4A_{22}+200a^2\left(A_{12}+2A_{66}\right)b^2+3360A_{11}b^4\right)\left(2+\beta\right)\pi^4}{256a^3b^3},$$

$$f_{19}=-\frac{3\left(660a^4A_{22}+995a^2\left(A_{12}+2A_{66}\right)b^2+3633A_{11}b^4\right)\beta\pi^3}{448a^3b^3},$$

$$f_{20}=-\frac{21\left(108a^4A_{22}+85a^2\left(A_{12}+2A_{66}\right)b^2+395A_{11}b^4\right)\beta\pi^3}{320a^3b^3},$$

$$f_{21}=-\frac{3\left(660a^4A_{22}+995a^2\left(A_{12}+2A_{66}\right)b^2+3633A_{11}b^4\right)\beta\pi^3}{448a^3b^3},$$

$$f_{22}=\frac{7\left(27a^4A_{22}+35a^2\left(A_{12}+2A_{66}\right)b^2+90A_{11}b^4\right)\left(2+\beta\right)\pi^4}{32a^3b^3},$$

$$f_{23}=\frac{7\left(27a^4A_{22}+35a^2\left(A_{12}+2A_{66}\right)b^2+90A_{11}b^4\right)\left(2+\beta\right)\pi^4}{32a^3b^3},$$

$$f_{24}=\frac{9\left(99a^4A_{22}+200a^2\left(A_{12}+2A_{66}\right)b^2+3360A_{11}b^4\right)\left(2+\beta\right)\pi^4}{256a^3b^3},$$

$$f_{25}=-\frac{21\left(108a^4A_{22}+85a^2\left(A_{12}+2A_{66}\right)b^2+395A_{11}b^4\right)\beta\pi^3}{320a^3b^3},$$

$$f_{26}=-\frac{3\left(660a^4A_{22}+995a^2\left(A_{12}+2A_{66}\right)b^2+3633A_{11}b^4\right)\beta\pi^3}{448a^3b^3},$$

$$f_{27}=-\frac{3\left(660a^4A_{22}+995a^2\left(A_{12}+2A_{66}\right)b^2+3633A_{11}b^4\right)\beta\pi^3}{448a^3b^3},$$

$$f_{28}=\frac{7\left(27a^4A_{22}+35a^2\left(A_{12}+2A_{66}\right)b^2+90A_{11}b^4\right)\left(2+\beta\right)\pi^4}{32a^3b^3},$$

$$f_{29}=\frac{9\left(99a^4A_{22}+200a^2\left(A_{12}+2A_{66}\right)b^2+3360A_{11}b^4\right)\left(2+\beta\right)\pi^4}{256a^3b^3},$$

$$f_{30}=\frac{7\left(27a^4A_{22}+35a^2\left(A_{12}+2A_{66}\right)b^2+90A_{11}b^4\right)\left(2+\beta\right)\pi^4}{32a^3b^3},$$

$$f_{31}=\frac{7\left(27a^4A_{22}+35a^2\left(A_{12}+2A_{66}\right)b^2+90A_{11}b^4\right)\left(2+\beta\right)\pi^4}{16a^3b^3},$$

$$f_{32}=-\frac{3\left(660a^4A_{22}+995a^2\left(A_{12}+2A_{66}\right)b^2+3633A_{11}b^4\right)\beta\pi^3}{224a^3b^3},$$

$$f_{33} = \frac{7\left(27a^4 A_{22} + 35a^2\left(A_{12} + 2A_{66}\right)b^2 + 90A_{11}b^4\right)\left(2+\beta\right)\pi^4}{16a^3b^3},$$

$$f_{34} = -\frac{3\left(660a^4 A_{22} + 995a^2\left(A_{12} + 2A_{66}\right)b^2 + 3633A_{11}b^4\right)\beta\pi^3}{224a^3b^3},\ f_{35} = 0$$

APPENDIX C

h_c in the coefficients below denote with the notation $(\ )_0$. c_3, c_4, d_3 and d_4 below are obtained for face sheets which are made of two symmetrical layers.

$$a_0 = \frac{a^{11} b \bar{m}}{18480},\ a_1 = \frac{a^9\left(33b^2 A_{11} + a^2 A_{66}\pi^2\right)}{13860b},\ a_2 = \frac{a^5\left(A_{12}+A_{66}\right)b^5\left(-15+\pi^2\right)^2}{4\pi^8},\ a_3 = 0,$$

$$a_4 = 0,\ a_5 = 0,\ a_6 = 0,\ a_7 = -\frac{5a^3\left(3a^2\left(A_{12}-A_{66}\right)\left(-63+4\pi^2\right)+A_{11}b^2\left(-15+4\pi^2\right)\right)}{64b\pi^2},$$

$$a_8 = -\frac{5a^3\left(7a^2\left(A_{12}-A_{66}\right)\left(-12455+912\pi^2\right)+20A_{11}b^2\left(-40607+2640\pi^2\right)\right)}{110592b\pi^2},$$

$$a_9 = -\frac{5a^3\left(3a^2\left(A_{12}-A_{66}\right)\left(-63+4\pi^2\right)+A_{11}b^2\left(-15+4\pi^2\right)\right)}{64b\pi^2},$$

$$a_{10} = -\frac{5a^3\left(7a^2\left(A_{12}-A_{66}\right)\left(-12455+912\pi^2\right)+20A_{11}b^2\left(-40607+2640\pi^2\right)\right)}{110592b\pi^2},\ a_{11} = 0,$$

$$a_{12} = -\frac{5a^3\left(3a^2\left(A_{12}-A_{66}\right)\left(-63+4\pi^2\right)+A_{11}b^2\left(-15+4\pi^2\right)\right)}{32b\pi^2},\ a_{13} = 0,\ a_{14} = 0,$$

$$a_{15} = -\frac{5a^3\left(7a^2\left(A_{12}-A_{66}\right)\left(-12455+912\pi^2\right)+20A_{11}b^2\left(-40607+2640\pi^2\right)\right)}{55296b\pi^2},\ a_{16} = 0,$$

$$a_{17} = 0$$

$$b_0 = \frac{ab^{11}\bar{m}}{18480},\ b_1 = \frac{a^5\left(A_{12}+A_{66}\right)b^5\left(-15+\pi^2\right)^2}{4\pi^8},\ b_2 = \frac{b^9\left(33a^2 A_{22} + b^2 A_{66}\pi^2\right)}{13860a},$$

$$b_3 = 0,\ b_4 = 0,\ b_5 = 0,\ b_6 = 0,$$

$$b_7 = \frac{5b^3\left(a^2 A_{22}\left(15-4\pi^2\right)+3\left(A_{12}-A_{66}\right)b^2\left(63-4\pi^2\right)\right)}{64a\pi^2},$$

$$b_8 = \frac{b^3\left(7a^2 A_{22}\left(15-4\pi^2\right)+15\left(12A_{12}-A_{66}\right)b^2\left(63-4\pi^2\right)\right)}{256a\pi^2},$$

$$b_9 = \frac{5b^3\left(a^2 A_{22}\left(15-4\pi^2\right)+3\left(A_{12}-A_{66}\right)b^2\left(63-4\pi^2\right)\right)}{64a\pi^2},$$

$$b_{10} = \frac{b^3\left(7a^2 A_{22}\left(15-4\pi^2\right)+15\left(12A_{12}-A_{66}\right)b^2\left(63-4\pi^2\right)\right)}{256a\pi^2},\ b_{11} = 0,$$

$$b_{12} = \frac{5b^3\left(a^2A_{22}\left(15-4\pi^2\right)+3\left(A_{12}-A_{66}\right)b^2\left(63-4\pi^2\right)\right)}{32a\pi^2},\ b_{13}=0,\ b_{14}=0,$$

$$b_{15} = \frac{b^3\left(7a^2A_{22}\left(15-4\pi^2\right)+15\left(12A_{12}-A_{66}\right)b^2\left(63-4\pi^2\right)\right)}{128a\pi^2},\ b_{16}=0,\ b_{17}=0$$

$$c_0 = \frac{9}{4}ab\overline{m},\ c_1=0,\ c_2=0,$$

$$\begin{aligned}
c_3 = \frac{1}{12a^3b^3}\pi^2(&3b^4(3\left(A_{11}^{f_{B1}}+A_{11}^{f_{B2}}\right)\beta^2h_c^2+8(A_{11}^{f_{B1}}\left(\left(3+\beta\left(3+\beta\right)\right)h_c^2+3\left(2+\beta\right)h_ch_{f_{B1}}+4h_{f_{B1}}^2\right)+\\
&A_{11}^{f_{B2}}\left(\left(3+\beta\left(3+\beta\right)\right)h_c^2+3\left(2+\beta\right)h_c\left(2h_{f_{B1}}+h_{f_{B2}}\right)+4\left(3h_{f_{B1}}^2+3h_{f_{B1}}h_{f_{B2}}+h_{f_{B2}}^2\right)\right))\pi^2)+\\
&a^4(-45\left(A_{22}^{f_{B1}}+A_{22}^{f_{B2}}\right)\beta^2h_c^2+24(A_{22}^{f_{B1}}\left(\left(3+\beta\left(3+\beta\right)\right)h_c^2+3\left(2+\beta\right)h_ch_{f_{B1}}+4h_{f_{B1}}^2\right)+\\
&A_{22}^{f_{B2}}\left(\left(3+\beta\left(3+\beta\right)\right)h_c^2+3\left(2+\beta\right)h_c\left(2h_{f_{B1}}+h_{f_{B2}}\right)+4\left(3h_{f_{B1}}^2+3h_{f_{B1}}h_{f_{B2}}+h_{f_{B2}}^2\right)\right))\pi^2)+\\
&2a^2b^2(A_{12}^{f_{B1}}\left(-21\beta^2h_c^2+8\left(\left(3+\beta\left(3+\beta\right)\right)h_c^2+3\left(2+\beta\right)h_ch_{f_{B1}}+4h_{f_{B1}}^2\right)\pi^2\right)+\\
&A_{12}^{f_{B2}}\left(-21\beta^2h_c^2+8\left(\left(3+\beta\left(3+\beta\right)\right)h_c^2+3\left(2+\beta\right)h_c\left(2h_{f_{B1}}+h_{f_{B2}}\right)+4\left(3h_{f_{B1}}^2+3h_{f_{B1}}h_{f_{B2}}+h_{f_{B2}}^2\right)\right)\pi^2\right)+\\
&2(-3\left(A_{66}^{f_{B1}}+A_{66}^{f_{B2}}\right)\beta^2h_c^2+8(A_{66}^{f_{B1}}\left(\left(3+\beta\left(3+\beta\right)\right)h_c^2+3\left(2+\beta\right)h_ch_{f_{B1}}+4h_{f_{B1}}^2\right)+\\
&A_{66}^{f_{B2}}\left(\left(3+\beta\left(3+\beta\right)\right)h_c^2+3\left(2+\beta\right)h_c\left(2h_{f_{B1}}+h_{f_{B2}}\right)+4\left(3h_{f_{B1}}^2+3h_{f_{B1}}h_{f_{B2}}+h_{f_{B2}}^2\right)\right))\pi^2)))
\end{aligned}$$

,

$$\begin{aligned}
c_4 = -\frac{1}{6a^3b^3}\beta h_c(&39b^4\left(A_{11}^{f_{B1}}\left(2+\beta\right)h_c+2A_{11}^{f_{B1}}h_{f_{B1}}+A_{11}^{f_{B2}}\left(\left(2+\beta\right)h_c+2\left(2h_{f_{B1}}+h_{f_{B2}}\right)\right)\right)+\\
&10a^4\left(A_{22}^{f_{B1}}\left(2+\beta\right)h_c+2A_{22}^{f_{B1}}h_{f_{B1}}+A_{22}^{f_{B2}}\left(\left(2+\beta\right)h_c+2\left(2h_{f_{B1}}+h_{f_{B2}}\right)\right)\right)+\\
&14a^2b^2(A_{12}^{f_{B1}}\left(2+\beta\right)h_c+2A_{12}^{f_{B1}}h_{f_{B1}}+A_{12}^{f_{B2}}\left(\left(2+\beta\right)h_c+2\left(2h_{f_{B1}}+h_{f_{B2}}\right)\right)+\\
&2\left(A_{66}^{f_{B1}}\left(2+\beta\right)h_c+2A_{66}^{f_{B1}}h_{f_{B1}}+A_{66}^{f_{B2}}\left(\left(2+\beta\right)h_c+2\left(2h_{f_{B1}}+h_{f_{B2}}\right)\right)\right)))\pi^3
\end{aligned}$$

$$,\ c_5=0,\ c_6=0,\ c_7=-\frac{5a^3\left(3a^2\left(A_{12}-A_{66}\right)\left(-63+4\pi^2\right)+A_{11}b^2\left(-15+4\pi^2\right)\right)}{32b\pi^2},\ c_8=0,$$

$$c_9=-\frac{5a^3\left(3a^2\left(A_{12}-A_{66}\right)\left(-63+4\pi^2\right)+A_{11}b^2\left(-15+4\pi^2\right)\right)}{32b\pi^2},\ c_{10}=0,$$

$$c_{11}=\frac{5b^3\left(a^2A_{22}\left(15-4\pi^2\right)+3\left(A_{12}-A_{66}\right)b^2\left(63-4\pi^2\right)\right)}{32a\pi^2},\ c_{12}=0,$$

$$c_{13}=\frac{5b^3\left(a^2A_{22}\left(15-4\pi^2\right)+3\left(A_{12}-A_{66}\right)b^2\left(63-4\pi^2\right)\right)}{32a\pi^2},\ c_{14}=0,$$

$$c_{15}=\frac{5\left(21a^4A_{22}+10a^2\left(A_{12}+2A_{66}\right)b^2+21A_{11}b^4\right)\pi^4}{8a^3b^3},\ c_{16}=0,$$

$$c_{17}=\frac{5\left(21a^4A_{22}+10a^2\left(A_{12}+2A_{66}\right)b^2+21A_{11}b^4\right)\pi^4}{8a^3b^3},\ c_{18}=0,$$

$$c_{19}=\frac{7\left(27a^4A_{22}+35a^2\left(A_{12}+2A_{66}\right)b^2+90A_{11}b^4\right)\pi^4}{16a^3b^3},$$

$$c_{20}=\frac{15\left(21a^4A_{22}+10a^2\left(A_{12}+2A_{66}\right)b^2+21A_{11}b^4\right)\pi^4}{8a^3b^3},$$

$$c_{21}=\frac{7\left(27a^4A_{22}+35a^2\left(A_{12}+2A_{66}\right)b^2+90A_{11}b^4\right)\pi^4}{16a^3b^3},\ c_{22}=0,\ c_{23}=0,\ c_{24}=0,$$

$$c_{25}=\frac{15\left(21a^4A_{22}+10a^2\left(A_{12}+2A_{66}\right)b^2+21A_{11}b^4\right)\pi^4}{8a^3b^3},$$

$$c_{26}=\frac{7\left(27a^4A_{22}+35a^2\left(A_{12}+2A_{66}\right)b^2+90A_{11}b^4\right)\pi^4}{16a^3b^3},$$

$$c_{27}=\frac{7\left(27a^4A_{22}+35a^2\left(A_{12}+2A_{66}\right)b^2+90A_{11}b^4\right)\pi^4}{16a^3b^3},\ c_{28}=0,\ c_{29}=0,\ c_{30}=0,$$

$$c_{31}=0,\ c_{32}=\frac{7\left(27a^4A_{22}+35a^2\left(A_{12}+2A_{66}\right)b^2+90A_{11}b^4\right)\pi^4}{8a^3b^3},\ c_{33}=0,$$

$$c_{34}=\frac{7\left(27a^4A_{22}+35a^2\left(A_{12}+2A_{66}\right)b^2+90A_{11}b^4\right)\pi^4}{8a^3b^3},\ c_{35}=-abq_z$$

$$d_0=\frac{15}{16}ab\overline{m},\ d_1=0,\ d_2=0,$$

$$\begin{aligned}d_3=&-\frac{1}{6a^3b^3}\beta h_c(39b^4\left(A_{11}^{f_{B1}}\left(2+\beta\right)h_c+2A_{11}^{f_{B1}}h_{f_{B1}}+A_{11}^{f_{B2}}\left(\left(2+\beta\right)h_c+2\left(2h_{f_{B1}}+h_{f_{B2}}\right)\right)\right)+\\&10a^4\left(A_{22}^{f_{B1}}\left(2+\beta\right)h_c+2A_{22}^{f_{B1}}h_{f_{B1}}+A_{22}^{f_{B2}}\left(\left(2+\beta\right)h_c+2\left(2h_{f_{B1}}+h_{f_{B2}}\right)\right)\right)+\\&14a^2b^2(A_{12}^{f_{B1}}\left(2+\beta\right)h_c+2A_{12}^{f_{B1}}h_{f_{B1}}+A_{12}^{f_{B2}}\left(\left(2+\beta\right)h_c+2\left(2h_{f_{B1}}+h_{f_{B2}}\right)\right)+\\&2\left(A_{66}^{f_{B1}}\left(2+\beta\right)h_c+2A_{66}^{f_{B1}}h_{f_{B1}}+A_{66}^{f_{B2}}\left(\left(2+\beta\right)h_c+2\left(2h_{f_{B1}}+h_{f_{B2}}\right)\right)\right)))\pi^3\end{aligned}$$

,

$$d_4=\frac{1}{576a^3b^3}\pi^2(96b^4(-73\left(A_{11}^{f_{B1}}+A_{11}^{f_{B2}}\right)\beta^2h_c^2+60(A_{11}^{f_{B1}}\left(\left(3+\beta\left(3+\beta\right)\right)h_c^2+3\left(2+\beta\right)h_ch_{f_{B1}}+4h_{f_{B1}}^2\right)+$$
$$A_{11}^{f_{B2}}\left(\left(3+\beta\left(3+\beta\right)\right)h_c^2+3\left(2+\beta\right)h_c\left(2h_{f_{B1}}+h_{f_{B2}}\right)+4\left(3h_{f_{B1}}^2+3h_{f_{B1}}h_{f_{B2}}+h_{f_{B2}}^2\right)\right))\pi^2)+$$
$$5a^4(-133\left(A_{22}^{f_{B1}}+A_{22}^{f_{B2}}\right)\beta^2h_c^2+96(A_{22}^{f_{B1}}\left(\left(3+\beta\left(3+\beta\right)\right)h_c^2+3\left(2+\beta\right)h_ch_{f_{B1}}+4h_{f_{B1}}^2\right)+$$
$$A_{22}^{f_{B2}}\left(\left(3+\beta\left(3+\beta\right)\right)h_c^2+3\left(2+\beta\right)h_c\left(2h_{f_{B1}}+h_{f_{B2}}\right)+4\left(3h_{f_{B1}}^2+3h_{f_{B1}}h_{f_{B2}}+h_{f_{B2}}^2\right)\right))\pi^2)+$$
$$8a^2b^2(A_{12}^{f_{B1}}\left(-365\beta^2h_c^2+192\left(\left(3+\beta\left(3+\beta\right)\right)h_c^2+3\left(2+\beta\right)h_ch_{f_{B1}}+4h_{f_{B1}}^2\right)\pi^2\right)+$$
$$A_{12}^{f_{B2}}\left(-365\beta^2h_c^2+192\left(\left(3+\beta\left(3+\beta\right)\right)h_c^2+3\left(2+\beta\right)h_c\left(2h_{f_{B1}}+h_{f_{B2}}\right)+4\left(3h_{f_{B1}}^2+3h_{f_{B1}}h_{f_{B2}}+h_{f_{B2}}^2\right)\right)\pi^2\right)+$$
$$2(-275\left(A_{66}^{f_{B1}}+A_{66}^{f_{B2}}\right)\beta^2h_c^2+192(A_{66}^{f_{B1}}\left(\left(3+\beta\left(3+\beta\right)\right)h_c^2+3\left(2+\beta\right)h_ch_{f_{B1}}+4h_{f_{B1}}^2\right)+$$
$$A_{66}^{f_{B2}}\left(\left(3+\beta\left(3+\beta\right)\right)h_c^2+3\left(2+\beta\right)h_c\left(2h_{f_{B1}}+h_{f_{B2}}\right)+4\left(3h_{f_{B1}}^2+3h_{f_{B1}}h_{f_{B2}}+h_{f_{B2}}^2\right)\right))\pi^2)))$$

, $d_5=0$, $d_6=0$, $d_7=0$,

$$d_8=-\frac{5a^3\left(7a^2\left(A_{12}-A_{66}\right)\left(-12455+912\pi^2\right)+20A_{11}b^2\left(-40607+2640\pi^2\right)\right)}{55296b\pi^2},\ d_9=0,$$

$$d_{10}=-\frac{5a^3\left(7a^2\left(A_{12}-A_{66}\right)\left(-12455+912\pi^2\right)+20A_{11}b^2\left(-40607+2640\pi^2\right)\right)}{55296b\pi^2},\ d_{11}=0,$$

$$d_{12}=\frac{b^3\left(7a^2A_{22}\left(15-4\pi^2\right)+15\left(12A_{12}-A_{66}\right)b^2\left(63-4\pi^2\right)\right)}{128a\pi^2},\ d_{13}=0,$$

$$d_{14}=\frac{b^3\left(7a^2A_{22}\left(15-4\pi^2\right)+15\left(12A_{12}-A_{66}\right)b^2\left(63-4\pi^2\right)\right)}{128a\pi^2},\ d_{15}=0,$$

$$d_{16}=\frac{3\left(99a^4A_{22}+200a^2\left(A_{12}+2A_{66}\right)b^2+3360A_{11}b^4\right)\pi^4}{128a^3b^3},\ d_{17}=0,$$

$$d_{18}=\frac{3\left(99a^4A_{22}+200a^2\left(A_{12}+2A_{66}\right)b^2+3360A_{11}b^4\right)\pi^4}{128a^3b^3},\ d_{19}=0,\ d_{20}=0,\ d_{21}=0,$$

$$d_{22}=\frac{7\left(27a^4A_{22}+35a^2\left(A_{12}+2A_{66}\right)b^2+90A_{11}b^4\right)\pi^4}{16a^3b^3},$$

$$d_{23}=\frac{7\left(27a^4A_{22}+35a^2\left(A_{12}+2A_{66}\right)b^2+90A_{11}b^4\right)\pi^4}{16a^3b^3},$$

$$d_{24}=\frac{9\left(99a^4A_{22}+200a^2\left(A_{12}+2A_{66}\right)b^2+3360A_{11}b^4\right)\pi^4}{128a^3b^3},\ d_{25}=0,\ d_{26}=0,\ d_{27}=0,$$

$$d_{28}=\frac{7\left(27a^4A_{22}+35a^2\left(A_{12}+2A_{66}\right)b^2+90A_{11}b^4\right)\pi^4}{16a^3b^3},$$

$$d_{29} = \frac{9\left(99a^4 A_{22} + 200a^2\left(A_{12} + 2A_{66}\right)b^2 + 3360 A_{11} b^4\right)\pi^4}{128a^3 b^3},$$

$$d_{30} = \frac{7\left(27a^4 A_{22} + 35a^2\left(A_{12} + 2A_{66}\right)b^2 + 90 A_{11} b^4\right)\pi^4}{16a^3 b^3},$$

$$d_{31} = \frac{7\left(27a^4 A_{22} + 35a^2\left(A_{12} + 2A_{66}\right)b^2 + 90 A_{11} b^4\right)\pi^4}{8a^3 b^3},\ d_{32} = 0,$$

$$d_{33} = \frac{7\left(27a^4 A_{22} + 35a^2\left(A_{12} + 2A_{66}\right)b^2 + 90 A_{11} b^4\right)\pi^4}{8a^3 b^3},\ d_{34} = 0,\ d_{35} = 0$$

$$e_0 = \frac{9}{4}ab\overline{m},\ e_1 = 0,\ e_2 = 0,\ e_3 = 0,\ e_4 = 0,$$

$$e_5 = \frac{48a^4\left(A_{44}\right)_0 b^2\left(2+\beta\right)k_{44}\pi^4 + 48a^2\left(A_{55}\right)_0 b^4\left(2+\beta\right)k_{55}\pi^4}{32a^3 b^3 \pi^2},$$

$$e_6 = -\frac{\beta\left(10a^2\left(A_{44}\right)_0 k_{44} + 21b^2\left(A_{55}\right)_0 k_{55}\right)\pi}{12ab},$$

$$e_7 = -\frac{5a^3\left(3a^2\left(A_{12} - A_{66}\right)\left(-63 + 4\pi^2\right) + A_{11}b^2\left(-15 + 4\pi^2\right)\right)}{32b\pi^2},\ e_8 = 0,$$

$$e_9 = -\frac{5a^3\left(3a^2\left(A_{12} - A_{66}\right)\left(-63 + 4\pi^2\right) + A_{11}b^2\left(-15 + 4\pi^2\right)\right)}{32b\pi^2},\ e_{10} = 0,$$

$$e_{11} = \frac{5b^3\left(a^2 A_{22}\left(15 - 4\pi^2\right) + 3\left(A_{12} - A_{66}\right)b^2\left(63 - 4\pi^2\right)\right)}{32a\pi^2},\ e_{12} = 0,$$

$$e_{13} = \frac{5b^3\left(a^2 A_{22}\left(15 - 4\pi^2\right) + 3\left(A_{12} - A_{66}\right)b^2\left(63 - 4\pi^2\right)\right)}{32a\pi^2},\ e_{14} = 0,$$

$$e_{15} = \frac{5\left(21a^4 A_{22} + 10a^2\left(A_{12} + 2A_{66}\right)b^2 + 21A_{11}b^4\right)\pi^4}{8a^3 b^3},\ e_{16} = 0,$$

$$e_{17} = \frac{5\left(21a^4 A_{22} + 10a^2\left(A_{12} + 2A_{66}\right)b^2 + 21A_{11}b^4\right)\pi^4}{8a^3 b^3},\ e_{18} = 0,$$

$$e_{19} = \frac{7\left(27a^4 A_{22} + 35a^2\left(A_{12} + 2A_{66}\right)b^2 + 90 A_{11} b^4\right)\pi^4}{16a^3 b^3},$$

$$e_{20} = \frac{15\left(21a^4 A_{22} + 10a^2\left(A_{12} + 2A_{66}\right)b^2 + 21A_{11}b^4\right)\pi^4}{8a^3 b^3},$$

$$e_{21}=\frac{7\left(27a^4A_{22}+35a^2\left(A_{12}+2A_{66}\right)b^2+90A_{11}b^4\right)\pi^4}{16a^3b^3},\ e_{22}=0,\ e_{23}=0,\ e_{24}=0,$$

$$e_{25}=\frac{15\left(21a^4A_{22}+10a^2\left(A_{12}+2A_{66}\right)b^2+21A_{11}b^4\right)\pi^4}{8a^3b^3},$$

$$e_{26}=\frac{7\left(27a^4A_{22}+35a^2\left(A_{12}+2A_{66}\right)b^2+90A_{11}b^4\right)\pi^4}{16a^3b^3},$$

$$e_{27}=\frac{7\left(27a^4A_{22}+35a^2\left(A_{12}+2A_{66}\right)b^2+90A_{11}b^4\right)\pi^4}{16a^3b^3},\ e_{28}=0,\ e_{29}=0,\ e_{30}=0,$$

$$e_{31}=0,\ e_{32}=\frac{7\left(27a^4A_{22}+35a^2\left(A_{12}+2A_{66}\right)b^2+90A_{11}b^4\right)\pi^4}{8a^3b^3},\ e_{33}=0,$$

$$e_{34}=\frac{7\left(27a^4A_{22}+35a^2\left(A_{12}+2A_{66}\right)b^2+90A_{11}b^4\right)\pi^4}{8a^3b^3},\ e_{35}=-abq_z$$

$$f_0=\frac{15}{16}ab\overline{m},\ f_1=0,\ f_2=0,\ f_3=0,\ f_4=0,$$

$$f_5=-\frac{\beta\left(10a^2\left(A_{44}\right)_0k_{44}+21b^2\left(A_{55}\right)_0k_{55}\right)\pi}{12ab},$$

$$f_6=\frac{34560a^4\left(A_{44}\right)_0b^2\left(2+\beta\right)k_{44}\pi^4+165888a^2\left(A_{55}\right)_0b^4\left(2+\beta\right)k_{55}\pi^4}{55296a^3b^3\pi^2},\ f_7=0,$$

$$f_8=-\frac{5a^3\left(7a^2\left(A_{12}-A_{66}\right)\left(-12455+912\pi^2\right)+20A_{11}b^2\left(-40607+2640\pi^2\right)\right)}{55296b\pi^2},\ f_9=0,$$

$$f_{10}=-\frac{5a^3\left(7a^2\left(A_{12}-A_{66}\right)\left(-12455+912\pi^2\right)+20A_{11}b^2\left(-40607+2640\pi^2\right)\right)}{55296b\pi^2},$$

$$f_{11}=0,\ f_{12}=\frac{b^3\left(7a^2A_{22}\left(15-4\pi^2\right)+15\left(12A_{12}-A_{66}\right)b^2\left(63-4\pi^2\right)\right)}{128a\pi^2},\ f_{13}=0,$$

$$f_{14}=\frac{b^3\left(7a^2A_{22}\left(15-4\pi^2\right)+15\left(12A_{12}-A_{66}\right)b^2\left(63-4\pi^2\right)\right)}{128a\pi^2},\ f_{15}=0,$$

$$f_{16}=\frac{3\left(99a^4A_{22}+200a^2\left(A_{12}+2A_{66}\right)b^2+3360A_{11}b^4\right)\pi^4}{128a^3b^3},\ f_{17}=0,$$

$$f_{18}=\frac{3\left(99a^4A_{22}+200a^2\left(A_{12}+2A_{66}\right)b^2+3360A_{11}b^4\right)\pi^4}{128a^3b^3},\ f_{19}=0,\ f_{20}=0,\ f_{21}=0,$$

$$f_{22}=\frac{7\left(27a^4A_{22}+35a^2\left(A_{12}+2A_{66}\right)b^2+90A_{11}b^4\right)\pi^4}{16a^3b^3},$$

$$f_{23}=\frac{7\left(27a^4A_{22}+35a^2\left(A_{12}+2A_{66}\right)b^2+90A_{11}b^4\right)\pi^4}{16a^3b^3},$$

$$f_{24}=\frac{9\left(99a^4A_{22}+200a^2\left(A_{12}+2A_{66}\right)b^2+3360A_{11}b^4\right)\pi^4}{128a^3b^3},\ f_{25}=0,\ f_{26}=0,\ f_{27}=0,$$

$$f_{28}=\frac{7\left(27a^4A_{22}+35a^2\left(A_{12}+2A_{66}\right)b^2+90A_{11}b^4\right)\pi^4}{16a^3b^3},$$

$$f_{29}=\frac{9\left(99a^4A_{22}+200a^2\left(A_{12}+2A_{66}\right)b^2+3360A_{11}b^4\right)\pi^4}{128a^3b^3},$$

$$f_{30}=\frac{7\left(27a^4A_{22}+35a^2\left(A_{12}+2A_{66}\right)b^2+90A_{11}b^4\right)\pi^4}{16a^3b^3},$$

$$f_{31}=\frac{7\left(27a^4A_{22}+35a^2\left(A_{12}+2A_{66}\right)b^2+90A_{11}b^4\right)\pi^4}{8a^3b^3},\ f_{32}=0,$$

$$f_{33}=\frac{7\left(27a^4A_{22}+35a^2\left(A_{12}+2A_{66}\right)b^2+90A_{11}b^4\right)\pi^4}{8a^3b^3},\ f_{34}=0,\ f_{35}=0$$

APPENDIX D

$$A_1 = \frac{a_0}{\left(\Delta t\right)^2} + a_1,\ A_2 = a_2,\ A_3 = a_3 + a_7 W_{1b}^n + a_{11} W_{2b}^n,\ A_4 = a_4 + a_8 W_{2b}^n + a_{14} W_{1s}^n + a_{15} W_{2s}^n,$$

$$A_5 = a_5 + a_9 W_{1s}^n + a_{12} W_{1b}^n,\ A_6 = a_6 + a_{10} W_{2s}^n + a_{13} W_{1b}^n + a_{16} W_{1s}^n,$$

$$A_7 = \frac{a_0}{\Delta t}\dot{U}^n + \frac{a_0}{\left(\Delta t\right)^2} U^n - a_{17}$$

$$B_1 = b_1,\ B_2 = \frac{b_0}{\left(\Delta t\right)^2} + b_2,\ B_3 = b_3 + b_7 W_{1b}^n + b_{11} W_{2b}^n,\ B_4 = b_4 + b_8 W_{2b}^n + b_{14} W_{1s}^n + b_{15} W_{2s}^n,$$

$$B_5 = b_5 + b_9 W_{1s}^n + b_{12} W_{1b}^n,\ B_6 = b_6 + b_{10} W_{2s}^n + b_{13} W_{1b}^n + b_{16} W_{1s}^n,\ B_7 = \frac{b_0}{\Delta t}\dot{V}^n + \frac{b_0}{\left(\Delta t\right)^2} V^n - b_{17}$$

$$C_1 = c_1 + c_7 W_{1b}^n + c_8 W_{2b}^n + c_9 W_{1s}^n + c_{10} W_{2s}^n,\ C_2 = c_2 + c_{11} W_{1b}^n + c_{12} W_{2b}^n + c_{13} W_{1s}^n + c_{14} W_{2s}^n,$$

$$C_3 = \frac{c_0}{\left(\Delta t\right)^2} + c_3 + c_{15}\left(W_{1b}^n\right)^2 + c_{19}\left(W_{2b}^n\right)^2 + c_{20}\left(W_{1s}^n\right)^2 + c_{21}\left(W_{2s}^n\right)^2 + c_{31} W_{2b} W_{1s},$$

$$C_4 = c_4 + c_{16}\left(W_{2b}^n\right)^2 + c_{22}\left(W_{1b}^n\right)^2 + c_{23}\left(W_{1s}^n\right)^2 + c_{24}\left(W_{2s}^n\right)^2 + c_{32} W_{1b}^n W_{2s}^n,$$

$$C_5 = c_5 + c_{17}\left(W_{1s}^n\right)^2 + c_{25}\left(W_{1b}^n\right)^2 + c_{26}\left(W_{2b}^n\right)^2 + c_{27}\left(W_{2s}^n\right)^2 + c_{33} W_{1b}^n W_{2s}^n,$$

$$C_6 = c_6 + c_{18}\left(W_{2s}^n\right)^2 + c_{28}\left(W_{1b}^n\right)^2 + c_{29}\left(W_{2b}^n\right)^2 + c_{30}\left(W_{1s}^n\right)^2 + c_{34} W_{2b}^n W_{1s}^n,$$

$$C_7 = \frac{c_0}{\Delta t}\dot{W}_{1b}^n + \frac{c_0}{\left(\Delta t\right)^2} W_{1b}^n - c_{35}$$

$$D_1 = d_1 + d_7 W_{1b}^n + d_8 W_{2b}^n + d_9 W_{1s}^n + d_{10} W_{2s}^n,\ D_2 = d_2 + d_{11} W_{1b}^n + d_{12} W_{2b}^n + d_{13} W_{1s}^n + d_{14} W_{2s}^n,$$

$$D_3 = d_3 + d_{15}\left(W_{1b}^n\right)^2 + d_{19}\left(W_{2b}^n\right)^2 + d_{20}\left(W_{1s}^n\right)^2 + d_{21}\left(W_{2s}^n\right)^2 + d_{31} W_{2b}^n W_{1s}^n +,$$

$$D_4 = \frac{d_0}{\left(\Delta t\right)^2} + d_4 + d_{16}\left(W_{2b}^n\right)^2 + d_{22}\left(W_{1b}^n\right)^2 + d_{23}\left(W_{1s}^n\right)^2 + d_{24}\left(W_{2s}^n\right)^2 + d_{32} W_{1b} W_{2s},$$

$$D_5 = d_5 + d_{17}\left(W_{1s}^n\right)^2 + d_{25}\left(W_{1b}^n\right)^2 + d_{26}\left(W_{2b}^n\right)^2 + d_{27}\left(W_{2s}^n\right)^2 + d_{33} W_{1b} W_{2s},$$

$$D_6 = d_6 + d_{18}\left(W_{2s}^n\right)^2 + d_{28}\left(W_{1b}^n\right)^2 + d_{29}\left(W_{2b}^n\right)^2 + d_{30}\left(W_{1s}^n\right)^2 + d_{34} W_{2b} W_{1s},$$

$$D_7 = \frac{d_0}{\Delta t}\dot{W}_{2b}^n + \frac{d_0}{\left(\Delta t\right)^2} W_{2b}^n - d_{35}$$

$$E_1 = e_1 + e_7 W_{1b}^n + e_8 W_{2b}^n + e_9 W_{1s}^n + e_{10} W_{2s}^n,\ E_2 = e_2 + e_{11} W_{1b}^n + e_{12} W_{2b}^n + e_{13} W_{1s}^n + e_{14} W_{2s}^n,$$

$$E_3 = e_3 + e_{15}\left(W_{1b}^n\right)^2 + e_{19}\left(W_{2b}^n\right)^2 + e_{20}\left(W_{1s}^n\right)^2 + e_{21}\left(W_{2s}^n\right)^2 + e_{31} W_{2b} W_{1s},$$

$$E_4 = e_4 + e_{16}\left(W_{2b}^n\right)^2 + e_{22}\left(W_{1b}^n\right)^2 + e_{23}\left(W_{1s}^n\right)^2 + e_{24}\left(W_{2s}^n\right)^2 + e_{32} W_{1b} W_{2s},$$

$$E_5 = \frac{e_0}{\left(\Delta t\right)^2} + e_5 + e_{17}\left(W_{1s}^n\right)^2 + e_{25}\left(W_{1b}^n\right)^2 + e_{26}\left(W_{2b}^n\right)^2 + e_{27}\left(W_{2s}^n\right)^2 + e_{33} W_{1b} W_{2s},$$

$$E_6 = e_6 + e_{18}\left(W_{2s}^n\right)^2 + e_{28}\left(W_{1b}^n\right)^2 + e_{29}\left(W_{2b}^n\right)^2 + e_{30}\left(W_{1s}^n\right)^2 + e_{34} W_{2b} W_{1s},$$

$$E_7 = \frac{e_0}{\Delta t}\dot{W}_{1s}^n + \frac{e_0}{\left(\Delta t\right)^2} W_{1s}^n - e_{35}$$

$$F_1 = f_1 + f_7 W_{1b}^n + f_8 W_{2b}^n + f_9 W_{1s}^n + f_{10} W_{2s}^n,\ F_2 = f_2 + f_{11} W_{1b}^n + f_{12} W_{2b}^n + f_{13} W_{1s}^n + f_{14} W_{2s}^n,$$

$$F_3 = f_3 + f_{15}\left(W_{1b}^n\right)^2 + f_{19}\left(W_{2b}^n\right)^2 + f_{20}\left(W_{1s}^n\right)^2 + f_{21}\left(W_{2s}^n\right)^2 + f_{31} W_{2b} W_{1s},$$

$$F_4 = f_4 + f_{16}\left(W_{2b}^n\right)^2 + f_{22}\left(W_{1b}^n\right)^2 + f_{23}\left(W_{1s}^n\right)^2 + f_{24}\left(W_{2s}^n\right)^2 + f_{32} W_{1b} W_{2s},$$

$$F_5 = f_5 + f_{17}\left(W_{1s}^n\right)^2 + f_{25}\left(W_{1b}^n\right)^2 + f_{26}\left(W_{2b}^n\right)^2 + f_{27}\left(W_{2s}^n\right)^2 + f_{33} W_{1b} W_{2s},$$

$$F_6 = \frac{f_0}{\left(\Delta t\right)^2} + f_6 + f_{18}\left(W_{2s}^n\right)^2 + f_{28}\left(W_{1b}^n\right)^2 + f_{29}\left(W_{2b}^n\right)^2 + f_{30}\left(W_{1s}^n\right)^2 + f_{34} W_{2b} W_{1s},$$

$$F_7 = \frac{f_0}{\Delta t}\dot{W}_{2s}^n + \frac{f_0}{\left(\Delta t\right)^2} W_{2s}^n - f_{35}$$

CURRICULUM VITAE

Name Surname: Sedat SÜSLER

Place and Date of Birth: İzmir, 27 April 1982

E-Mail: sedatsusler@gmail.com

EDUCATION:

B.Sc.: Aeronautical Engineering, Faculty of Aeronautics and Astronautics, ITU

M.Sc.: Aerospace Engineering, Institute of Science and Technology, ITU

PUBLICATIONS, PRESENTATIONS AND PATENTS ON THE THESIS:

- **Susler S.**, Turkmen H. S. and Kazancı Z., 2012: The Nonlinear Dynamic Behaviour of Tapered Laminated Plates Subjected to Blast Loading. *Shock and Vibration*, 19(6), 1235-1255.
- **Susler S.**, Kazancı Z. and Turkmen H. S., 2010: Dynamic Behaviour of Tapered Plates Subjected to Blast Loading. *10th International Conference on Computational Structures Technology (CST2010)*, September 14-17, 2010 Valencia, Spain.
- **Susler S.**, Kazancı Z. and Turkmen H. S., 2011: Analysis of Laminated Plates with Parabolic Thickness Variation. *13th International Conference on Civil Structural and Environmental Engineering Computing (CC2011)*, September 6-9, 2011 Chania, Crete, Greece.
- **Susler S.**, Kazancı Z. and Turkmen H. S., 2012: Nonlinear Dynamic Behaviour of Tapered Sandwich Plates Subjected to Blast Loading. *15th European Conference on Composite Materials (ECCM15)*, June 24-28, 2012 Venice, Italy.
- Baştürk S., **Susler S.**, Uyanık H., Turkmen H. S., Lopresto V., Genna S. and Kazancı Z., 2015: Experimental and Numerical Analysis of a Laminated Basalt Composite Plate Subjected to Blast Load. *20th International Conference on Composite Materials (ICCM20)*, July 19-24, 2015 Copenhagen, Denmark.

OTHER PUBLICATIONS, PRESENTATIONS AND PATENTS:

- Ustaoğlu H. B., Ayhün S., Simitçioğlu G., **Süsler S.**, Akay E., Doğan V. Z., Mecitoğlu Z., Türkmen H. S. and Atamer S., 2015: Static and Dynamic Analysis of Plastic Fuel Tanks Used in Buses. *Procedia Engineering*, 101, 509-517.

- Turkmen H. S., **Susler S.** and Kazancı Z., 2013: Dynamic Behaviour of Laminated Plates Subjected to Thermomechanical Loads. *3rd South East European Conference on Computational Mechanics-an ECCOMAS and IACM Special Interest Conference (SEECCM III)*, June 12-14, 2013 Kos, Greece.

- **Susler S.**, Kazancı Z. and Turkmen H. S., 2013: Dynamic Behaviour of Laminated Plates Subjected to a Combined Loading. *6th International Conference on Recent Advances in Space Technologies (RAST2013)*, June 12-14, 2013 Istanbul, Turkey.

- Ustaoğlu H. B., Ayhün S., Simitçioğlu G., **Süsler S.**, Akay E., Doğan V. Z., Mecitoğlu Z., Türkmen H. S. and Atamer S., 2015: Static and Dynamic Analysis of Plastic Fuel Tanks Used in Buses. *3rd International Conference on Material and Component Performance Under Variable Amplitude Loading (VAL2015)*, March 23-26, 2015 Prague, Czech Republic.

- Simitçioğlu G., Ustaoğlu B., Atamer S., Doğan V. Z., Türkmen H. S., Mecitoğlu Z., Ayhün S., Akay E., **Süsler S.**, Erginsoy Y. E. and Çakır M, 2015: Otobüslerde Kullanılan Plastik Yakıt Tanklarının Statik ve Dinamik Analizler Yardımıyla Dayanımının İncelenmesi. *TUMTMK XIX. Ulusal Mekanik Kongresi*, August 24-28, 2015 Trabzon, Turkey.